March 2015

Synthesis, Characterization and Surface Modification of Polydimethylsiloxane and Its Composites

Yan Wang

SYNTHESIS, CHARACTERIZATION AND SURFACE MODIFICATION OF POLYDIMETHYLSILOXANE AND ITS COMPOSITES

A Dissertation Presented

by

YAN WANG

Submitted to the Graduate School of the
University of Massachusetts in partial fulfillment
of the degree requirements for the degree of

DOCTOR OF PHILOSOPHY

February 2015

Polymer Science and Engineering Department

SYNTHESIS, CHARACTERIZATION AND SURFACE MODIFICATION OF POLYDIMETHYLSILOXANE AND ITS COMPOSITES

A Dissertation Presented

by

YAN WANG

Approved as to style and content by:

_____
Thomas J. McCarthy, Chair

_____
Maria M. Santore, Member

_____
Vincent M. Rotello, Member

_____
David A. Hoagland, Department Head
Polymer Science and Engineering

To my parents and Wei Zhao

ACKNOWLEDGMENTS

I would like to first thank my advisor, Prof. Thomas J. McCarthy, for all his help and support during the past several years. He is a great advisor and teacher, using both his words and actions to teach me how to become a creative, passionate, independent and collaborative researcher. He taught me how to get inspiration from other fields and generate innovative research ideas, how to systematically solve a problem, and when it is time to close the door on a project. He also provided me with the opportunity to work on both independent and collaborative projects, from which I continuously improve my critical thinking, communication and leadership skills.

I acknowledge my two other committee members, Prof. Santore and Prof. Rotello for their valuable suggestions on my PhD thesis work. It is my honor to have such accomplished researchers on my committee. Thanks to all the past and current McCarthy group members, Pei, Peiwen, Joe, Dennis, Fang, Minchao, Connor, Dan, Liming, Satchel and Jack, I have plenty of great memories both inside and outside the lab. I grew a lot both academically and socially with their help. Particularly, I thank Peiwen and Joe, who gave me enormous advice and support at the beginning of my PhD life. I quickly got adapted to the research environment in Amherst, and learned from them how to become a productive researcher. I also want to thank Jack, for all the enjoyable conversations with him about research and life.

I appreciate all the help from my collaborators and ‘great helpers’ inside and outside the Polymer Science and Engineering department, including Joe White, Dannielle Ryman, Jiaming Zhuang, Lei Zhang, Michael Beaulieu, Dan King, Yucheng Chen, Polina Ware, Brian Cromer, Connor Evans, Irem Kosif, Wenxu Zhang and Ying Zhou. I would also like to thank all my classmates, all my friends in

the department, and the great softball team members. My friendship with them is a much cherished part of my life in Amherst.

I would like to thank MRSEC, CHM, CUMIRP, and Henkel for their financial support. I also thank the staff members including Lisa, Maria, Alyssa, Sekar, Greg and Dave for making my life in Amherst easier.

Finally, I especially thank Wei Zhao and my parents. Their unconditional love and support help me overcome many obstacles in my personal and professional life. Therefore, I dedicate this thesis to them.

ABSTRACT

SYNTHESIS, CHARACTERIZATION, AND SURFACE MODIFICATION OF POLYDIMETHYLSILOXANE AND ITS COMPOSITES

FEBRUARY 2015

YAN WANG, B.S., TSINGHUA UNIVERSITY

M.S., UNIVERSITY OF MASSACHUSETTS AMHERST

Ph.D., UNIVERSITY OF MASSACHUSETTS AMHERST

Directed by: Professor Thomas J. McCarthy

Silicone elastomers are widely employed in composite, coatings, biomedical, sealant and electronics applications. This dissertation highlights new methodologies and formulation approaches to improve the performance of siloxane polymers, including the mechanical properties, surface properties, optical properties and transport properties. It also provides an in-depth understanding about dip-coating deposition on chemically patterned surfaces.

The first chapter presents the process of transforming sand into siloxane polymers of excellent mechanical strength. History, properties and applications of siloxane polymers are systematically discussed. Another focus of this chapter is wetting, including the concepts of contact angles and capillary bridge ruptures.

Five interconnected projects are discussed following the introduction. Base-catalyzed siloxane equilibration is fully utilized in the first and second projects. First, extremely stretchable silicone elastomers are prepared by copolymerizing silica particles and octamethylcyclotetrasiloxane with siloxane equilibration. It is demonstrated that Stöber silica particles can actively participate in the chemical cross-linking of linear PDMS, serving as SiO_4 linking group reservoirs. Second,

permanently hydrophilic silicones are obtained by grafting PEO-PDMS copolymers to cross-linked silicones via siloxane equilibration.

High power light-emitting diodes require a transparent encapsulant of high refractive index and low water permeability. The third project concerns the uniform incorporation of high refractive index inorganic fillers into siloxane polymers. Silicone composites with tailored refractive indices, different molecular structures, tunable mechanical properties and excellent transparency are achieved via sol-gel chemistry.

In the fourth project, the high water transport rate in pure silicone is clarified, for both linear and cross-linked silicones. This high water transport rate results from the special structural features of silicone. Incorporation of water-resistant coating layers, silanized fillers and polyimide blocks are shown to be several effective approaches to decrease the water permeability of silicones.

The fifth project deals with dip-coating deposition on chemically patterned surfaces. The mechanisms of capillary bridge deformation and rupture for dip-coating deposition on chemically and topographically patterned surfaces are compared. Ordered inorganic and organic individual crystal arrays are successfully patterned on smooth and chemically patterned surfaces prepared by photolithography.

TABLE OF CONTENTS

Page

LIST OF TABLES

Table Page

LIST OF FIGURES

Figure Page

CHAPTER 1

INTRODUCTION

1.1 Development of Organosilanes and Siloxane Polymers

Oxygen and silicon are the two most abundant elements in earth crust. Silicon exists in the earth crust mainly in the form of Si-O (sand and other silicates) and never elemental Si, for the reasons that there is plenty of oxygen on Earth and the Si-O bond has a large bond energy (108 kcal/mol).[1] A carbon-based reduction process has been in practice to prepare silicon since early in the last century, in which sand is heated at 3000 ^{o}C in a furnace equipped with graphite electrodes (Equation 1-1).

$$SiO_2 + 2\ C \rightarrow Si + 2\ CO \qquad \text{Equation 1-1}$$

The first chlorosilanes were produced by heating amorphous silicon in an HCl gas stream. A colorless liquid mixture was obtained after purification of the product. This liquid mixture consisted of chlorosilanes (Equation 1-2).

$$Si + HCl \rightarrow SiCl_4 + HSiCl_3 \qquad \text{Equation 1-2}$$

Tetraethylsilane was the first organosilicon compound synthesized (Equation 1-3). Friedel and Crafts heated $SiCl_4$ with diethylzinc to prepare the first organosilicon compounds. Ladenburg hydrolyzed one of these, $C_2H_5SiCl_3$, and prepared the first siloxane polymer $(C_2H_5SiO_{1.5})_n$.

$$2\ (C_2H_5)_2Zn + SiCl_4 \rightarrow (C_2H_5)_4Si + 2\ ZnCl_2 \qquad \text{Equation 1-3}$$

In 1900, Grignard reagents were discovered and published, which led to Kipping's method of organosilicon compound synthesis (Equation 1-4). He reacted Grignard reagents with chlorosilanes to prepare organosilanes. Kipping also did some

research on siloxane polymers. He found that hydrolysis of dichlorosilanes yields oligosiloxanes $(R_2SiO)_2$, while silicone resin $(RSiO_{1.5})_n$ is given after hydrolysis of trichlorosilanes.

$$C_2H_5MgI + SiCl_4 \rightarrow (C_2H_5)_4Si + (C_2H_5)_3SiCl + (C_2H_5)_2SiCl_2 + C_2H_5SiCl_3 \qquad \text{Equation 1-4}$$

Doing industrial research before World War II, Hyde from Corning Glass Works repeated Kipping's synthetic approach and prepared some phenyl group - containing siloxane oligomers. At about the same time (1938), a chemist from the GE Research Laboratory, Rochow, focused his research on methylpolysiloxanes. Methylpolysiloxane seemed a more promising research area to him than the product of diphenyldichlorosilane hydrolysis/condensation. He also reacted the Grignard reagent (C_2H_5MgCl) with $SiCl_4$, and carefully distilled the product to isolate $(C_2H_5)_2SiCl_2$ and $C_2H_5SiCl_3$ as pure compounds.

However, Dow Chemical was the major producer of magnesium in the USA at that time, and GE had less accessibility to Grignard reagents than Dow Corning, Inc. This was an incentive for Rochow to develop an alternative approach to prepare chlorosilanes without Grignard reagents. In 1945, Rochow published[2] a paper reporting the direct synthesis of organosilicon compounds. This publication was delayed by World War II (wartime security consideration). It is noted that Richard Müller discovered this reaction independently in Germany at around the same time.[3] After some other scale up tests, plant scale production of silicone fluid and silicone rubbers was realized, which significantly benefited the military. Today the direct synthesis of organochlorosilanes (Equation 1-5) is used by many companies, including Dow-Corning, Union Carbide, Wacker-Chemie, and Bayer.

$$CH_3Cl \xrightarrow[Si/Cu]{} (CH_3)_4Si + (CH_3)_3SiCl + (CH_3)_2SiCl_2 + CH_3SiCl_3 + SiCl_4$$ Equation 1-5

1.2 Preparation, Properties and Applications of Siloxane Polymers

A siloxane polymer is formed by alternating silicon and oxygen atoms, and the silicon atoms are connected with organic substituents. Polydimethylsiloxane (PDMS) is the most common type of siloxane polymer. It is a liquid material with special properties.[4] In PDMS, one silicon atom is connected with one oxygen atom and two methyl groups. Kipping realized its structural similarity to ketones in 1904, and proposed the name 'silicone' for siloxane polymers.[5] There are four different structural units for methylpolysiloxane (Figure 1-1). M units can end block siloxane chain ends, D units can constitute chains or rings, T units can serve as chain extender or cross-links, and Q units can be considered as "double" cross-links.

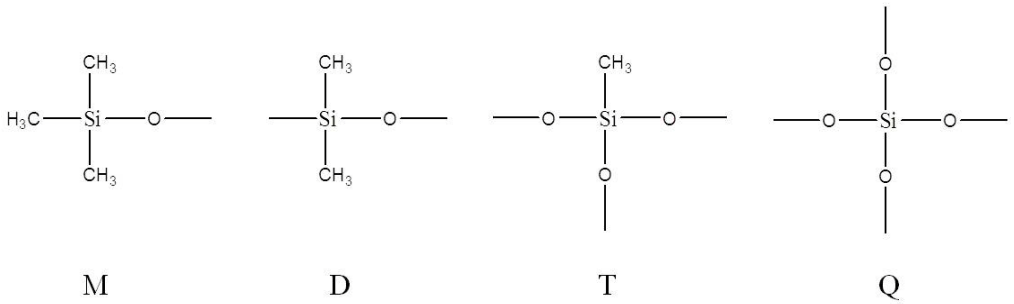

Figure 1-1 Common molecular units in silicones

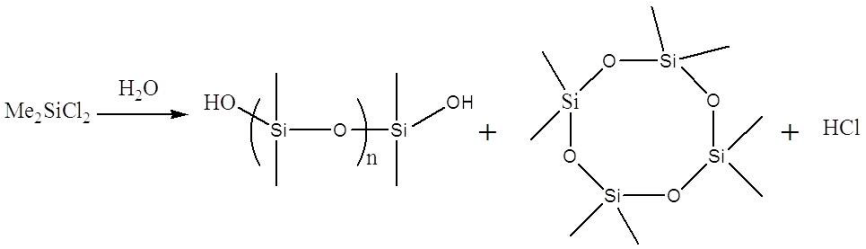

Figure 1-2 Synthesis of PDMS by hydrolysis and condensation

Hydrolysis/condensation reaction of dimethyldichlorosilane results in the formation of linear PDMS (Figure 1-2). Octamethylcyclotetrasiloxane (D_4) is the

byproduct of this reaction that can be removed via distillation.[6] The problem with this synthetic approach is that the degree of polymerization is hard to control. Better control of linear PDMS molecular weight can be accomplished by acid or base catalyzed ring opening polymerization of D_4, with appropriate addition of hexamethyldisiloxane (MM) chain stoppers (Figure 1-3). Aside from the molecular weight control, it is also possible to incorporate other functional groups as end groups in linear silicone by this acid or base catalyzed synthetic method. For example, vinyl-terminated PDMS is achieved when MM is replaced by divinyltetramethyldisiloxane.

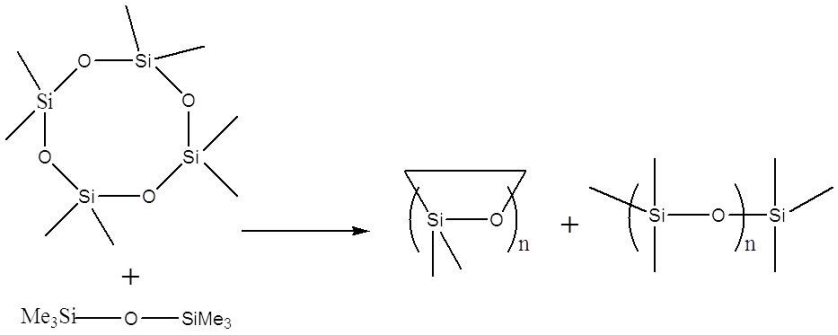

Figure 1-3 Synthesis of PDMS by acid or base catalyzed siloxane equilibration

In the case of base-catalyzed polymerization of D_4, the viscosity changes of the reaction mixture with time show an interesting trend. The viscosity reaches a maximum value before it drops to an equilibrium value. Molecular weight of the products is expected to change with time in a similar fashion.[7] This is because D_4 is more reactive towards base nucleophiles than MM at the beginning of the reaction. (Silicon connected to two oxygen atoms is more electropositive than silicon bonded to one oxygen atom.) Consequently, D_4 quickly polymerizes into very long linear chains as soon as the reaction starts. MM gets attacked by base at a later stage of the reaction. Then these MMs function as chain endblockers, cleaving long PDMS chains into shorter ones.

PDMS has many special properties. It has the lowest T_g (-125 ^oC) of the common polymers because of its unusual chain flexibility. This chain flexibility contributes to the low melting point of PDMS (-40 ^oC) as well. The bond angle of Si-O-Si is around 143^o, which is much greater than the usual tetrahedral C-C-C bond angle (~110^o), and it is interesting that this 143^o bond angle is deformable. Si-O has a longer bond length (1.64 $\overset{o}{A}$) than C-C (1.54 $\overset{o}{A}$) bond.[6] Moreover, Rochow pointed out that the 51% ionic Si-O bond is more ionic and less directional than the C-C bond.[4] The large bond angle, long bond length and ionic nature of the bond together allow the free rotation and vibration of siloxane chains.[8] In addition, PDMS chains have weak intermolecular interactions between each other, and the methyl groups on PDMS chains have large degrees of rotational and vibrational freedom. They contribute to the superior gas permeability, good hydrophobicity and low surface energy (20-23 dyn/cm) of PDMS.[6,9] Finally, the bond dissociation energy of Si-O (450 kJ/mol) is larger than that of C-C bond (350 kJ/mol), so PDMS has excellent thermal, oxidative, chemical and biological stability.[10] There is a large business involving silicone fluids worldwide, since they have applications including lubricants, deodorants, mold release coatings,[6] analytical chemistry,[11] heating oil baths, and surfactants.[10]

1.3 Cross-linking of Siloxane Polymers

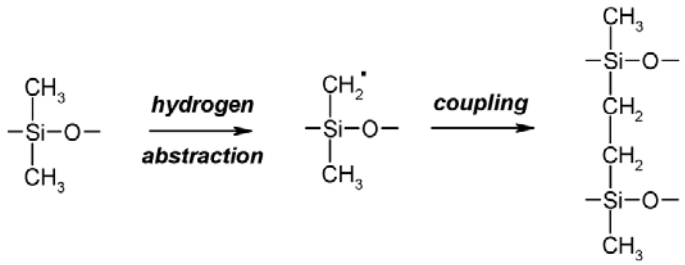

Figure 1-4 Mechanism of radical cross-linking of PDMS[12]

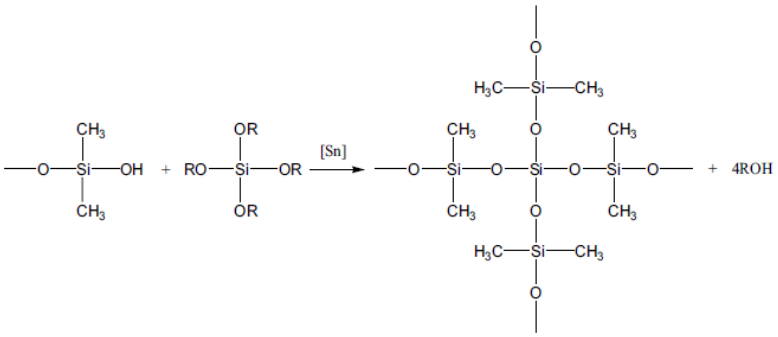

Figure 1-5 Mechanism of condensation curing of PDMS[13]

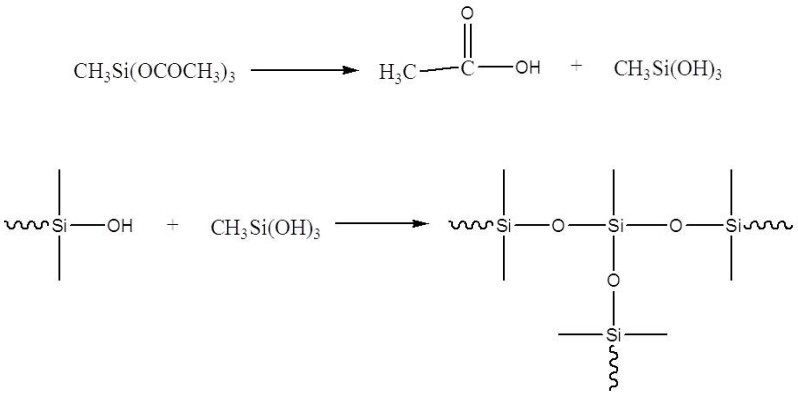

Figure 1-6 Cross-linking of one-component RTV silicone[10]

The cross-linked silicone elastomers have unique commercial value in the market. They have a wide range of medical applications, such as catheters, breast implants and contact lenses.[6] They are also applied in sealants, adhesives, tubing, and

electrical insulation.[10] Radical cross-linking, condensation curing, and hydrosilylation are the three most common approaches to obtain cross-linked PDMS networks.[13] Alkyl peroxide is frequently used in the 'peroxidic' cross-linking. The radicals abstract hydrogen from PDMS chains, leading to the coupling of two methylene radicals and formation of ethylene bridges (Figure 1-4).[12] Room temperature vulcanizing (RTV) silicone is a good example of the condensation curing of PDMS. (Figure 1-5) The two component system which consists of poly(dimethylsiloxane)-α,ω-diol and multifunctional alkoxysilane is well studied. Organo-tin compounds such as dialkyltin dicarboxylates and tin dicarboxylates are known as effective catalyst for the curing condensation.[14] Another example is one-component RTV silicone. A homogeneous mixture of silanol-terminated polysiloxane, methyltriacetoxysilane and dibutyltin dilaurate catalyst is sealed in an airtight package. It gradually cures into elastomer in the air by absorbing moisture (Equation 1-6).

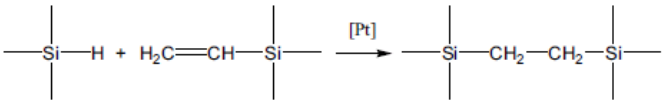

Figure 1-7 Mechanism of cross-linking of PDMS via hydrosilylation[13]

The commercial silicone, Dow Corning Sylgard 184, is the crucial substance in wrinkling studies and soft lithography research.[15,16] Its cross-linking mechanism is hydrosilylation, which refers to the reaction between Si-H and the unsaturated bonds (Figure 1-7).[13] Development in technology provides other alternatives to cross-link PDMS. For instance, Papautsky and coworkers claimed it is possible to cross-link photosensitive PDMS with photoinitiator 2,2-dimethoxy-2-phenyl acetophenone using light with wavelengths below 365 nm.[17]

1.4 Compounding of Siloxane Polymers

Unfilled silicone elastomers are normally weak and soft. Reinforcement of the elastomer with silica can improve its tensile strength from ~ 0.34 MPa to 50 times this value.[18] Dow Corning Sylgard 184, for example, contains 30-50 wt% dimethylvinylated and trimethylated silica in its base, and these silica fillers comprise 10-30 wt% of the curing agents.[19] These reinforcing fillers account for the good mechanical strength of this commercial product. For the PDMS/silica composite, the stiffness of the composite increases compared to that of the pure polymer, because the fillers are more rigid than the soft matrix, and also because of additional 'cross-links' formed between the fillers and polymer. In addition, the size of the particle aggregates, the particle morphology and the particle surface characteristics all affect the stiffness.[20]

$$SiCl_4 + 2H_2 + O_2 \xrightarrow{1800^oC} SiO_2 + 4HCl \qquad \text{Equation 1-6}$$

Fumed silica, such as Cab-O-Sil, Aerosil and Wacker HDK, is generally blended into PDMS prepolymer to provide reinforcement.[5] It is named as fumed silica, because it is prepared in a flame (Equation 1-6), has very large surface area and a three-dimensional structure (it is actually the white smoke from the flame). This method of compounding is straightforward, the composite contains nearly no impurities, and many well developed blending instruments such as the SpeedMixer are commercially available.[21] However, this approach also has its drawbacks: It is energy consuming; The particle aggregation is uncontrollable; An undesirable inhomogeneous composite material is usually achieved.

Silica fillers can also be generated *in-situ* in the cross-linked silicone network. Sol-gel chemistry is widely utilized to prepare silica-filled PDMS. Bokobza and

coworkers prepared a well cured PDMS network by carrying out a hydrosilylation reaction between 1,3,5,7-tetramethylcyclotetrasiloxane and vinyl-terminated PDMS. The cross-linked PDMS was then swollen in tetraethoxysilane (TEOS). Subsequently, silica was generated in the cross-linked network in the presence of water under the constraint from the polymer, so that large aggregates of silica were prevented.[20] Silica/PDMS composites can be also obtained in a one-pot synthesis by means of the sol-gel process. Avnir and coworkers grew silica particles using TEOS hydrolysis in an emulsion composed of PDMS and ethanol. The emulsion was stabilized by PDMS/polyether surfactants.[22] Brook and coworkers prepared almost monodisperse *in-situ* - formed silica in PDMS by mixing hydroxy-terminated PDMS, TEOS and aminopropyl-terminated dimethylsiloxane oligomer (AT-PDMS). TEOS, as both cross-linker and silica precursor, can absorb water from the air and undergo hydrolysis. AT-PDMS mainly resides at the silicone air interface, functioning as a stabilizer to inhibit particle aggregation.[23]

PDMS properties can be improved in various aspects by the addition of other mineral particles. Researchers found that titania can increase the compressibility and thermal stability of PDMS.[24] Quake and coworkers mixed iron powder and carbon black with PDMS, resulting in a magnetic layer.[25] Carbon nanotubes, with large surface area to volume ratio, became the center of research in the area of composite preparation. The large surface of fillers is the premise of strong filler-matrix interaction, as well as the pronounced reinforcement effect. Wagner and coworkers blended single-wall carbon nanotubes into PDMS. They report that the material mechanical properties improvement is related to the filler content.[26] Giannelis and coworkers mixed layered mica-type silicates with PDMS via melt processing. The delaminated silicate/PDMS nanocomposites exhibit lower swelling ratio in toluene,

and better thermal stability due to the strong particle-polymer interaction.[27] Wen and coworkers transformed non-conducting PDMS into conductive composites by integrating silver microparticles into PDMS. The composite is shown to have excellent electrical conductivity, and can find applications in microfabricated devices. This strategy is more advantageous compared to patterning metallic structures on PDMS, because the adhesion of metal to PDMS is weak.[28]

1.5 Contact Angles

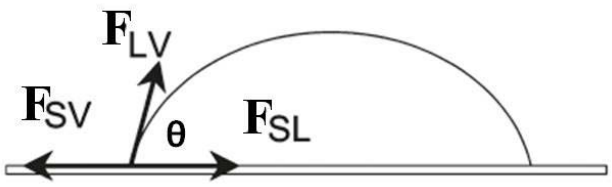

Figure 1-8 Forces and contact angle in Young's statement

Gao and McCarthy systematically summarized their work in wetting from 2006 to 2009 in the paper 'Wetting 101°'.[29] Thomas Young was the first scientist to characterize surface wettability with contact angle. In his 1804 statement,[30] he used a force balance equation (Equation 1-7) at the three-phase contact line of a liquid drop on any type of surface (Figure 1-8).

$$F_{SV} = F_{LV}\cos\theta + F_{SL} \qquad \text{Equation 1-7}$$

Unfortunately, this equation was misinterpreted by Wenzel, and the well recognized form of Young's equation nowadays is,

$$\cos\theta = \frac{\gamma_{SV} - \gamma_{SL}}{\gamma_{LV}} \qquad \text{Equation 1-8}$$

Equation 1-8 is a faulty interpretation of Young's statement, because γ_{SV} , γ_{SL} and γ_{LV} represent surface free energies at solid/air, solid/liquid and liquid/air interfaces, respectively. The forces, which are tensors in the original equation (Equation 1-7) are mistakenly substituted by energy terms (scalars). In Equation 1-7 and Equation 1-8, θ is the static contact angle.

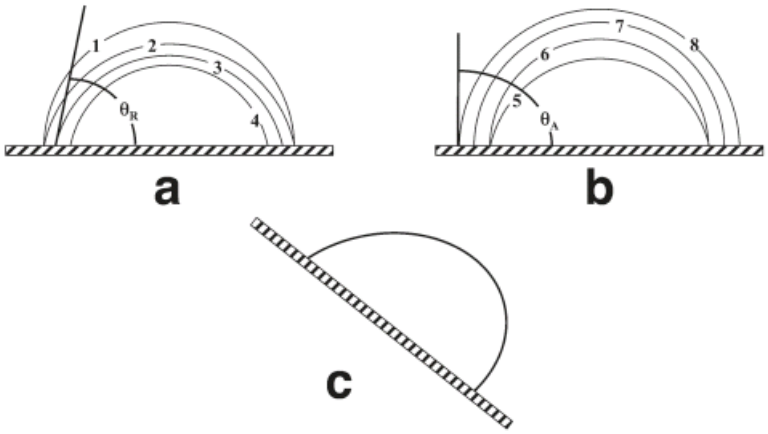

Figure 1-9 (a)Receding (θ_R) contact angles of a sessile drop with shrinking contact line diameters; (b)Advancing (θ_A) contact angles of a sessile drop with expanding contact line diameters; (c) A droplet sliding down a tilted surface.

Another problem with Equation 1-8 is that a sessile liquid drop can reside on a surface at a metastable state when a static contact angle value is measured, so the wettability of a surface cannot be accurately characterized with a single static contact angle value. It is suggested that both advancing contact angle (θ_A) and receding contact angle (θ_R) values need to be reported to demonstrate the wettability of a surface.[29] When the liquid is withdrawn from a sessile drop, the water contact line recedes, maintaining the same contact angle θ_R (Figure 1-9(a)). Similarly, the water contact line advances with the same contact angle θ_A when more water is injected into the sessile drop (Figure 1-9(b)). Both θ_A and θ_R values rely on surface chemistry and

topography. Static contact angle, since it corresponds to a metastable state of the drop, is an arbitrary value between θ_A and θ_R.

It is depicted in Figure 1-9(c) that θ_A has to be reached at the downhill side of the drop, and θ_R has to be reached at the uphill side of the drop, before a drop can actually slide down a tilted surface. It implies contact angle hysteresis is another important parameter to evaluate surface hydrophobicity. Contact angle hysteresis $\Delta\theta$ is defined as the difference between the two contact angles (Equation 1-9).[31]

$$\Delta\theta = \theta_A - \theta_R \qquad \text{Equation 1-9}$$

The chemical heterogeneity of surfaces and surface roughness greatly affect $\Delta\theta$. For instance, rougher surfaces usually have a larger $\Delta\theta$.[32] Contact angle hysteresis is related with the activation energy needed to move a liquid drop from one metastable state to another. Contact angle hysteresis can be also scrutinized based on the three-phase contact line.[33]

1.6 Capillary Bridge Ruptures

Gao and McCarthy previously recorded tensile capillary bridge rupture of a sessile droplet between two hydrophobic surfaces as they are separated,[34] and demonstrated that contact angle hysteresis and the force-separation curves of capillary bridges are interconnected.[35] They further made the conjecture that tensile microcapillary bridge rupture at receding contact lines results in microdroplet formation at pinning sites.[36] This conjecture was partially justified by a simple dip-coating experiment with a hydrophobized silicon wafer containing $3\,\mu m \times 6\,\mu m \times 40\,\mu m$ staggered rhombus posts.[37]

Cheng and McCarthy examined sessile capillary bridge rupture of a water droplet on a chemically patterned surface made by photolithography.[38] Photolithography is a technique used in the mass production of optoelectronics and microelectronics like integrated circuits.[39] They patterned hydrophilic (silica) features on a hydrophobic surface (1,3,5,7-Tetramethylcyclotetrasiloxane-modified silicon wafer surface). It was illustrated that after the depinning process of sessile droplets from hydrophilic circular arcs pointing up, tiny droplets cling to the hydrophilic arcs due to the sessile capillary bridge breakup.

Wang and McCarthy studied shear distortion of capillary bridges between two parallel chemically patterned surfaces.[40] Tensile and sessile capillary bridge ruptures are simultaneously observed in this special case. The capillary bridge tends to maintain the same mean curvature (same Laplace pressure) everywhere, and it distorts accordingly.

1.7 References

1. Seyferth, D., Dimethyldichlorosilane and the direct synthesis of methylchlorosilanes. The key to the silicones industry. *Organometallics* **2001,** *20* (24), 4978-4992.

2. Rochow, E. G., The Direct Synthesis of Organosilicon Compounds. *J Am Chem Soc* **1945,** *67* (6), 963-965.

3. Müller, R., Über Silicone (I). Zur angewandten Chemie der Silicone (Synthese). *Chem. Tech.* **1950,** *2*, 7-13.

4. Rochow, E. G., An Introduction to the Chemistry of the Silicones. Second ed.; John Wiley & Sons, Inc: 1946.

5. Buddy D. Ratner, A. S. H., Frederick J. Schoen, Jack E. Lemons, Biomaterial Science: An Introduction to Materials in Medicine. Elservier, Inc.

6. Clarson, S. J., Silicones and Silicone-modified Materials. American Chemical Society: 2000.

7. Kantor, S. W.; Grubb, W. T.; Osthoff, R. C., The Mechanism of the Acid-Catalyzed and Base-Catalyzed Equilibration of Siloxanes. *J Am Chem Soc* **1954,** *76* (20), 5190-5197.

8. Zheng, P. W.; McCarthy, T. J., Rediscovering Silicones: Molecularly Smooth, Low Surface Energy, Unfilled, UV/Vis-Transparent, Extremely Cross-Linked, Thermally Stable, Hard, Elastic PDMS. *Langmuir* **2010,** *26* (24), 18585-18590.

9. Lane, T. H.; Burns, S. A., Silica, silicon and silicones ... unraveling the mystery. *Curr Top Microbiol* **1996,** *210*, 3-12.

10. Odian, G., Principles of Polymerization. fourth ed.; Wiley Interscience.

11. Seethapathy, S.; Gorecki, T., Applications of polydimethylsiloxane in analytical chemistry: A review. *Anal Chim Acta* **2012,** *750*, 48-62.

12. Baquey, G.; Moine, L.; Degueil-Castaing, M.; Lartigue, J. C.; Maillard, B., Decomposition of di-tert-butyl peroxide in siloxane: An approach of the free radical cross-linking of silicones. *Macromolecules* **2005,** *38* (23), 9571-9583.

13. Mashak, A.; Rahimi, A., Silicone Polymers in Controlled Drug Delivery Systems: A Review. *Iran Polym J* **2009,** *18* (4), 279-295.

14. Vanderweij, F. W., The Action of Tin-Compounds in Condensation-Type Rtv Silicone Rubbers. *Makromol Chem* **1980,** *181* (12), 2541-2548.

15. Breid, D.; Crosby, A. J., Effect of stress state on wrinkle morphology. *Soft Matter* **2011,** *7* (9), 4490-4496.

16. Qin, D.; Xia, Y. N.; Whitesides, G. M., Soft lithography for micro- and nanoscale patterning. *Nat Protoc* **2010,** *5* (3), 491-502.

17. Bhagat, A. A. S.; Jothimuthu, P.; Papautsky, I., Photodefinable polydimethylsiloxane (PDMS) for rapid lab-on-a-chip prototyping. *Lab Chip* **2007,** *7* (9), 1192-1197.

18. Michael J. Sullivan, S. A., Edmund A. Hebert Golf Ball Surface Patterns Comprising Variable Width/Depth Multiple Channels. 2013.

19. *Sylgard 184 Silicone Elastomer Kit Material Safety Data Sheet*.

20. Dewimille, L.; Bresson, B.; Bokobza, L., Synthesis, structure and morphology of poly (dimethylsiloxane) networks filled with in situ generated silica particles. *Polymer* **2005,** *46* (12), 4135-4143.

21. Rajan, G. S.; Sur, G. S.; Mark, J. E.; Schaefer, D. W.; Beaucage, G., Preparation and characterization of some unusually transparent poly(dimethylsiloxane) nanocomposites. *J Polym Sci Pol Phys* **2003,** *41* (16), 1897-1901.

22. Sertchook, H.; Elimelech, H.; Avnir, D., Composite particles of silica/poly(dimethylsiloxane). *Chem Mater* **2005,** *17* (18), 4711-4716.

23. Rajendra, V.; Gonzaga, F.; Brook, M. A., Nearly Monodisperse Silica Microparticles Form in Silicone (Pre)elastomer Mixtures. *Langmuir* **2012,** *28* (2), 1470-1477.

24. McCarthy, D. W.; Mark, J. E.; Clarson, S. J.; Schaefer, D. W., Synthesis, structure, and properties of hybrid organic-inorganic composites based on polysiloxanes. II. Comparisons between poly(methylphenylsiloxane) and poly(dimethylsiloxane), and between titania and silica. *J Polym Sci Pol Phys* **1998,** *36* (7), 1191-1200.

25. Unger, M. A.; Chou, H. P.; Thorsen, T.; Scherer, A.; Quake, S. R., Monolithic microfabricated valves and pumps by multilayer soft lithography. *Science* **2000,** *288* (5463), 113-116.

26. Frogley, M. D.; Ravich, D.; Wagner, H. D., Mechanical properties of carbon nanoparticle-reinforced elastomers. *Compos Sci Technol* **2003,** *63* (11), 1647-1654.

27. Burnside, S. D.; Giannelis, E. P., Synthesis and Properties of New Poly(Dimethylsiloxane) Nanocomposites. *Chem Mater* **1995,** *7* (9), 1597-1600.

28. Niu, X. Z.; Peng, S. L.; Liu, L. Y.; Wen, W. J.; Sheng, P., Characterizing and patterning of PDMS-based conducting composites. *Adv Mater* **2007,** *19* (18), 2682-+.

29. Gao, L. C.; McCarthy, T. J., Wetting 101 degrees. *Langmuir* **2009,** *25* (24), 14105-14115.

30. Young, T., An Essay on the Cohesion of Fluids *Philosophical Transactions of the Royal Society* **1805,** *95*, 65-87.

31. Furmidge, C. G., Studies at Phase Interfaces .1. Sliding of Liquid Drops on Solid Surfaces and a Theory for Spray Retention. *J Coll Sci Imp U Tok* **1962,** *17* (4), 309-&.

32. Fadeev, A. Y.; McCarthy, T. J., Trialkylsilane monolayers covalently attached to silicon surfaces: Wettability studies indicating that molecular topography contributes to contact angle hysteresis. *Langmuir* **1999,** *15* (11), 3759-3766.

33. Gao, L. C.; McCarthy, T. J., Contact angle hysteresis explained. *Langmuir* **2006,** *22* (14), 6234-6237.

34. Gao, L. C.; McCarthy, T. J., Teflon is hydrophilic. Comments on definitions of hydrophobic, shear versus tensile hydrophobicity, and wettability characterization. *Langmuir* **2008,** *24* (17), 9183-9188.

35. De Souza, E. J.; Gao, L. C.; McCarthy, T. J.; Arzt, E.; Crosby, A. J., Effect of contact angle hysteresis on the measurement of capillary forces. *Langmuir* **2008,** *24* (4), 1391-1396.

36. Krumpfer, J. W.; McCarthy, T. J., Contact angle hysteresis: a different view and a trivial recipe for low hysteresis hydrophobic surfaces. *Faraday Discuss* **2010,** *146*, 103-111.

37. Krumpfer, J. W.; McCarthy, T. J., Dip-Coating Crystallization on a Superhydrophobic Surface: A Million Mounted Crystals in a 1 cm(2) Array. *J Am Chem Soc* **2011,** *133* (15), 5764-5766.

38. Cheng, D. F.; McCarthy, T. J., Using the Fact that Wetting Is Contact Line Dependent. *Langmuir* **2011,** *27* (7), 3693-3697.

39. Xia, Y. N.; Whitesides, G. M., Soft lithography. *Annu Rev Mater Sci* **1998,** *28*, 153-184.

40. Wang, L. M.; McCarthy, T. J., Shear Distortion and Failure of Capillary Bridges. Wetting Information Beyond Contact Angle Analysis. *Langmuir* **2013,** *29* (25), 7776-7781.

CHAPTER 2

SILICA CAN BE AN ACTIVE PARTICIPANT IN CROSS-LINKED SILICONE SYNTHESIS

2.1 Introduction

2.1.1 Background

Polydimethylsiloxane (PDMS), which contains only linear chains, is a liquid material with special properties. Cross-linked PDMS has a wide range of applications including coatings,[1] gas separation membranes,[2,3] and soft lithography[4,5] because of its exceptional properties. It has high temperature stability,[6] high gas permeability,[3] excellent electrical properties and biocompatibility.[6] Many methods have been investigated to cross-link PDMS, among which radical cross-linking, condensation curing, and hydrosilylation are the most common approaches to obtain cross-linked PDMS networks.[6,7]

Cross-linked PDMS has relatively poor mechanical strength (tofu-like), especially tensile strength, in its unfilled state due to the weak intermolecular forces. Reinforcement of PDMS by mineral fillers such as silica (SiO_2) particles can significantly improve the mechanical strength of the material.[8] Silica-filled PDMS can be fabricated using two major methods according to the literature. One is blending silica filler particles into PDMS prepolymer before cross-linking reactions. The other is filling PDMS with in-situ generated silica particles.[9, 10] Particle-particle interaction and particle-polymer interaction are believed to contribute to the enhancement of material properties.[11] Many researchers have claimed that tensile strength improvement of silica-filled siloxane polymer is attributed to hydrogen bonding between silica particles, along with the hydrogen bonding between silica and

PDMS.[12] Macosko and coworkers reported that linear PDMS chains can bridge fumed silica particles when they are mixed together, and that silica networks can be formed through physical forces.[13] Cohen-Addad performed theoretical studies on mixtures of silica and siloxane, and ascribed the gel like structure to adsorption of PDMS on silica by hydrogen bonds.[14]

Other researchers have believed that there is more than only physical absorption between silica and PDMS. As early as the 1950s, Warrick and coworkers demonstrated that the polysiloxane backbone may react with silanol groups on fillers, when a mixture of silica and silicone were heated at 150 ^{o}C for 1 hour.[15] Li and Schatz used an ammonia (NH_3)-modified swelling method to study silica-filled silicone. A combination of toluene and NH_3 were used to wash the material. The insoluble part under NH_3-modified swelling condition was considered as 'chemically bound silicone', because free PDMS chains and PDMS chains attached to silica through hydrogen bonding can be both removed by a mixture of toluene and NH_3. They claimed the PDMS used contain a small amount of potassium hydroxide (KOH), and further concluded the active silanolate groups lead to the formation of covalent bonds between silica and PDMS.[16,17] Our group recently reported fabrication of low hysteresis surfaces by modifying silicon wafers with linear silicone through a thermally activated reaction. It was proposed that the thin hydrated silica layer at the surface of the wafer played an important role in the reaction. Silica can absorb water as a desiccant and react with water via the silica - silicic acid equilibrium, and then silicone chains are equilibrated with the surface silanols in the presence of the silicic acid catalyst.[18] All of these reports suggest that covalent bonds can be formed between silica and PDMS.

2.1.2 Objectives

A recent paper from Zheng and McCarthy demonstrates self-healing and cross-linked silicone synthesis by anionic copolymerization of D_4 and bis-D_4, in which the ethylene bridges serve as cross-links.[19] In this work, the aforementioned chemical reaction between silica and PDMS,[18] along with the anionic copolymerization,[19] were used to prepare a new type of 'living silicone'. The aim was to demonstrate that silica particles can play the role of cross-linkers (SiO_4 linkage group reservoirs, Qs) in the cross-linked silicone synthesis. Swelling tests, calcination tests and fluorescence microscopy were utilized to elucidate the 'corrosion' of silica and 'migration' of SiO_4 linkage groups in the reaction. Furthermore, mechanical properties, chemical stress relaxation, living and self-healing properties of the silica cross-linked silicone were systematically investigated. Another aim of this work was to explore the potential applications of this living DQ silicone, such as its application in modulus gradient material fabrication.

2.2 Experimental Section

2.2.1 Sample Preparation

Stöber particles (1 μm in diameter) were synthesized following Stöber's method.[20] ÅngströmSpheres (commercial amorphous silica particles of 1 μm and 10 μm in diameter, density ~ 1.8 g/cm^3, surface area ~ 2-6 m^2/g) were purchased from Fiber Optic Center, Inc. Quartz powders (crystalline silica) and trimethylsiloxy terminated polydimethylsiloxane (M_w ~116 500) were obtained from Gelest, Inc. Fluorescence-dye (5/6-Fluorescein-isothiocyanate, FITC) modified silica nanoparticles were prepared with a literature method,[21] and these nanoparticles were provided by other research labs. Toluene, ammonium hydroxide, and KOH were all

purchased from Fisher Scientific Inc., and they were used as received. Benzoyl peroxide (BPO, 97%) was provided by Sigma-Aldrich, Inc. It was recrystallized before use.

The particles or powders except FITC - labeled particles were dispersed in acetone with sonication to get a uniform suspension, after which the suspension was mixed with D_4. Then all the acetone was removed by heating the mixture at 60 ^oC, and a relatively uniform dispersion was maintained. A small amount (0.4 wt%) of initiator (tetramethylammonium siloxanolate) was added to the dispersion of silica in D_4, and subsequently the mixture was poured into a Teflon mold and heated at 105 ^oC for prescribed lengths of time (Silica loading in the silicone was 1.665 wt%, 3.330 wt% and 4.995 wt%). A control experiment was carried out by letting the same amount of initiator react only with D_4. 0.04 g of each product was soaked in 20 mL toluene at room temperature and shaken vigorously in a Vortex mixer overnight for swelling tests.

2.2.2 Fluorescence Microscopy Characterization and Calcination Tests

1.665 wt% FITC - labeled silica particles and 0.4 wt% tetramethylammonium siloxanolate were blended into D_4 using a FlackTech, Inc. SpeedMixer DAC 150.1., which operated at 3500 rpm for 4 min. In addition, 1.665 wt% FITC - labeled silica particles were blended into D_4 with the SpeedMixer under the same conditions, as a control sample. Both samples were heated at 105 ^oC for 44 h. Fluorescence microscopy experiments using these samples were conducted on a Zeiss Axiovert 200 microscope with a 100 × objective.

In another experiment, amorphous silica particles and D_4 were 'copolymerized' in the presence of potassium KOH initiator. The product was calcined at 260 ^{o}C in a tube furnace (Thermolyne 79300) under nitrogen for 7 h.

2.2.3 Mechanical Properties Characterization

Advanced rheometer 2000 was utilized to evaluate the temperature dependence of the material viscoelastic properties. 40 mm Aluminum parallel plates were installed to obtain the modulus data at the frequency of 1 Hz. Thickness of the cross-linked silicone was controlled at around 800 μm.

The cross-linked silicone was punched into a dogbone sample with a length of 21.67 mm, width of 5 mm and thickness of 0.97 mm. Tensile testing was carried out with an Instron 5800 R fitted with a 50 N load cell. A sample was tested at a constant cross-head speed of 50 mm/min at room temperature.

The modulus of silicone elastomer was also determined by a contact adhesion test. The major component of the customized contact adhesion testing device is a nanopositioner (Burleigh Inchworm Nanopositioner) which simultaneous records the vertical displacement (d) and the normal force (P) of a polystyrene probe. The probe first compresses the sample, and then retracts. If K represents the initial slope for the normal force versus displacement curve during the probe retraction, a represents the probe radius, and ν is the poisson's ratio of the elastomer, Young's modulus can be determined as $E = \frac{K}{2a}(1-\nu^2)$.

2.3 Results and Discussion

2.3.1 Silica Particles Actually Participate in the Cross-linked Silicone Synthesis

Table 2-1 Swelling tests of products of tetramethylammonium - siloxanolate initiated (a) copolymerization of D_4 and commercial amorphous silica, (b) copolymerization of D_4 and lab-made Stöber silica particles, (c) copolymerization of D_4 and crystalline silica, (d) polymerization of D_4.

Sample number	**Weight percentage of tetramethylammonium siloxanolate in silicone (wt %)**	**Type of particles**	**Weight percentage of silica in silicone (wt %)**	**Reaction time(h)**	**Status of silicone after soaked in toluene overnight**
a	0.4	Commercial Stöber particles (1 μm in diameter)	1.665	7	Swell
b	0.4	Lab-Made Stöber particles (1 μm in diameter)	1.665	7	Swell
c	0.4	Quartz powders (Irregular shape)	1.665	7	Dissolve
d	0.4	NA	0	7	Dissolve

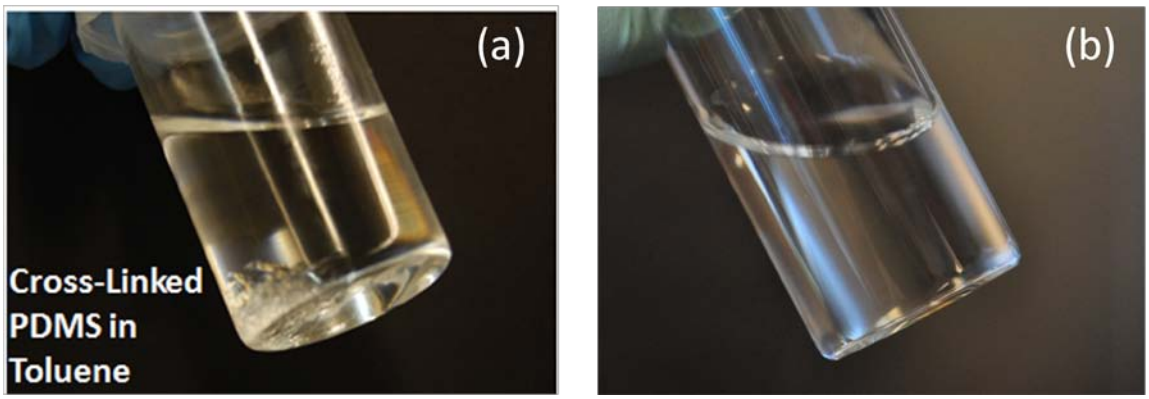

Figure 2-1 (a) Silicone samples swell in toluene. (b) Silicone samples dissolve in toluene.

Table 2-1 shows the recipe and reaction time of a series of anionic polymerizations. Composition of initiator and particles, reaction time and reaction temperature were held constant to study the effect of different particles on the reaction. ÅngströmSpheres (commercial amorphous silica) from Fiber Optic Center Inc. contain more than 99% amorphous silica, having a large amount of silanol groups. Stöber particles were prepared by tetraethoxysilane hydrolysis, and liquid phase synthesis of silica is a typical method to fabricate amorphous silica. Quartz powders are crystalline silica with a purity of around 97%. Thus, the particles copolymerized with D_4 represent amorphous and crystalline silica, respectively. Swelling experiments indicate that copolymerization of amorphous silica and D_4 yield a polymer network (physically or chemically cross-linked) that swells in toluene (Figure 2-1(a)), while reactions between crystalline silica and D_4 is insufficient to support a cross-linked PDMS network formation. When no silica is involved in the reaction, the product can completely dissolve in the excess amount of toluene (Figure 2-1(b)), implying the formation of only linear chains.

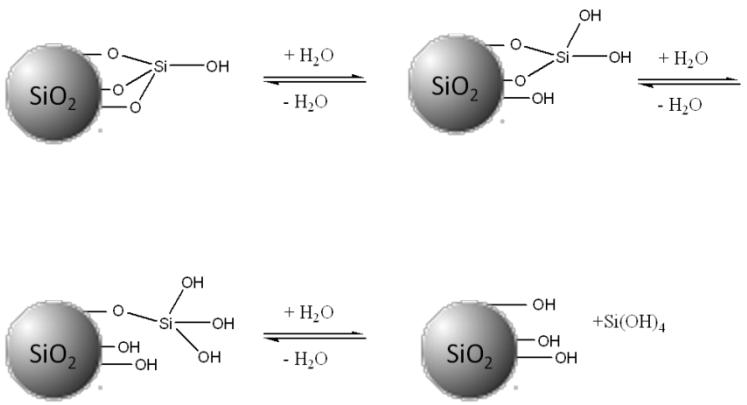

Figure 2-2 Equilibrium of silica particles and water

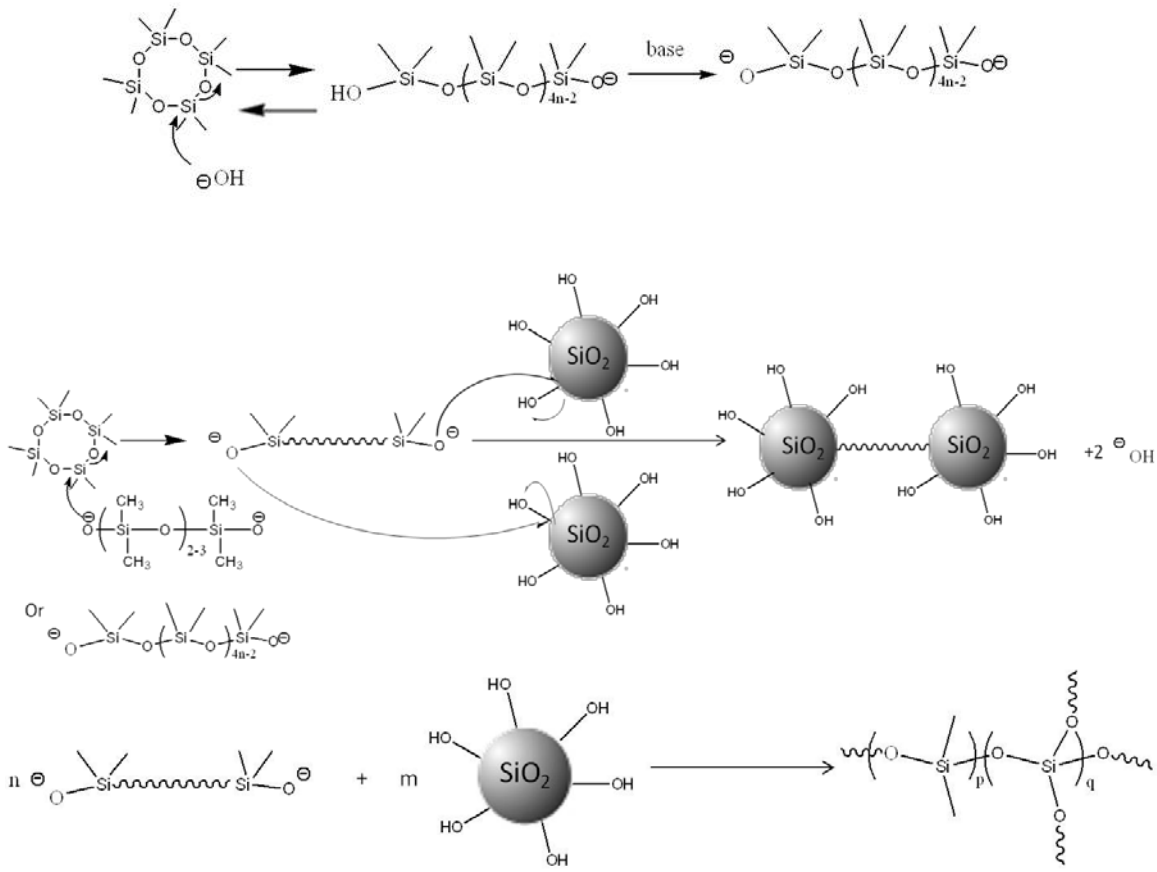

Figure 2-3 Schematic illustration for the preparation of cross-linked silicone with silica particles, D_4 and tetramethylammonium siloxanolate

D_4 undergoes anionic ring opening polymerization in the presence of base initiator, and the polymer is expected to consist of only linear chains. These linear chains are in equilibration with D_4 rings, which is known as siloxane equilibration (Figure 2-3).[22] Our swelling experiment results also supported this argument, as the polymer can completely dissolve in its good solvent. Water can be absorbed easily from the environment by silica, resulting in a hydrated surface layer in which silica and water are equilibrated in the mechanism of silicic acid equilibrium (Figure 2-2). If base initiator, D_4 and silica are mixed together, these two equilibration reaction are combined together. A more complex equilibration among siloxane, silanol and water exists. Amorphous silica can be copolymerized with D_4 to make cross-linked silicone due to this equilibration. Figure 2-3 shows the probable cross-linking mechanism.

Oligodimethysiloxandiolate catalyst molecules themselves bring living silanolate chain ends to the reaction system. The silanolate groups resulting from anionic polymerization of D_4 initiated by base can 'attack' SiO_2 particles, and then SiO_4 linkage groups can leave silica and become part of silicone. Silica actually provides cross-links in cross-linked silicone synthesis. In our experiment, the final equilibrium is not reached. Only silica at the particle surface is 'dissolved' and equilibrated to produce DQ silicone resin. When the final equilibrium is reached and all the Q get dissolved, DQ silicone prepared with 1.665 wt% silica is expected to have a cross-linking density of 267 mol/m^3.

Water has lower permeability in quartz than in amorphous silica which stems from the compact crystalline structure of quartz. Although quartz and amorphous silica have similar surface silanol density (4-5 SiOH/nm^2), [23, 24] the hydrated layer is thicker for amorphous silica, meaning there are larger number of reactive Qs and silanols in amorphous silica. After the surface silanols are consumed and involved as Qs in the network, other reactive dimethylsilanolate group can further react with silanols in the inner hydrated layer. The silica particle undergoes gradual 'corrosion' by the living network. Besides, larger quantities of impurities in quartz powder (97 % purity) than those in ÅngströmSpheres (99 % purity) or Stöber particles may impede the reaction between siloxane and silanols. These explain the ineffectiveness of quartz powder in yielding cross-linked silicone. It is consistent with the proposed reaction mechanism as shown in Figure 2-3.

A comparison between D_4 and silica copolymerization and D_4 polymerization illustrates the role of amorphous silica as 'cross-linker'. The Pomanteer-Lentz swelling method[16,17] was utilized to rule out the possibility that the cross-linked

silicone is a physical network sustained by hydrogen bonding. 0.04 g sample a as shown in Table 2-1 was swollen in a mixture of 12 mL toluene and 6 mL concentrated ammonium hydroxide, and shaken on a vortex mixer overnight. A large part of the sample is insoluble in the mixture, demonstrating that the cross-linked network is mainly chemically cross-linked. This swelling experiment result is consistent with the reaction mechanism described in Figure 2-3.

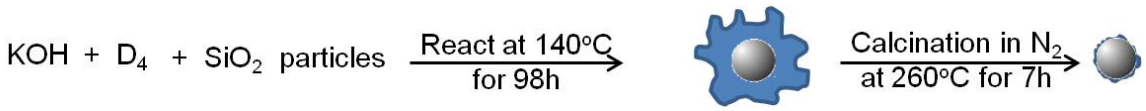

Figure 2-4 Schematic illustration of a silica particle equilibrated with D_4 and its surface morphology after calcination. The blue block indicates the living PDMS network.

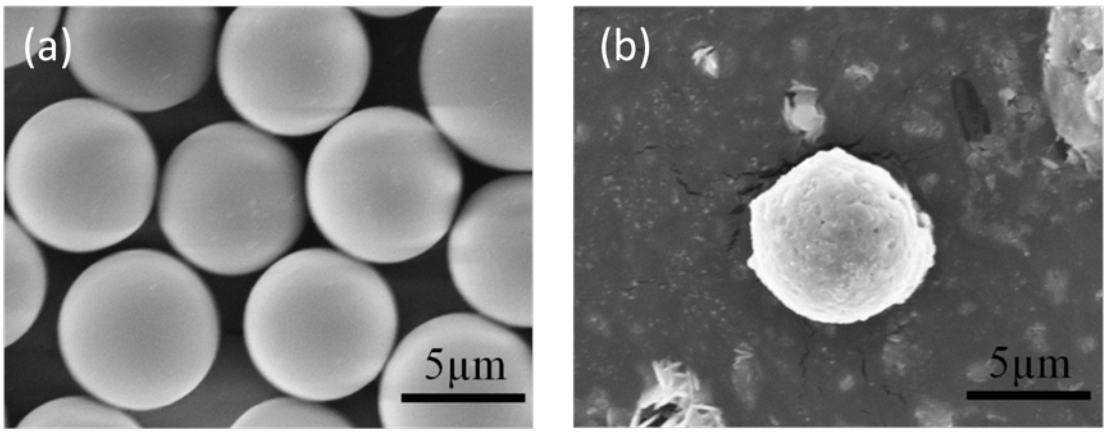

Figure 2-5 SEM images of (a) ÅngströmSpheres (10 µm in diameter). (b) ÅngströmSphere (10 µm in diameter) after equilibration with the cross-linked PDMS and calcination.

Another experiment was designed to support the conclusion that silanolate group on linear PDMS chain can react with silica particles. Kantor and coworkers reported KOH can convert D_4 to linear PDMS at 140 ^{o}C, behaving similarly to quaternary ammonium bases as catalyst. [25] Therefore, 1 wt% KOH and 1.665 wt% ÅngströmSpheres (10 µm in diameter) were added to D_4, which were heated together

at 140 ^{o}C for 98 h to ensure thorough equilibration between the silica and the PDMS network (Figure 2-4). The cross-linked PDMS network, which is expected to be hydroxyl group terminated, was then calcined at 260 ^{o}C in tube furnace (Thermolyne 79300) in an atmosphere of nitrogen for 7 h. The sample was placed in the center of the tube before the tube was evacuated and purged with nitrogen. As shown in Figure 2-5(a), the commercial ÅngströmSpheres are relatively monodisperse in size and have smooth surfaces. Note that the actual particle size is smaller than claimed by the manufacturer. In comparison, it is exhibited in Figure 2-5(b) that particles incorporated in the cross-linked network and then calcined have a rough surface morphology. It is reported that trimethylsilyl-terminated PDMS with 5 wt% KOH completely degrades at 225 ^{o}C in nitrogen,[26] and that the temperature of PDMS degradation depends mainly on the type of polymer side groups and the purity of the sample.[27] Pure trimethylsilyl-terminated PDMS has its thermal oxidation degradation beginning at 290 ^{o}C if heated in air at a very slow heating rate (1 ^{o}C/min).[28] These imply that depolymerization of linear PDMS segments occurs without any oxidation of PDMS under our calcination condition. Hence, the rough silica surface in Figure 2-5(b) can be explained: The living chain ends randomly instead of uniformly react with silica surface silanols, leading to the random 'corrosion' of silica particles. Part of the particle may not be covered by the living network at all, while other parts may be deeply corroded.

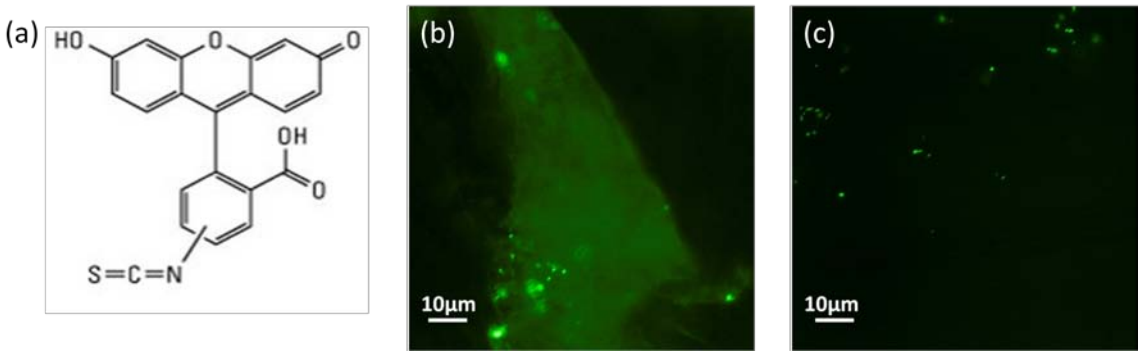

Figure 2-6 (a) Chemical structure of fluorescent dye FITC; (b) Cross-linked silicone formed by copolymerization of D_4 and FITC-labeled silica nanoparticles; (c) Silicone composites prepared by mixing FITC-labeled silica nanoparticles and trimethylsiloxy-terminated polydimethylsiloxane (M_w ~116 500).

The concept that silica particles can serve as SiO_4 linkage group reservoirs was also demonstrated by copolymerization of D_4 and FITC-labeled silica particles. It is observed in the triangle-shaped silicone product (Figure 2-6(b)) that fluorescence dye distributes uniformly in the sample. However, in the control sample where base catalyst is not involved, only the particles show fluorescence (Figure 2-6(c)). In the silicone composite formed by copolymerization of D_4 and FITC-labeled silica particles (Figure 2-6(b)), the FITC groups get dragged ‘everywhere’ in the sample probably due to siloxane equilibration. The corrosion and dissolution of FITC labeled silica particles in the base-catalyzed copolymerization are directly revealed under the fluorescence microscope.

2.3.2 Special Mechanical Properties of DQ Silicone

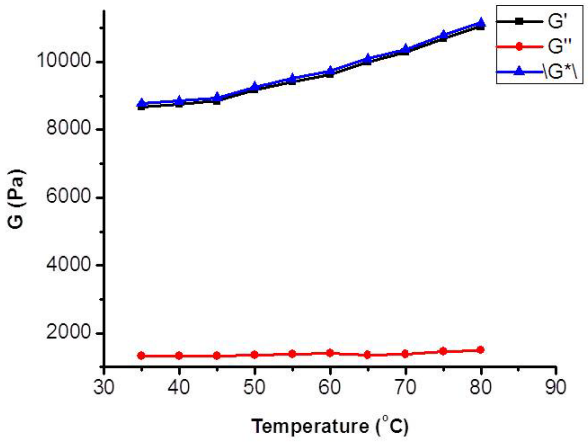

Figure 2-7 Temperature dependence of viscoelastic properties for DQ silicone containing 4.995 wt%

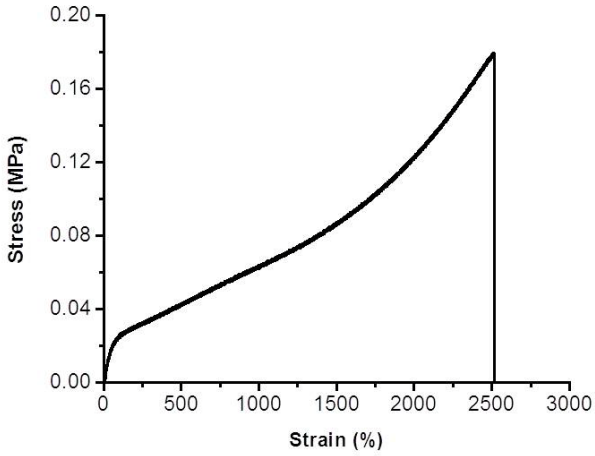

ÅngströmSpheres (1 μm in diameter).

Figure 2-8 Stress versus strain plot for DQ silicone containing 4.995 wt% ÅngströmSpheres (1 μm in diameter) under tensile test

The DQ silicone formed by copolymerization of D_4 and amorphous silica also has special mechanical properties. DQ silicone prepared with 4.995 wt% commercial amorphous silica was characterized with both rheometry tests and tensile tests.

Rheometry measurements (Figure 2-7) display that the DQ silicone is very soft, with a storage modulus of $G' = 8678Pa$ and a loss modulus of $G'' = 1325Pa$ at 35 ^{o}C. Temperature sweep test data also revealed that the storage modulus of the material increases with the increase of temperature, which agrees with the affine network model prediction and shows that the DQ silicone is a cross-linked network.[29] Standard tensile strain measurement (Figure 2-8) gives an elongation at break value of 2549%, indicating that the material is very 'stretchy'. Commercial silicones like Sylgard 184 also contains a large amount of silica (about 50 wt % additives and silica fillers), but Sylgard 184 (10:1 mixing ratio) is reported to have an elongation at break of only 140%.[30] This implies the superior stretchability of our living silicone should not only be ascribed to a filler reinforcement effect, but also to chemical stress relaxation. The fast stretching process of the sample at the speed of 50 mm/min generates large quantities of heat which accumulate locally and raise the temperature of the sample. There is a remarkable chemical stress relaxation effect above a certain temperature,[31] which can delay the breakage of PDMS.

2.3.3 Applications of DQ Silicone

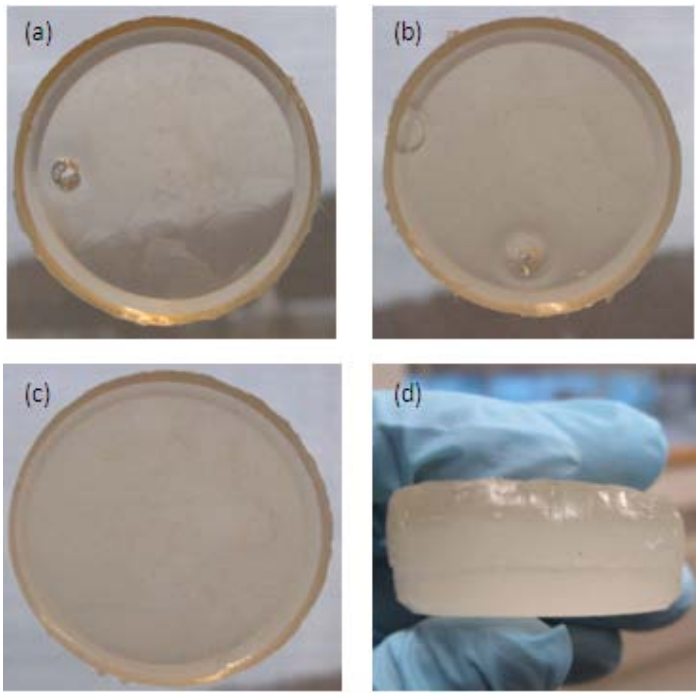

Figure 2-9 DQ silicone with commercial Stöber particles (1 μm in diameter) containing (a) 1.665 wt%, (b) 3.330 wt%, (c) 4.995 wt %, (d) A single piece of silicone formed from materials (a)-(c).

Table 2-2 Contact adhesion test characterization of the gradient modulus silicone containing various amounts of commercial Stöber particles (1 μm in diameter)

SiO_2 content in the layer (wt %)	**Modulus (MPa)**
1.665	0.449311
3.330	0.507781
4.995	0.567168

The cross-linked silicone formed by copolymerization of D_4 and amorphous silica has many interesting properties. The reactive tetramethylammonium dimethylsilanolate end groups in the network can react with the network and catalyze the equilibration between cyclics and the network, endowing the silicone with 'self-healing' properties.[19] Three disk-shaped PDMS samples (Figure 2-9) containing 1.665 wt%, 3.330 wt% and 4.995 wt% ÅngströmSpheres (1 μm in diameter) were prepared in Teflon containers to have diameters of 40 mm and thicknesses of around 5 mm.

The three samples were placed overlapping with each other and wrapped with Teflon tape before being heated in an oven at 105 ^{o}C overnight. After heating, no clear interface was observed between any two layers (Figure 2-9(d)), and the layers cannot be pulled apart by hand. This demonstrates that the DQ silicone is 'living'. Modulus of the three layers was then characterized with a contact adhesion test, and the measurement results are shown in Table 2-2, which suggests that a modulus gradient silicone elastomer is successfully prepared.

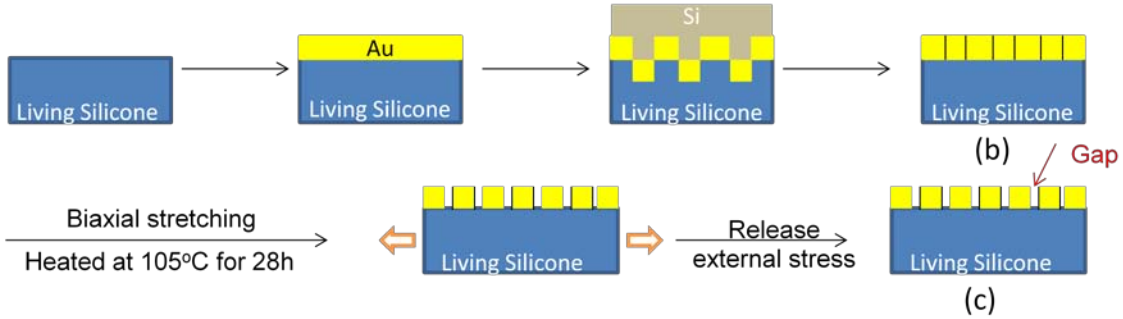

Figure 2-10 Schematic illustration of patterning gold islands on DQ silicone

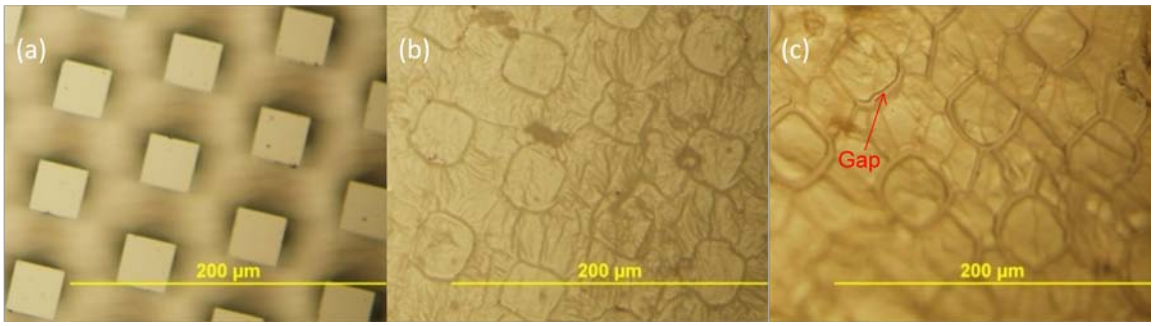

Figure 2-11 (a) Post-containing surface; (b) Gold surface just after imprinting with the post-containing surface; (c) Gold surface after biaxial stretching and chemical stress relaxation.

Chemical stress relaxation due to siloxane equilibration was demonstrated in the tensile test of DQ silicone. We investigated other applications of the chemical stress relaxation. For instance, when polymers were coated with a thin film of gold and subjected to external stretch, the gold film fractures and forms gold islands. These

gold islands cannot be preserved when the external stretch is released. However, these fractured gold structures might stay when the stress built up in the stretched polymer is relaxed.

As depicted in Figure 2-10, in order to preserve the fracture pattern, DQ silicone containing 1.665 wt% silica was sputter coated with a thin layer of gold. The sample was imprinted with a post-containing surface (Figure 2-11(a)), so that square-shaped crack traces were left on the gold layer (Figure 2-11(b)). Subsequently, the sample was biaxially stretched along the directions parallel to the sides of the squares and heated at 105 ^{o}C at the same time. It is observed that the gaps stay open after external stress is released. A square-shaped fracture pattern is displayed on a free-standing DQ silicone sample (Figure 2-11(c)). The process described in Figure 2-10 is a convenient way to make an array of structures.

2.4 Conclusions

Silica is widely used as a filler in cross-linked silicones to improve material properties, particularly mechanical strength. This reinforcement effect is generally attributed to the high modulus of silica particles and hydrogen bonding between silica and PDMS chains. We report that Stöber silica particles actively participate in the chemical cross-linking of linear PDMS prepared by anionic ring-opening polymerization of D_4. The silica particles serve as Q reservoirs for the growing siloxane network and cross-links are equilibrated into the matrix during polymerization. Scanning electron microscopy and a series of swelling tests demonstrate the erosion of silica particles and the presence of covalent bonds between silica and PDMS. The living (self healing and chemical stress relaxing) nature of

these materials is reported as well as their use in preparing controlled modulus and gradient modulus materials.

2.5 References

1. Juchniewicz, M.; Stadnik, D.; Biesiada, K.; Olszyna, A.; Chudy, M.; Brzozka, Z.; Dybko, A., Porous crosslinked PDMS-microchannels coatings. *Sensor Actuat B-Chem* **2007,** *126* (1), 68-72.

2. Aoki, T., Macromolecular design of permselective membranes. *Prog Polym Sci* **1999,** *24* (7), 951-993.

3. Rao, H. X.; Liu, F. N.; Zhang, Z. Y., Preparation and oxygen/nitrogen permeability of PDMS crosslinked membrane and PDMS/tetraethoxysilicone hybrid membrane. *J Membrane Sci* **2007,** *303* (1-2), 132-139.

4. Choi, K. M.; Rogers, J. A., A photocurable poly(dimethylsiloxane) chemistry designed for soft lithographic molding and printing in the nanometer regime. *J Am Chem Soc* **2003,** *125* (14), 4060-4061.

5. Rogers, J. A.; Nuzzo, R. G., Recent progress in soft lithography. *Mater Today* **2005,** *8* (2), 50-56.

6. Cai, G. P.; Weber, W. P., Synthesis of terminal Si-H irregular tetra-branched star polysiloxanes. Pt-catalyzed hydrosilylation with unsaturated epoxides. Polysiloxane films by photo-acid catalyzed crosslinking. *Polymer* **2004,** *45* (9), 2941-2948.

7. Li, H. Y.; Yu, D. S.; Zhang, J. Y., A novel and facile method for direct synthesis of cross-linked polysiloxanes by anionic ring-opening copolymerization with Ph-12-POSS/D-4/Ph8D4. *Polymer* **2005,** *46* (14), 5317-5323.

8. McCarthy, D. W.; Mark, J. E.; Clarson, S. J.; Schaefer, D. W., Synthesis, structure, and properties of hybrid organic-inorganic composites based on polysiloxanes. II. Comparisons between poly(methylphenylsiloxane) and poly(dimethylsiloxane), and between titania and silica. *J Polym Sci Pol Phys* **1998,** *36* (7), 1191-1200.

9. Dewimille, L.; Bresson, B.; Bokobza, L., Synthesis, structure and morphology of poly (dimethylsiloxane) networks filled with in situ generated silica particles. *Polymer* **2005,** *46* (12), 4135-4143.

10. Rajendra, V.; Gonzaga, F.; Brook, M. A., Nearly Monodisperse Silica Microparticles Form in Silicone (Pre)elastomer Mixtures. *Langmuir* **2012,** *28* (2), 1470-1477.

11. Camenzind, A.; Schweizer, T.; Sztucki, M.; Pratsinis, S. E., Structure & strength of silica-PDMS nanocomposites. *Polymer* **2010,** *51* (8), 1796-1804.

12. Shim, S. E.; Isayev, A. I., Rheology and structure of precipitated silica and poly(dimethyl siloxane) system. *Rheol Acta* **2004,** *43* (2), 127-136.

13. Aranguren, M. I.; Mora, E.; Degroot, J. V.; Macosko, C. W., Effect of Reinforcing Fillers on the Rheology of Polymer Melts. *J Rheol* **1992,** *36* (6), 1165-1182.

14. Cohenaddad, J. P., Sol or Gel-Like Behavior of Ideal Silica Siloxane Mixtures - Percolation Approach. *Polymer* **1992,** *33* (13), 2762-2767.

15. Warrick, E. L.; Lauterbur, P. C., Filler Phenomena in Silicone Rubber. *Ind Eng Chem* **1955,** *47* (3), 486-491.

16. Vondracek, P.; Schatz, M., Nh3-Modified Swelling of Silica-Filled Silicone-Rubber. *J Appl Polym Sci* **1979,** *23* (9), 2681-2694.

17. Li, Y. F.; Xia, Y. X.; Xu, D. P.; Li, G. L., Surface-Reaction of Particulate Silica with Polydimethylsiloxanes. *J Polym Sci Pol Chem* **1981,** *19* (12), 3069-3079.

18. Krumpfer, J. W.; McCarthy, T. J., Rediscovering Silicones: "Unreactive" Silicones React with Inorganic Surfaces. *Langmuir* **2011,** *27* (18), 11514-11519.

19. Zheng, P. W.; McCarthy, T. J., A Surprise from 1954: Siloxane Equilibration Is a Simple, Robust, and Obvious Polymer Self-Healing Mechanism. *J Am Chem Soc* **2012,** *134* (4), 2024-2027.

20. Stober, W.; Fink, A.; Bohn, E., Controlled Growth of Monodisperse Silica Spheres in Micron Size Range. *J Colloid Interf Sci* **1968,** *26* (1), 62-&.

21. Estevez, M. C.; O'Donoghue, M. B.; Chen, X. L.; Tan, W. H., Highly Fluorescent Dye-Doped Silica Nanoparticles Increase Flow Cytometry Sensitivity for Cancer Cell Monitoring. *Nano Res* **2009,** *2* (6), 448-461.

22. Kantor, S. W.; Grubb, W. T.; Osthoff, R. C., The Mechanism of the Acid-Catalyzed and Base-Catalyzed Equilibration of Siloxanes. *J Am Chem Soc* **1954,** *76* (20), 5190-5197.

23. Rimola, A.; Sodupe, M.; Tosoni, S.; Civalleri, B.; Ugliengo, P., Interaction of glycine with isolated hydroxyl groups at the silica surface: First principles B3LYP periodic simulation. *Langmuir* **2006,** *22* (15), 6593-6604.

24. Kohr, J.; Engelhardt, H., Characterization of Quartz Capillaries for Capillary Electrophoresis. *J Chromatogr A* **1993,** *652* (2), 309-316.

25. Gilbert, A. R.; Kantor, S. W., Transient Catalysts for the Polymerization of Organosiloxanes. *J Polym Sci* **1959,** *40* (136), 35-58.

26. Grassie, N.; Macfarlane, I. G., Thermal-Degradation of Polysiloxanes .1. Poly(Dimethylsiloxane). *Eur Polym J* **1978,** *14* (11), 875-884.

27. Gelest Catalog.

28. Camino, G.; Lomakin, S. M.; Lazzari, M., Polydimethylsiloxane thermal degradation - Part 1. Kinetic aspects. *Polymer* **2001,** *42* (6), 2395-2402.

29. Colby, R., Polymer Physics.

30. MSDS sheet of Dow Corning Sylgard 184.

31. Osthoff, R. C.; Bueche, A. M.; Grubb, W. T., Chemical Stress Relaxation of Polydimethylsiloxane Elastomers. *J Am Chem Soc* **1954,** *76* (18), 4659-4663.

CHAPTER 3
SILICONE SURFACE MODIFICATION BY SILOXANE EQUILIBRATION

3.1 Introduction

3.1.1 Background

PDMS has demonstrated great performance in biomaterial applications such as the artificial heart, artificial skin and ophthalmologic devices.[1] It is compatible with blood, and can endure the hydrolytic and enzymatic degradation medium of the human body.[2] The organic substituent (methyl group) conveys hydrophobicity to the material.[3] Adsorption of protein from the tears and blood, as well as cell adhesion to the hydrophobic PDMS-based materials poses a problem for the proper function of the silicone material. Additionally, hydrophobic PDMS implants can be 'sensed' by the human body, leading to inflammation.[4] Poly(ethylene oxide) (PEO) is widely used for the modification of hydrophobic polymer to impart hydrophilicity and solve biofouling and biocontact issues, because the PEO chain is flexible, hydrophilic, nontoxic and nonimmunogenic.[5] PDMS-based materials with hydrophilic surfaces have applications in microfluidic devices and microcontact printing.[6] Microcontact printing uses PDMS stamps as the 'solvent' to dissolve the 'ink', and self-assembled monolayers of the 'ink' are formed on the substrate after contact of the stamp and the substrate.[7] The hydrophilization of PDMS extends the variety of 'ink' molecules, allowing the printing of polar molecules. Delamarche and coworkers attached amine-functionalized silanes to PDMS stamps, which subsequently react with PEO moieties. The PDMS stamp is PEGylated after a four step grafting procedure.[8]

A number of efforts have been made to improve the hydrophilicity of PDMS. An enormous literature is concerned with physical techniques, including oxygen

plasma, UV/Ozone, corona discharge, etc. For oxygen plasma treatment, the PDMS surface is exposed to a mixture of radicals, ions, photons, electrons and other species.[6] X-ray photoelectron spectroscopy (XPS) data show a decrease in carbon content and an increase in oxygen content for oxygen plasma treated PDMS, indicating that a silica-like inorganic layer (SiO_x, $1<x<2$) is gradually generated in this oxidative process. Yunus and coworkers adopted transmission electron microscopy (TEM) to observe the silica layer on the oxygen plasma - treated silicone samples.[9] Water contact angle values close to zero can be achieved immediately after treatment. However, this type of PDMS surface modification is not permanent, and 'hydrophobic recovery' is observed with time. This inherent disadvantage is the consequence of multiple reasons: (1) migration of the polar groups from the surface into the bulk, (2) migration of low molecular weight siloxane from the bulk to the surface, (3) condensation of surface silanol groups, (4) changes in the surface roughness, (5) adsorption of contaminants from the air to the high energy clean surface.[10]

UV-ozone treatment is less intense and likely less damaging than oxygen plasma, while it can reach to greater depths in PDMS.[11] The UV-ozone instrument is relatively inexpensive. In the instrument, ozone is formed from oxygen irradiated by UV light, followed by dissociation into oxygen atoms and oxygen molecules. Radicals are generated in PDMS after the UV exposure, and they can further react with oxygen atoms, oxygen molecules, and ozone. The organic portion is converted into volatile CO_2 and H_2O, leaving the SiO_x behind. Hence, the chemical changes of the PDMS surface are similar to those that occur with oxygen plasma treatment. It is reported that oxygen and water permeation rates of PDMS membranes can be reduced by the SiO_x thin film.[12]

Corona discharge is frequently used to treat inert polymer surfaces to improve their printability and adhesion.[13] Strong electromagnetic fields are applied in proximity to a charged thin wire so that the air is ionized in this region. The molecules in the excited state bombard the PDMS surface, and a hydrophilic surface is created. Again, unstable hydrophilicity is the disadvantage of this modification method.

Other common methods performed to modify the silicone surface involve hydrolysis, functionalization, etching, and chemical grafting, among which chemical grafting is the most frequently applied method.[14] The chemical grafting can be conducted either by the reaction between the silicone and reagents including monomers in solution, or by the covalent grafting of polymer chains to the silicone. Considerable efforts have been devoted to altering bulk properties as well as surface properties of silicone materials.

Sheardown and coworkers have synthesized methyl-triethoxysilylpropyl-poly(ethylene oxide), and copolymerized it with hydroxyl-terminated poly(dimethylsiloxane) and tetraethoxysilane. PEO segments tend to reside at the silicone/air interface. The modified surface was shown to be both hydrophilic and protein rejecting.[4] They also reported water contact angle changes of PEO-modified PDMS with time, which were attributed to PEO chain reorientation at the solid-air interface. In another study, Sheardown and coworkers grafted Si-H groups to cross-linked Sylgard 184 by equilibrating the Sylgard 184 with $(MeHSiO)_n$. Methyl-allyl-poly(ethylene oxide) was further grafted to the Si-H rich surface through hydrosilylation. (Figure 3-1)

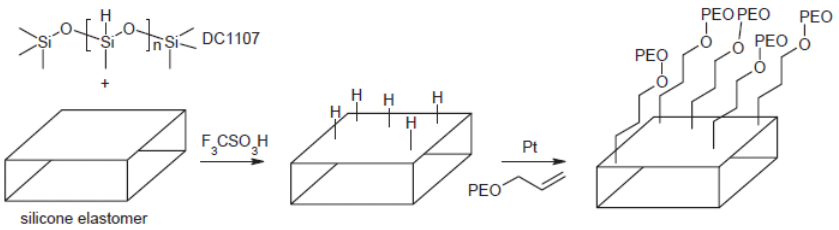

Figure 3-1 Schematic of surface modification[4]

Preparation of interpenetrating polymer networks (IPNs) is another approach to fabricate hydrophilic PDMS.[15] Abbasi and coworkers swelled cross-linked PDMS with 2-hydroxyethyl methacrylate (HEMA), azobisisobutyronitrile (AIBN), ethylene glycol dimethylacrylate (EGDMA) and toluene. The IPN was obtained by heating the mixture (Figure 3-2). The composite was demonstrated to be hydrophilic, and reported to have potential applications in soft contact lenses.

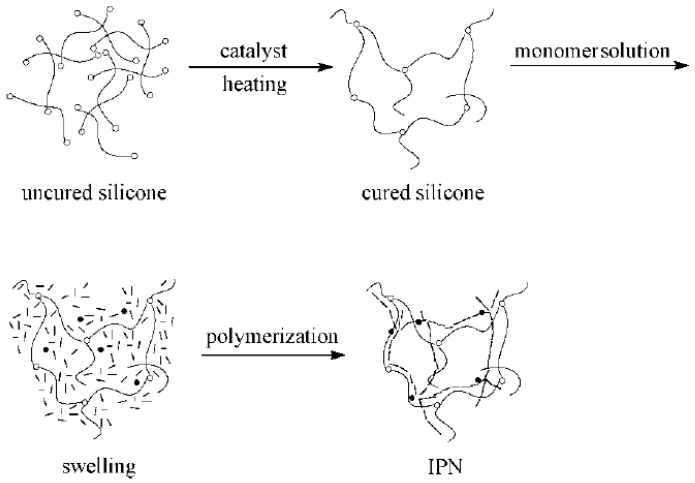

Figure 3-2 Schematic of the synthesis of PDMS/PHEMA IPN[15]

Similar strategies can be utilized to further hydrophobize the PDMS. Chaudhury and coworkers reacted perfluoroether allylamide with methyl hydrogen siloxanes and vinyl-terminated PDMS oligomers using hydrosilylation. The surface properties, especially the adhesive release properties, showed remarkable changes.[16]

3.1.2 Objectives

The objective of this work was to show the possibility of conducting silicone elastomer surface modification via base-catalyzed siloxane equilibration. An ethylene oxide-dimethylsiloxane block copolymer (PEO-PDMS) was employed to functionalize living silicone surfaces. The modified surface was analyzed with contact angle measurements, Attenuated Total Reflection Infrared (ATR-IR) spectroscopy, XPS and Atom Force Microscopy (AFM) to verify the chemical grafting of PEO segments. Thermal Gravimetric Analysis (TGA) measurements were carried out to quantify the PEO grafting content. Furthermore, the hydrolytic stability of the hydrophilic silicone prepared by siloxane equilibration was evaluated and compared with that of silicone hydrophilized using another approach. The goal was to assess advantages and disadvantages of PEO modified silicone by siloxane equilibration, for its use in applications such as microfluidic devices. Finally, silicone cross-linked by hydrosilylation was transformed into living silicone by a base catalyst. This activated surface was further modified with PEO-PDMS through siloxane equilibration.

3.2 Experimental Section

3.2.1 Preparation of Cross-linked Silicone

Cross-linked PDMS was prepared by two major approaches: (1) anionic copolymerization of octamethylcyclotetrasiloxane (D_4) and the dimer of D_4 (bis-D_4) (Figure 3-3);[17] (2) hydrosilylation of vinyl-terminated PDMS and polymethylhydrosiloxane in the presence of Karstedt's catalyst. (Figure 3-4).[18] In the first approach, benzoylperoxide (BPO - purchased from Aldrich) was recrystallized from methanol. D_4 and tetramethylammonium siloxanolate were purchased from Gelest, Inc. and used without further purification. 2.5 wt% BPO was slowly dissolved

in D_4 at 120 ^oC under nitrogen. The solution was stirred at this temperature for 2 h before being passed through an alumina column to render a product solution. The product solution (mixture of D_4 and bis-D_4) and 0.2 wt% tetramethylammonium siloxanolate were heated at 105 ^oC for 17 h in a sealed Teflon container to yield cross-linked living silicone (Figure 3-3).

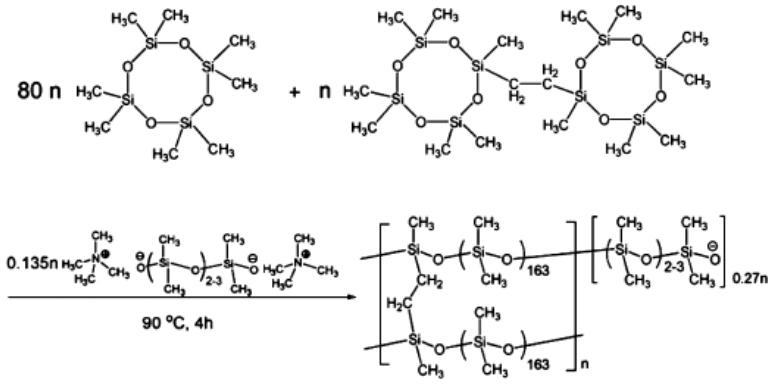

Figure 3-3 Anionic copolymerization of D_4 and bis-D_4

In the second approach, polymethylhydridosiloxane ('PDMS-H', M_w~1800-2100 g/mol), vinyl-terminated PDMS ('PDMS-Vinyl', M_w~28 000 g/mol), and platinum-divinyldisiloxane complex (Karstedt's catalyst) were all purchased from Gelest, Inc. and used as received. Cross-linked silicone was prepared by mixing PDMS-H and PDMS-vinyl in a molar ratio of H: vinyl=15:1. Hydrosilylation was catalyzed by 2 ppm of Pt catalyst (based on silicone product mass), and the reagents were heated at 105^o C overnight (Figure 3-4).

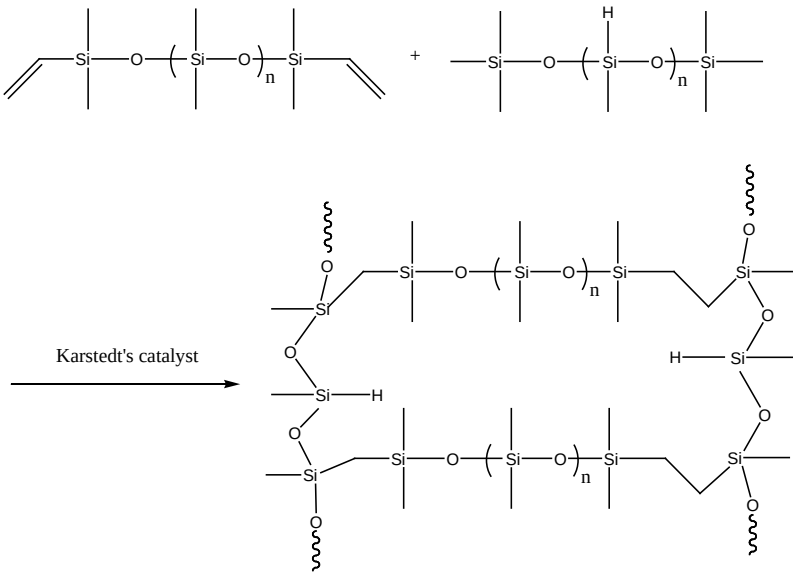

Figure 3-4 Preparation of cross-linked PDMS with hydrosilylation

3.2.2 Cross-linked Silicone Modification with PEO-PDMS

PEO-PDMS (75% non-siloxane, M_w~600 g/mol) was purchased from Gelest, Inc. and used as received. One side of a 2 mm thick living silicone sample was wetted with PEO-PDMS, and the sample was heated at 105 ^oC for 20 h in an oven. The sample was thoroughly cleaned with water, either by Soxhlet extraction for 15.5 h, or by fully rinsing.

Silicone cross-linked via hydrosilylation was wetted with a catalytic amount of tetramethylammonium siloxanolate and heated at 105 ^oC for 1 day to enrich the surface with silanolate groups. Then a small amount of PEO-PDMS was equilibrated with the activated surface at 105 ^oC for 20 h. Again, the sample was fully rinsed with water. The activated surface, in another experiment, was remolded against a penny at 105 ^oC for 4 h.

3.2.3 Sylgard 184 Silicone Surface Modification with Brook's method

Sylgard 184 silicone elastomer was fabricated by mixing prepolymer with cross-linker in the weight ratio of 10:1. The mixture was cast into a 2 mm thick sample in a polystyrene Petri dish. Disk-shaped samples with a diameter of around 1 cm were washed in hexane and acetone, fully dried in nitrogen, and further stirred in a solution containing 0.04 mL triflic acid, 6 mL PDMS-H and 10 mL methanol for 30 min at room temperature. Then the Si-H - functionalized silicone samples were washed with 50 mL methanol and 50 mL hexane, after which they were dried under vacuum for one day.

Polyethylene glycol 2000 (M_n~5000 g/mol) was provided by Fluka and used for thermal property studies. Allyloxy poly(ethylene oxide) (8-12 ethylene oxide repeat unit) was obtained from Gelest, Inc. PDMS-H - modified Sylgard 184 elastomer was immersed in a 80 wt% allyloxy poly(ethylene oxide) in isopropanol solution. One small drop of platinum-divinyltetramethyldisiloxane complex (purchased from Gelest, Inc.) was added to the solution to catalyze the PEO grafting reaction. The reaction was conducted for 15 h at room temperature, and then the PEO-modified silicone was fully washed with acetone and water and dried in a vacuum oven at room temperature.

3.2.4 Contact Angle Measurements

Dynamic contact angles were measured using a Rame-Hart telescopic goniometer and a Gilmont syringe with a 24-gauge, flat-tipped needle. Millipore water (>18.4 $M\Omega cm$) was used as probe liquid. Advancing (θ_A) and receding (θ_R) contact angle measurements were carried out when water was injected into or

withdraw from the sessile water drop. All reported contact angle data are the average value of five measurements on different locations of the sample.

3.2.5 ATR-IR Spectroscopy and XPS

A Perkin Elmer 100 FT-IR spectrometer was used to study the surface composition. A 45^{o} ZnSe internal reflection crystal was used to obtain ATR-IR spectra of original PDMS and modified PDMS. The silicone sample was placed in the sample holder to record the IR spectra. XPS spectra were collected with a 75° takeoff angle on a Physical Electronics Quantum 2000 with Al Kα excitation (15 kV, 25 W). The raw data were analyzed using Multipak software.

3.2.6 TGA Analysis

The thermal stability of modified and unmodified silicone networks was assessed with a TA Instrument TGA Q50. A 5-10 mg sample was loaded in a platinum pan, and heated from room temperature to 900 ^{o}C at an air flow rate of 60 mL/min. The sample mass and temperature were recorded at the same time.

3.2.7 Optical Profilometry and AFM

A Zygo NewView 7300 Profilometer was used to reveal the surface topography of PEO-modified living silicone after rinsing/extracting with water. The top surface map was displayed in MetroPro software. AFM measurements were performed with a Nanosurf easyScan2 AFM System equipped with an AppNano ACLA-10 silicon tip (N-type). Images were collected under both dynamic force (tapping) mode and phase contrast mode, so that height images and phase images were obtained simultaneously.

3.2.8 Hydrolytic Stability Studies

Around 0.5 g of the modified and unmodified silicone elastomers were washed with 75 mL deinonized (DI) water by magnetic stirring the water at 500 rpm. The samples were taken out of the water and fully dried in a nitrogen stream overnight after every 2 h of wash. Subsequently, the dried mass of samples was determined with a Denver Instrument Company A-250 balance. Mass versus wash time plots were constructed to demonstrate the sample hydrolytic stability.

3.3 Results and Discussion

3.3.1 Modification of Living Silicone via Siloxane Equilibration

A mixture of D_4 and bis-D_4 was prepared, and copolymerized in the presence of 0.2 wt% tetramethylammonium siloxanolate following the procedure described in Chapter 3.2.1. The product is a D_4 – bis-D_4 living silicone sample. The bottom of living silicone sample was wetted with a small amount of PEO-PDMS and equilibrated at 105 ^oC for 20 h to achieve modified silicone sample. The optical transparency of D_4 – bis-D_4 living silicone was altered after modification with PEO-PDMS. Figure 3-5 shows pictures of top views of ~2 mm thick living silicone samples before and after modification. The modified silicone sample becomes more opaque from the top to the bottom, although only its bottom surface touched the PEO-PDMS liquid. This result suggests PEO segments aggregate and microphase separate in the bulk silicone. It also implies that PEO-PDMS can diffuse and equilibrate through the entire 2 mm thick sample, and that siloxane equilibration is possibly the driving force for the PEO-PDMS migration. The PEO segments were covalently grafted to both the silicone surface and the bulk.

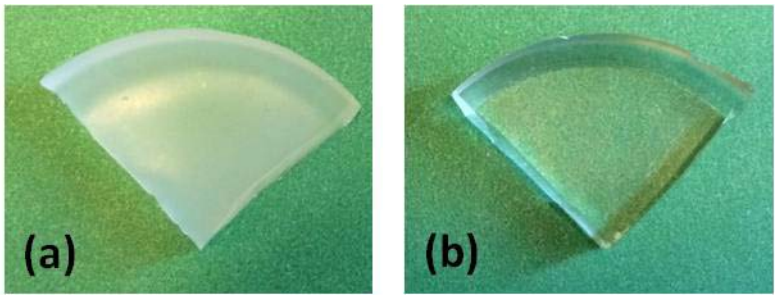

Figure 3-5 (a) Living silicone modified with PEO-PDMS at 105 ^{o}C; (b) Unmodified living silicone. Both samples were washed thoroughly with water for 15.5 h by Soxhlet extraction.

Table 3-1 Average advancing and receding water contact angles of PEO-PDMS - modified living silicone and unmodified living silicone. Both samples were washed thoroughly with water for 15.5 h by Soxhlet extraction.

Material	**Contact Angle θ_A/θ_R**	**Contact Angle after Two Months θ_A/θ_R**
(a) PEO-PDMS modified living silicone	0º/0º	0º/0º
(b) Unmodified living silicone	116º/72º	118º/70º

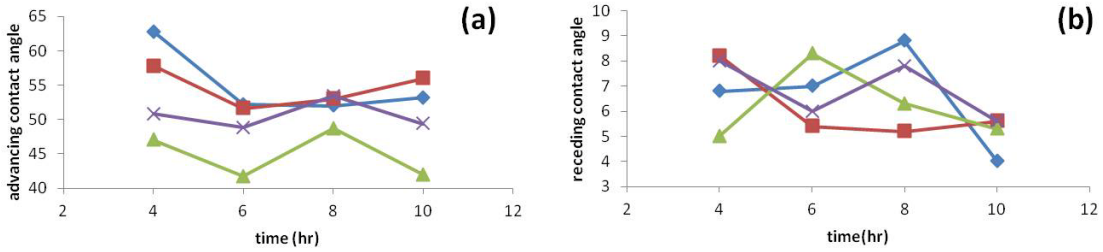

Figure 3-6 (a) Advancing contact angle and (b) Receding contact angle changes of PEO-PDMS - modified living silicones after washing with DI water. The samples were washed in DI water and taken out for analysis every 2 h, followed by overnight drying in air before mass measurement.

Contact angle measurement is one of the most sensitive surface probing methods. It is capable of acquiring surface information at the topmost surface, serving as a simple, low-cost and straightforward technique to monitor surface wettability changes. The water contact angle of Sylgard 184 silicone elastomer is reported to be 0^{o} (<3^{o}) immediately after oxygen plasma treatment,[19] yet recovery to its original

hydrophobic state may take place after 60 min of its exposure to air.[10] PEO is commonly adhered to silicone surface to improve protein resistance of silicone. Various water contact angles were observed after PEGylation of silicone. Grunlan and coworkers reported θ_A/θ_R = 61°/61° water contact angles for a glass slide grafted with functionalized PEO ($(EtO)_3Si-(CH_2)_3-(OCH_2CH_2)_8-OCH_3$). 81°-102° advancing contact angles, along with 70°-85° receding contact angles were reported when the aforementioned PEO was incorporated into silicone.[20] Similarly, Brook and coworkers discovered that PEO monomethyl ether grafted to Si-H-enriched silicone surfaces produced water contact angles ranging from 65° to 110° for advancing and less than 56° for receding.[21] The unreacted PEO reagents were either removed by Soxhlet extraction with CH_2Cl_2,[20] or flushed away by rinsing solvents (i.e. methanol and hexane).[21]

In the silicone modification with siloxane equilibration, prominent surface hydrophilicity enhancement was noticed in the modified samples that were Soxhlet extracted. Water serves as the washing solvent because our selected PEO-PDMS reagent is 'miscible with water in all concentrations'.[22] Dynamic contact angles are reduced to 0°/0° from 116°/72°, which means a drop of water spreads spontaneously on the modified silicone surface. Contact angle hysteresis experiences remarkable changes as well. It decreases from 44° to 0°. This uncommon and excellent surface wettability is an advantage of our modification method. It is further seen in Table 3-1 that the good water wettability of PEO-modified silicone does not deteriorate with time (at least for two months), and the 0°/0° contact angle is expected to be a permanent property of the modified sample. The samples just discussed are washed by Soxhlet extraction. When the samples are only washed in DI water at room

temperature, the water contact angles of modified samples are stabilized at θ_A/θ_R ~ $50^o/0^o$ after 10 h of washing (Figure 3-6). This value again suggests very good surface hydrophilicity. Therefore, siloxane equilibration is a simple and effective approach to anchor PEO chains onto and into silicone networks and generate permanently hydrophilic surfaces.

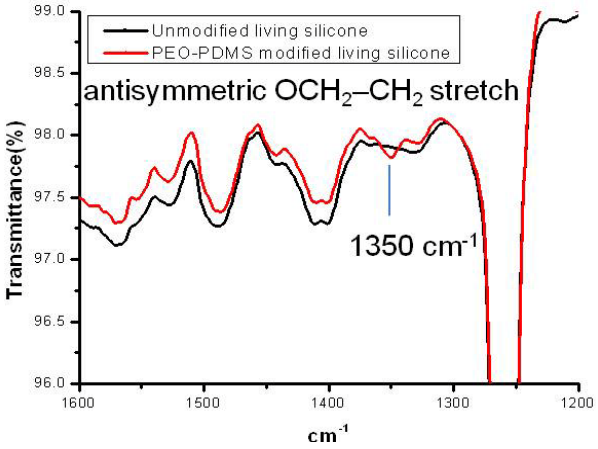

Figure 3-7 ATR-IR spectra of PEO-PDMS - modified living silicone and unmodified living silicone

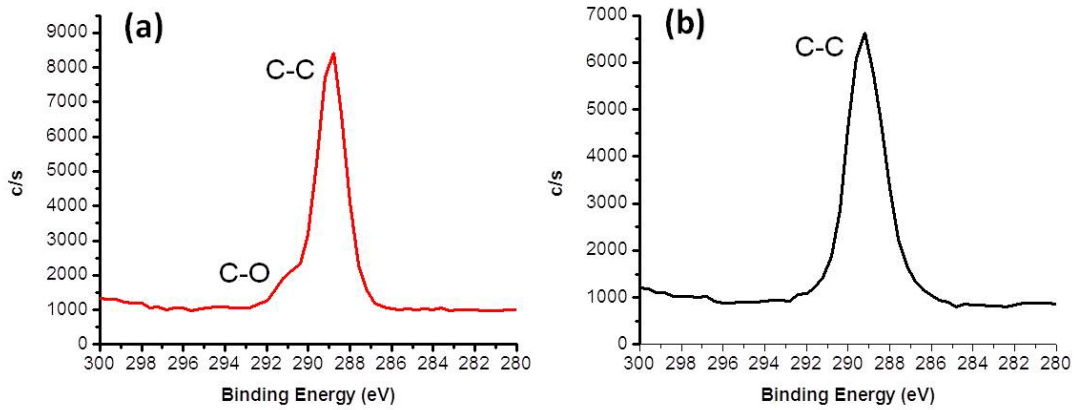

Figure 3-8 XPS spectra (75^o take-off angle) of (a) PEO-PDMS - modified living silicone; (b) Unmodified living silicone

The ATR-IR spectrum of PEO-PDMS modified living silicone show a characteristic absorption at around 1350 cm^{-1} (Figure 3-7), which corresponds to the

PEO antisymmetric $OCH_2–CH_2$ stretch. However, this peak is not present in the spectrum of the unmodified living silicone surface. The comparison indicates that PEO segments are successfully attached to the silicone surface. Figure 3-8 shows the C 1s XPS of the PEO modified and unmodified living silicone. The presence of carbon on the unmodified living silicone (Figure 3-8(b)) is due to the methyl groups of PDMS and the ethylene bridges in bis-D_4. It is verified by the single C-C peak at a binding energy of 289 eV. This value drifts from the 285 eV reference value, because the living silicone apparently affects the BaO neutralizer in XPS. In Figure 3-8(a), the appearance of the carbon peak (C-O in ethers) at around 291 eV (286.5 eV in literature[23]) indicates the surface coverage by PEO for the PEO-modified silicone samples, while no C-O peak is observed on the unmodified living silicone sample (Figure 3-8(b)).

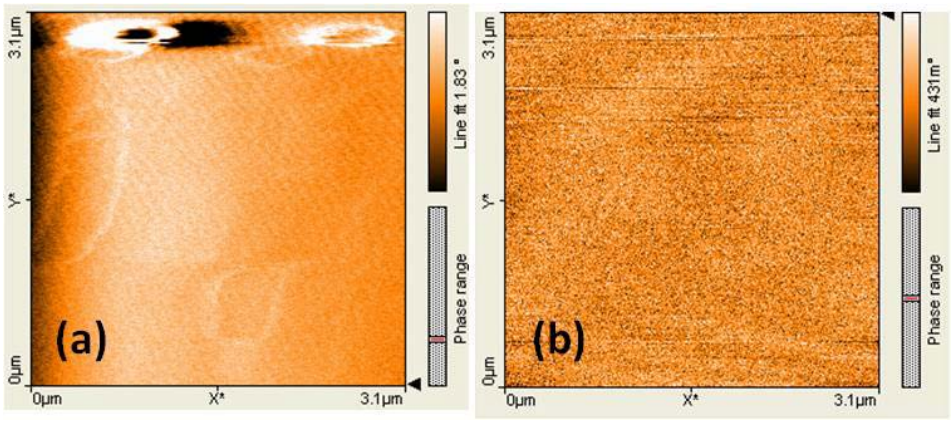

Figure 3-9 AFM phase images of (a) PEO-PDMS - modified living silicone; (b) Unmodified living silicone.

Figure 3-9 show AFM phase images of PEO-modified silicone and unmodified silicone. The modified silicone surface (Figure 3-9 (a)) contains peaks of PEO aggregates, while the unmodified silicone surface is relatively smooth (Figure 3-9 (b)). Likely the PEO islands form because the hydrophilic chain segments phase-segregate from the siloxane chains causes higher surface roughness.

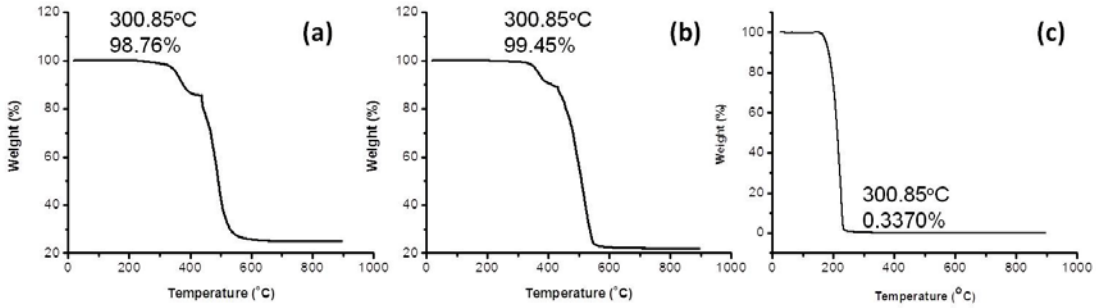

Figure 3-10 TGA curves of (a) PEO-PDMS - modified living silicone; (b) Unmodified living silicone; (c) PEO (M_n~ 5000).

The content of PEO that is incorporated into silicone was assessed using thermogravimetric analysis. All the TGA measurements in Figure 3-10 were conducted in the air atmosphere with a flow rate of 60 mL/min. It is noted from Figure 3-10 (c) that PEO is almost completely oxidized and vaporized at 300.85 ^{o}C (0.3370 wt% of PEO residue remains at this temperature). As shown in Figure 3-10(a)(b), both PEO-modified and unmodified living silicones display a dramatic weight loss between 300.85 ^{o}C and 550 ^{o}C. This phenomenon is attributed to the oxidation and decomposition of silicone. The residual mass above 550 ^{o}C is around 20 wt%, which comes from silica, silicon carbide and silicon/oxide/carbide. It is possible to calculate the PEO content in the modified living silicone from the residual mass of PEO modified and unmodified silicone at 300.58 ^{o}C. It is discovered that a very small amount of PEO segments are grafted to the sample ($\frac{99.45-98.76}{98.76+(99.45-98.76)}\times 100\ \ wt\% = 0.69\ \ wt\%$).

3.3.2 Hydrolytic Stability of PEGylated Silicone

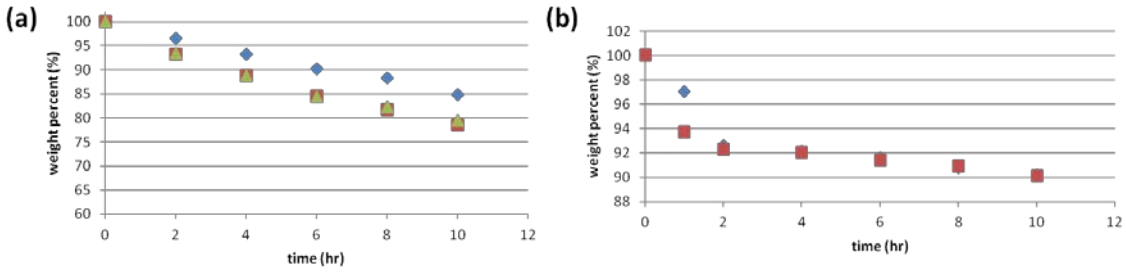

Figure 3-11 Hydrolytic stability of (a) PEO-PDMS modified living silicone; (b) Unmodified living silicone. Both samples were washed in DI water and taken out after certain times of washing, followed by overnight drying in air before mass measurement.

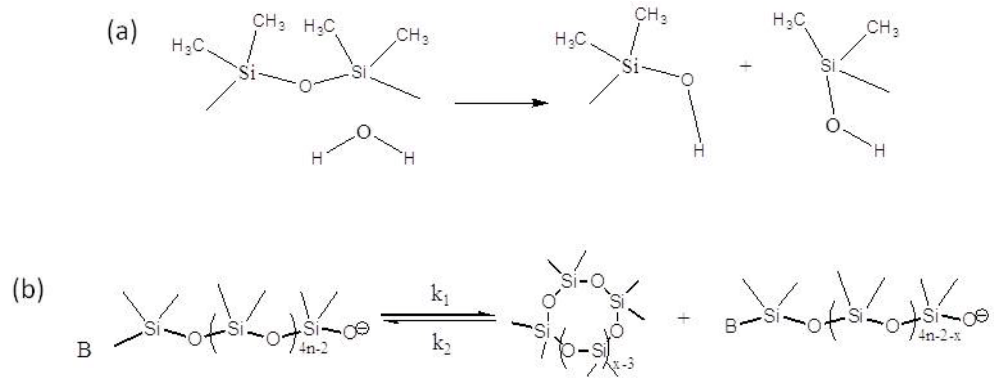

Figure 3-12 Degradation of silicone in water

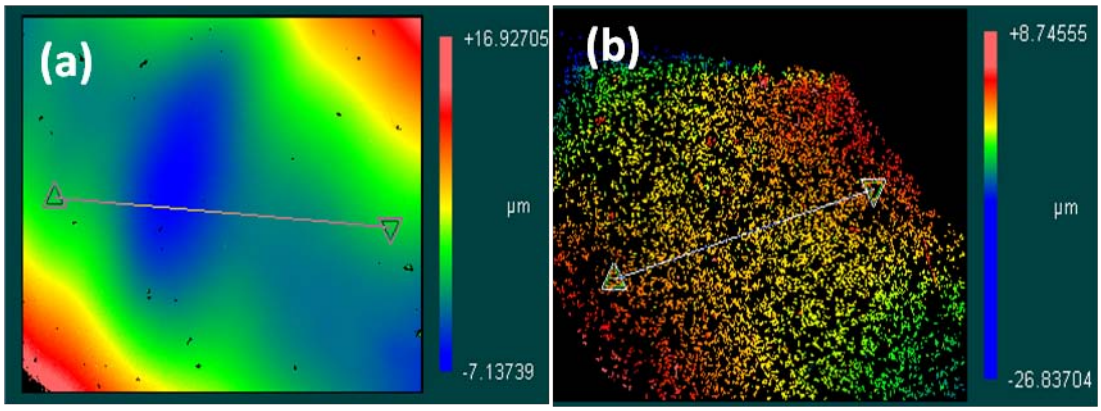

Figure 3-13 Optical profilometry measurements of PEO-PDMS - modified living silicone surfaces after the samples were washed in DI water for (a) 10 h and (b) 13 days.

The hydrolytic stability of microfluidic devices is of obvious importance, especially when the device is used for biological applications.[24] Hydrolytic stability provides direct insight into a material's operational life in this functional environment.[25] Silicone is widely used in microfluidic devices and biomedical studies, so its resistance to water 'corrosion' is crucial. The weight loss of silicone samples in water was monitored *in-situ*, and the measurement results are plotted in Figure 3-11. Silicone is known to react with water and degrade in steam (Figure 3-12(a)).[26] Low molecular weight cyclic species can be also removed with water, pushing siloxane equilibration reaction towards the 'degradation' side ($k_1 > k_2$). (Figure 3-12(b)) This explains the 10 wt% mass loss of the unmodified living silicone washed in water for 10 h at room temperature (Figure 3-11(b)). In contrast, PEO-modified silicone suffers around 20 wt% mass loss after 10 h of washing (Figure 3-11(a)). The significant weight loss can even be visualized by washing the PEO modified silicone for 10 h and 13 days, separately. Optical profilometry shows that the sample surface becomes much rougher when it is washed for 13 days than 10 h (Figure 3-13). It is possible that PEO segments play an important role in the more severe mass decrease: Water tends to associate with the hydrophilic PEO segments, so that PDMS chains can closely interact and react with water in the case of PEO-modified living silicone.

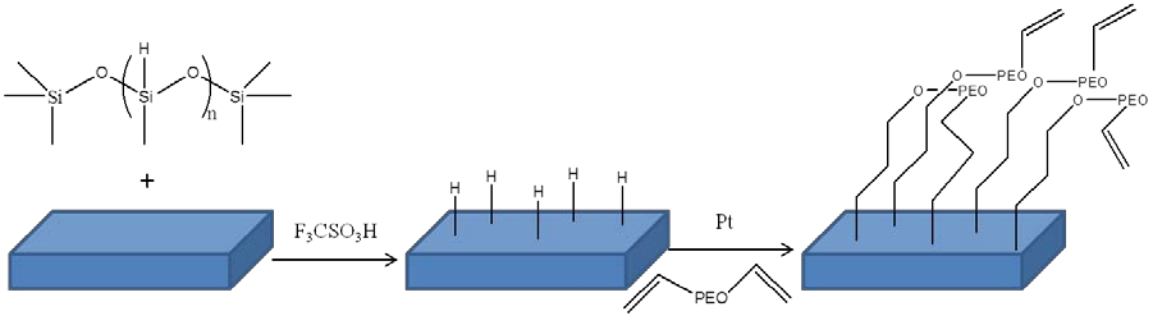

Figure 3-14 Sylgard 184 surface modification with PDMS-H (M_w~1800-2100) and divinyl-terminated PEO. The blue block is cross-linked Sylgard 184.

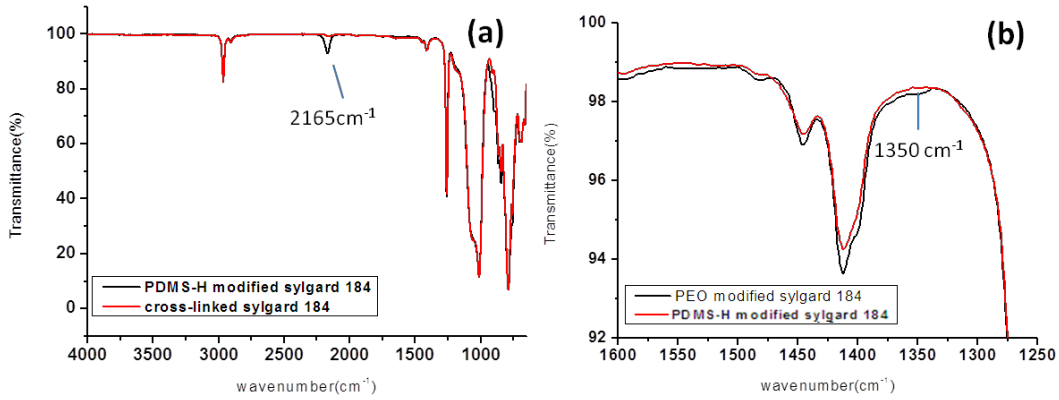

Figure 3-15 ATR-IR spectra of cross-linked Sylgard 184, PDMS-H - modified Sylgard 184 and PEO modified Sylgard 184.

Poor hydrolytic stability is one major drawback of silicone surface modification with siloxane equilibration. Brook and coworkers' work was reproduced to improve our understanding about this problem. Sylgard 184 was modified with PDMS-H through acid-catalyzed siloxane equilibration, and the allyloxy-terminated PEO was further tethered to the hydrido (Si-H)-enriched silicone surface, as shown in Figure 3-14. Surface characterization of the modified silicone samples was performed by ATR-IR. The absorption peak at 2165 cm^{-1}corrsponds to Si-H stretching in Figure 3-15(a), and the peak at 1350 cm^{-1} in Figure 3-15(b) is assigned to the antisymmetric OCH_2-CH_2 stretch. The IR results confirm that PEO is immobilized on the silicone surface after the two step reaction.

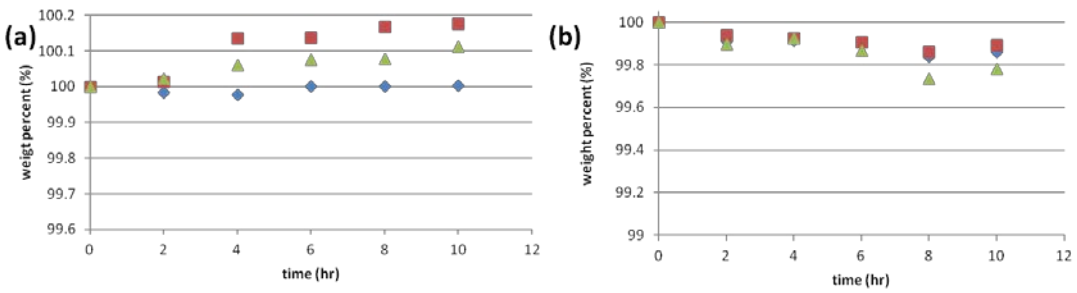

Figure 3-16 Hydrolytic stability of (a) PDMS-H - modified Sylgard 184; (b) PEO modified Sylgard 184. Both samples were washed in DI water and taken out every 2h, followed by dried overnight in air before weight measurement.

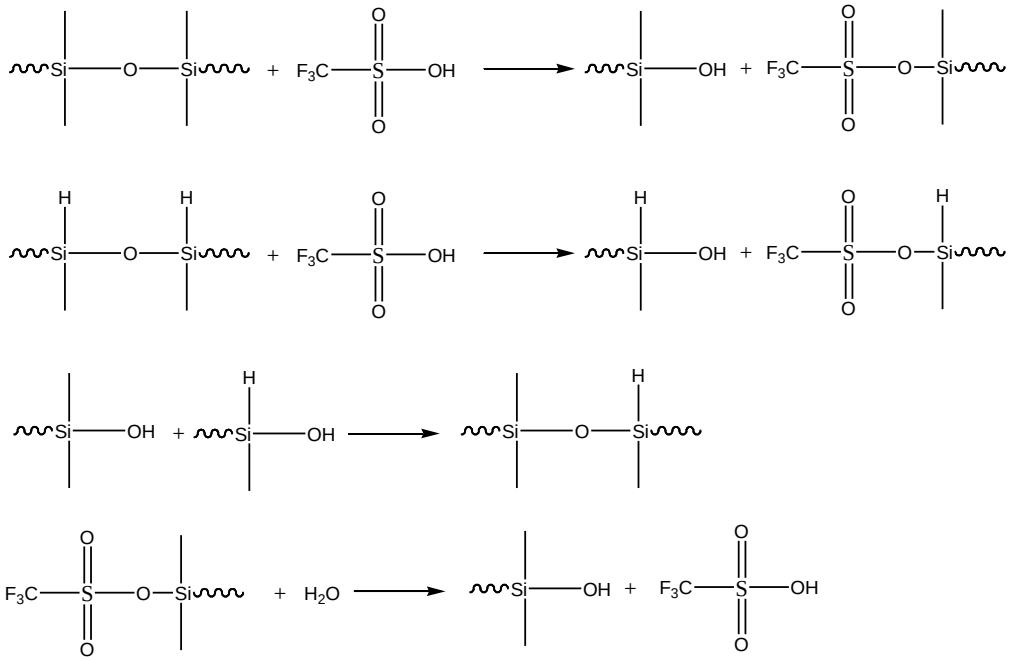

Figure 3-17 Sylgard surface modification with PDMS-H (M_w~1800-2100) in the presence of triflic acid

The hydrolytic stability of PDMS-H and PEO-modified Sylgard 184 were also evaluated by recording the sample mass loss in water. Although a somewhat improved hydrophilicity is observed on PEO-modified silicone ($117^o/40^o$) compared with PDMS-H modified silicone ($115^o/65^o$), both samples appear stable when they are washed with copious amounts of water (Figure 3-16). A possible reaction mechanism for acid-catalyzed grafting of Si-H to silicone surface is depicted in Figure 3-17. Since

Si-H-enriched silicone is washed thoroughly with methanol and hexane which may contain water, the catalytic amount of triflic acid is possibly all removed by the solvent. In other words, acid-catalyzed 'living' Sylgard 184 is 'killed' by water and solvent flushing, and it explains the almost zero mass loss of PDMS-H modified silicone in Figure 3-16(a).

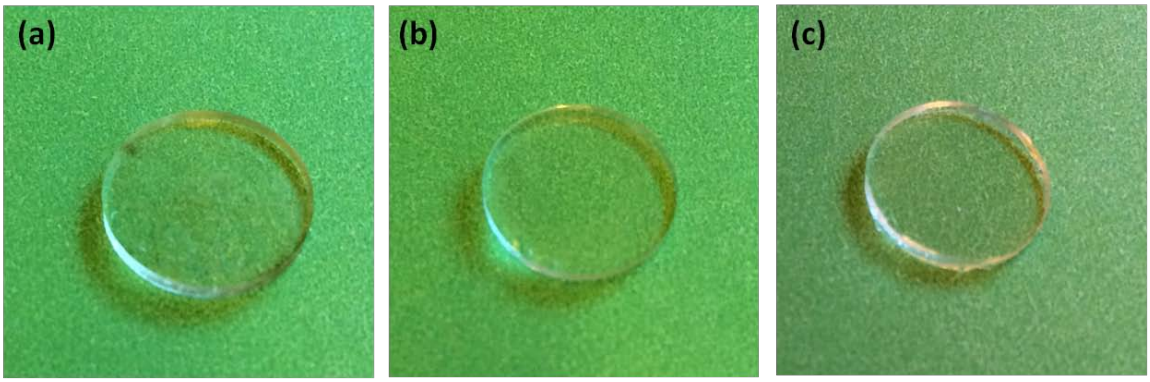

Figure 3-18 (a) PEO-modified Sylgard 184; (b) PDMS-H - modified Sylgard 184; (c) pristine Sylgard 184

Unlike silicone modification with base-catalyzed siloxane equilibration, in which a large quantity of PEO-PDMS is grafted inside and outside the silicone sample, silicone modification with Brook's approach only yields a surface coverage of covalently attached PEO segments. This surface coverage is verified by the contact angle measurement results and the excellent sample transparency (Figure 3-18(a)). Only the surface siloxane bonds are in close contact with water that is associated with the PEO segments, so PEO does not cause a significant change in the silicone hydrolytic stability (Figure 3-16(b)).

3.3.3 Surface Modification of Silicone Cross-linked by Hydrosilylation

Theoretically, any cross-linked silicone can be transformed into living silicone with base. The base can attack the cross-linked PDMS network, introducing reactive

dimethylsilanolate groups to the network (Figure 3-19).[27] These living silanolate groups lead to backbiting and interchain exchange reactions: cyclic oligomers are equilibrated with the network, and network reconstruction occurs continuously.

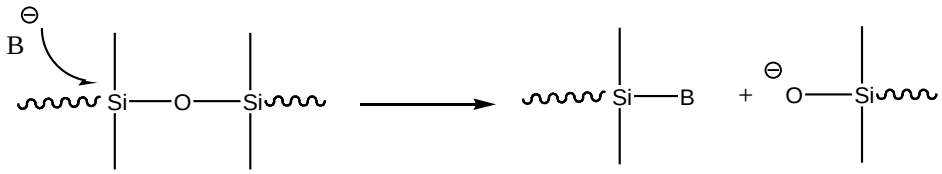

Figure 3-19 Schematic of base inducing living silanolate chain ends

Figure 3-20 (a) Cross-linked PDMS prepared by hydrosilylation of PDMS-Vinyl (M_w~28 000) and PDMS-H (M_w~1800-2100) (H: vinyl=15:1, 2 ppm Pt based on silicone mass); (b) A penny; (c) Cross-linked silicone equilibrated with tetramethylammonium siloxanolate and then remolded with a penny.

This idea was tested by equilibrating a smooth hydrosilylation cross-linked silicone surface with tetramethylammonium siloxanolate, after which the 'activated' surface was molded against a penny (Figure 3-20). The reverse impression of the penny is made on silicone. This silicone surface reshaping can be ascribed to chemical stress relaxation. It is also an experimental proof that the silicone surface is turned into living silicone.

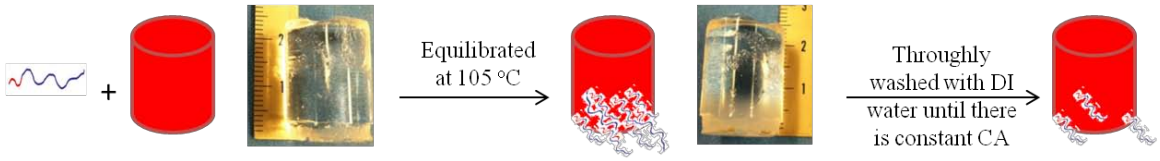

Figure 3-21 Schematics of silicone modification with PEO-PDMS. Blue segments indicate PEO blocks. The red segments indicate PDMS blocks. Red cylinder indicates cross-linked silicone.

Table 3-2 Average advancing and receding water contact angles of PEO-PDMS - modified living silicone washed in DI water.

Surface property change with time	
Washed in DI water for 1 day	$75^o/32^o$
Washed in DI water for 2 days	$76^o/33.5^o$
Washed in DI water for 11 days	$97^o/32^o$

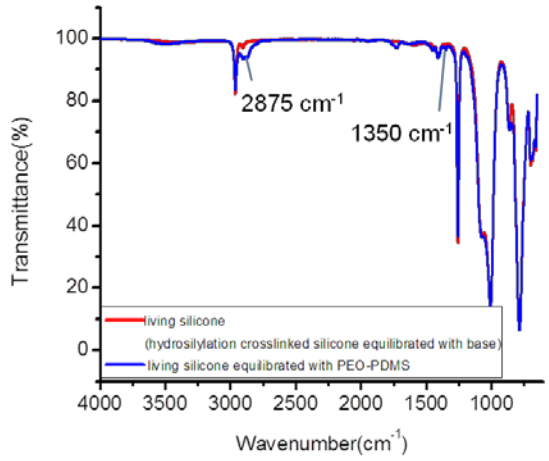

Figure 3-22 ATR-IR spectra of living silicone (hydrosilylation cross-linked silicone equilibrated with base) and living silicone equilibrated with PEO-PDMS.

As shown in Figure 3-21, the surface activated silicone elastomer was equilibrated with PEO-PDMS at 105 ^{o}C overnight. A diffusion front of PEO-PDMS is found at around 5 mm from the bottom of the sample, based on the observation of sample opacity. The physically absorbed, unreacted PEO-PDMS is expected to be rinsed away after a long washing process in DI water. Data in Table 3-2 reflect that the contact angle of silicone equilibrated with PEO-PDMS is $97^o/32^o$, whereas the surface has a water contact angle of $101^o/89^o$ before it is equilibrated with PEO-

PDMS. It suggests the surface modification with PEO was achieved on hydrosilylation cross-linked silicone. Appearance of CH_2 adsorption at 2875 cm^{-1} as well as antisymmetric $OCH_2 - CH_2$ stretch adsorption at 1350 cm^{-1} in ATR-IR spectra (Figure 3-22) further reinforce our conclusion.

3.4 Conclusions

Silicone elastomers with improved hydrophilicity were prepared by equilibrating dimethylsiloxane - ethylene oxide block copolymer with cross-linked PDMS in the presence of base. Siloxane equilibration is implicated as the grafting mechanism. The PEO segments are chemically attached to the elastomer, as shown by contact angle, ATR-IR and XPS measurements. Characterization with TGA revealed that there is only a small amount of PEO chains grafted to the cross-linked PDMS. The PEO chains can aggregate on the surface as indicated in AFM images of dried samples. The modified silicone elastomers, with PEO-PDMS grafted both 'onto' and 'into' the elastomer, maintain their hydrophilicity apparently indefinitely. However, poor hydrolytic stability of the PEO grafted silicone is one drawback of this modification scheme.

This simple, one-step silicone modification method can be applied to PDMS cross-linked by either anionic copolymerization or hydrosilylation. The resulting modified silicones may be valuable materials for microfluidic devices and microcontact printing stamps.

3.5 References

1. Vladkova, T., Surface modification of silicone rubber with poly(ethylene glycol) hydrogel coatings. *J Appl Polym Sci* **2004,** *92* (3), 1486-1492.

2. Khorasani, M. T.; Mirzadeh, H.; Kermani, Z., Wettability of porous polydimethylsiloxane surface: morphology study. *Appl Surf Sci* **2005,** *242* (3-4), 339-345.

3. Rochow, E. G.; Rochow, T. G., The Properties and Molecular Weights of Some Silicone Polymers. *J Phys Colloid Chem* **1951,** *55* (1), 9-16.

4. Chen, H.; Brook, M. A.; Sheardown, H., Silicone elastomers for reduced protein adsorption. *Biomaterials* **2004,** *25* (12), 2273-2282.

5. Jo, S.; Park, K., Surface modification using silanated poly(ethylene glycol)s. *Biomaterials* **2000,** *21* (6), 605-616.

6. Olah, A.; Hillborg, H.; Vancso, G. J., Hydrophobic recovery of UV/ozone treated poly(dimethylsiloxane): adhesion studies by contact mechanics and mechanism of surface modification. *Appl Surf Sci* **2005,** *239* (3-4), 410-423.

7. Sharpe, R. B. A.; Burdinski, D.; Huskens, J.; Zandvliet, H. J. W.; Reinhoudt, D. N.; Poelsema, B., Chemically patterned flat stamps for microcontact printing. *J Am Chem Soc* **2005,** *127* (29), 10344-10349.

8. Delamarche, E.; Geissler, M.; Bernard, A.; Wolf, H.; Michel, B.; Hilborn, J.; Donzel, C., Hydrophilic poly (dimethylsloxane) stamps for microcontact printing. *Adv Mater* **2001,** *13* (15), 1164-+.

9. Befahy, S.; Lipnik, P.; Pardoen, T.; Nascimento, C.; Patris, B.; Bertrand, P.; Yunus, S., Thickness and Elastic Modulus of Plasma Treated PDMS Silica-like Surface Layer. *Langmuir* **2010,** *26* (5), 3372-3375.

10. Bodas, D.; Rauch, J. Y.; Khan-Malek, C., Surface modification and aging studies of addition-curing silicone rubbers by oxygen plasma. *Eur Polym J* **2008,** *44* (7), 2130-2139.

11. Zhou, J. W.; Ellis, A. V.; Voelcker, N. H., Recent developments in PDMS surface modification for microfluidic devices. *Electrophoresis* **2010,** *31* (1), 2-16.

12. Fu, Y. J.; Qui, H. Z.; Liao, K. S.; Lue, S. J.; Hu, C. C.; Lee, K. R.; Lai, J. Y., Effect of UV-Ozone Treatment on Poly(dimethylsiloxane) Membranes: Surface Characterization and Gas Separation Performance. *Langmuir* **2010,** *26* (6), 4392-4399.

13. Goddard, J. M.; Hotchkiss, J. H., Polymer surface modification for the attachment of bioactive compounds. *Prog Polym Sci* **2007,** *32* (7), 698-725.

14. Abbasi, F.; Mirzadeh, H.; Katbab, A. A., Modification of polysiloxane polymers for biomedical applications: a review. *Polym Int* **2001,** *50* (12), 1279-1287.

15. Abbasi, F.; Mirzadeh, H.; Katbab, A. A., Bulk and surface modification of silicone rubber for biomedical applications. *Polym Int* **2002,** *51* (10), 882-888.

16. Thanawala, S. K.; Chaudhury, M. K., Surface modification of silicone elastomer using perfluorinated ether. *Langmuir* **2000,** *16* (3), 1256-1260.

17. Zheng, P. W.; McCarthy, T. J., A Surprise from 1954: Siloxane Equilibration Is a Simple, Robust, and Obvious Polymer Self-Healing Mechanism. *J Am Chem Soc* **2012,** *134* (4), 2024-2027.

18. Stein, J.; Lewis, L. N.; Gao, Y.; Scott, R. A., In situ determination of the active catalyst in hydrosilylation reactions using highly reactive Pt(0) catalyst precursors. *J Am Chem Soc* **1999,** *121* (15), 3693-3703.

19. Lee, S.; Voros, J., An aqueous-based surface modification of poly(dimethylsiloxane) with poly(ethylene glycol) to prevent biofouling. *Langmuir* **2005,** *21* (25), 11957-11962.

20. Murthy, R.; Cox, C. D.; Hahn, M. S.; Grunlan, M. A., Protein-resistant silicones: Incorporation of poly(ethylene oxide) via siloxane tethers. *Biomacromolecules* **2007,** *8* (10), 3244-3252.

21. Chen, H.; Zhang, Z.; Chen, Y.; Brook, M. A.; Sheardown, H., Protein repellant silicone surfaces by covalent immobilization of poly(ethylene oxide). *Biomaterials* **2005,** *26* (15), 2391-2399.

22. Gelest Catalog.

23. Kajiyama, T.; Tanaka, K.; Takahara, A., Depth Dependence of the Surface Glass-Transition Temperature of a Poly(Styrene-Block-Methyl Methacrylate) Diblock Copolymer Film on the Basis of Temperature-Dependent X-Ray Photoelectron-Spectroscopy. *Macromolecules* **1995,** *28* (9), 3482-3484.

24. Xu, J. J.; Gleason, K. K., Conformal, Amine-Functionalized Thin Films by Initiated Chemical Vapor Deposition (iCVD) for Hydrolytically Stable Microfluidic Devices. *Chem Mater* **2010,** *22* (5), 1732-1738.

25. Lai, Y. C., Novel Polyurethane Silicone Hydrogels. *J Appl Polym Sci* **1995,** *56* (3), 301-310.

26. Kole, S.; Srivastava, S. K.; Tripathy, D. K.; Bhowmick, A. K., Accelerated Hydrothermal Weathering of Silicone-Rubber, Epdm, and Their Blends. *J Appl Polym Sci* **1994,** *54* (9), 1329-1337.

27. Kantor, S. W.; Grubb, W. T.; Osthoff, R. C., The Mechanism of the Acid-Catalyzed and Base-Catalyzed Equilibration of Siloxanes. *J Am Chem Soc* **1954,** *76* (20), 5190-5197.

CHAPTER 4
SYNTHESIS OF TRANSPARENT SILICONE WITH HIGH REFRACTIVE INDEX

4.1 Introduction

4.1.1 Optical Properties of Polymer Composite

Epoxy resins are traditionally used as the encapsulants for light-emitting diodes (LEDs). The emergence of high-power LED devices makes silicone a more preferred packaging material than epoxy, because it is stable at high temperatures and high humidity, and can contain very low amounts of ionic impurities. However, the thermal conductivity and refractive index of silicone are concerns for it as a replacement for epoxy as an LED encapsulant.[1,2]

Addition of high refractive index particles into polymer matrices is a straightforward way to increase the refractive index of the composite material, because the refractive indices of a composite material (n_{comp}) is the result of both the refractive indices of the particles (n_p) and the polymer matrix (n_{poly}),[3]

$$n_{comp} = \varphi_p n_p + \varphi_{poly} n_{poly} \qquad \text{Equation 4-1}$$

where φ_p and φ_{poly} are the volume fraction of the particles and the polymer matrix.

Optical clarity is also a prerequisite for a material's application as LED packaging. The intensity of transmitted light I is,

$$\frac{I}{I_0} \sim \exp\left[-\frac{3V_P x r^3}{4\lambda^4}\left(\frac{n_p}{n_m}-1\right)\right] \qquad \text{Equation 4-2}$$

In Equation 4-2, I_0 is incident light intensity. n_p and n_m are refractive indices of the particles and the polymer matrix. V_p and r are the volume fraction and radius of particles, respectively. λ denotes the wavelength of incident light, and x denotes the optical path length.

It is shown in Equation 4-2 that transparency can be maximized (I is close to I_0) by eliminating refractive index mismatching of the particles and the polymer matrix. The refractive indices of the matrix and fillers have to be matched to the third decimal place. [4] There were some successful attempts to improve polymer composite transparency by introduction of fillers of core-shell structure. Li and coworkers prepared core–shell structured silica-titania (SiO_2-TiO_2) nanoparticles and blended them with epoxy. The refractive index of the nanoparticles is regarded as the weighted average of refractive indices of SiO_2, TiO_2 and the air. When the TiO_2 content is 36.5 wt%, the nanoparticles have a refractive index perfectly matching that of the epoxy, and optically transparent nanocomposite is produced regardless of the particle size.[5] Yang and coworkers synthesized nanosized zinc oxide (ZnO) particles, and then coated them with amorphous SiO_2 via Stöber's method. The addition of ZnO-SiO_2 core-shell nanoparticles into polycarbonate (PC) enhances the transparency of the nanocomposite compared to PC/ZnO/SiO_2 in which ZnO and SiO_2 are added individually.[6] Although transparent polymer composites can be prepared by carefully adjusting the refractive index of the fillers to match that of the polymer, no improvement in refractive index value can be expected for the composite.

It is also shown in Equation 4-2 that embedding small nanoparticles into polymer matrix is an effective way to avoid turbidity. But smaller particles have larger surface area/particle size ratio, leading to a higher tendency of aggregation.

The optical clarity of composite material can be deteriorated by particle agglomeration (increase of effective r). Significant amounts of research attention have been focused on two approaches to suppress particle aggregation: 1) Surface functionalization of the particles to improve their compatibility with the polymer matrix 2) *In situ* preparation of particles in the polymer via sol-gel chemistry.[7, 8]

4.1.2 Preparation of Transparent Polydimethylsiloxane (PDMS)/ Metal Oxide Composite with Co-solvent

In the surface functionalization approach, coupling agents should be carefully selected, with one side anchoring to the particles and the other side dispersing into the polymer. Paik and coworkers synthesized ligand molecules with diamine headgroup and siloxane double tails. (Figure 4-1) First, clear zirconia (ZrO_2) nanoparticle in toluene dispersion was purchased and ligand molecules are attached to the particle surface. Then the modified particle dispersion was mixed with PDMS, followed by thorough evaporation of toluene. It is reported the nanoparticles were well dispersed after the toluene solvent is 'exchanged' with PDMS.[9]

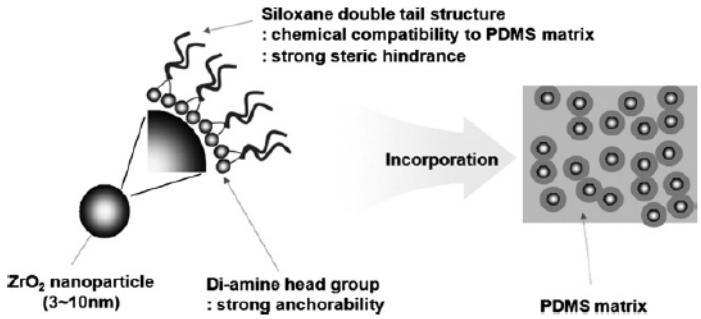

Figure 4-1 Dispersion strategy to prepare transparent nanocomposites

Using a co-solvent to inhibit severe particle agglomeration inside polymer matrices is a common method to prepare transparent composites. High refractive

index TiO_2 particles have been introduced to poly(bisphenol-A-co-epichlorohydrin) in this way. Hayashi and coworkers dispersed propionic acid - coated TiO_2 particles into *n*-butanol and toluene. The dispersion is further mixed with poly(bisphenol-A-co-epichlorohydrin) in *n*-butanol and toluene solution. Transparent composite film was obtained after thorough solvent removal.[10]

4.1.3 Mechanically Dispersing Modified Metal Oxide Particles into PDMS

In the paint industry, surface-modified fumed particles are usually incorporated into polymer via strong mechanical blending to reduce the particle distribution inhomogeneity. Controlling the particle dispersion and spacing within the polymer matrix has always been a significant issue because it is the premise for pronounced material properties improvement. The process of mechanically dispersing nanoparticles into a viscous polymer matrix involves four steps:[11]

1) Particles are mixed with liquid polymer,

2) The particle-air interfaces are displaced with particle-polymer interfaces,

3) Particle aggregates are broken up,

4) Particles are stabilized in the suspension by the dispersant.

In step 4, the repulsion between particles can come from electrostatic forces, or absorbed surfactant layers. These phenomena are called electrostatic stabilization and steric stabilization, separately.[12]

One challenge to achieve uniform particle dispersion is flocculation. It can occur to already dispersed particles if mixing is further carried out. Four basic types of interaction exist between a pair of particles: (Figure 4-2)

1) Hard sphere interactions: Interaction approaches infinity when the particles center to center distance is smaller than the diameter of hard sphere.

2) Electrostatic interactions: Interactions resulting from the surface charge or the ionic dispersant.

3) Steric interactions: Interactions resulting from nonionic dispersants or block copolymers.

4) Van der Waals attraction: Attractive interactions coming from fluctuations of electron density distribution.

Flocculation is the result when type 2 or type 3 interaction cannot overcome the universal Van der Waals attraction. Therefore, strong electrostatic interaction and steric interaction ensure uniform and stable particle dispersion.

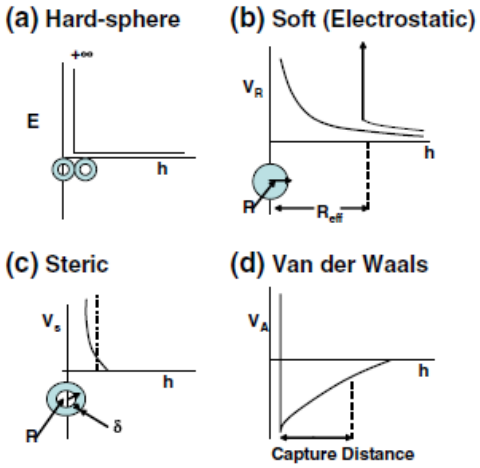

Figure 4-2 Interaction between particles

To prevent aggregation and flocculation, significant effort has been made to graft nanoparticles with ligands. The effectiveness of this strategy is determined by many parameters such as the ligand grafting density, relative molecular weight of the ligand and the polymer matrix.[13] Bates and coworkers investigated the silica particle dispersion in polystyrene and claimed uniform particle dispersion can be only obtained when the system is in the wet brush limit (the ligand molecular weight exceeds the polymer molecular weight).[14]

Another factor that makes uniform particle suspensions unstable is the sendimentation process. For a single particle, the balance among gravity, buoyancy and viscosity resistance leads to Stokes' law,[15]

$$u = \frac{(\rho_s - \rho_f) g D^2}{18\eta} \qquad \text{Equation 4-3}$$

where η is the viscosity of the polymer matrix, ρ_f is the density of the polymer, ρ_s is the particle density, D is the particle diameter, and g is the gravity acceleration. A direct conclusion from Stokes law is that particle sedimentation rate u decreases with the decrease of particle density and particle size. The sedimentation rate also decreases with the increase of polymer matrix density and viscosity.

Li and coworkers modified ZnO nanoparticles with 3-methacryloxypropyltrimethoxysilane. It is reported that these modified inorganic fillers can be well dispersed in two-component Room Temperature Vulcanized silicone with sonication. The transparent ZnO/silicone nanocomposite has neither flocculation nor sedimentation problems.[2]

4.1.4 In-situ Synthesis of Inorganic Phase in PDMS from Sol–gel Precursors

Sol-gel processes prove to be broadly applicable approaches to loading inorganic fillers into polymer matrix. This *in situ* precipitation of inorganic domains typically involves two steps: hydrolysis of metal alkoxides to metal hydroxides, polycondensation of metal hydroxides to form a network structure. Mark and coworkers generated silica fillers *in situ* after PDMS curing using sol-gel chemistry.[16] Bequcage and coworkers mixed polydimethylsiloxane- α,ω -diol with tetraethylorthosilicate (TEOS), and then added a tin salt as polycondensation catalyst showing that silica fillers can be generated *in situ* during PDMS curing.[17] Pure metal oxide films derived from sol-gel process have the tendency of cracking in the air due to surface tension. The existence of flexible PDMS chains in the composite helps release the stress and eliminate the cracking problem.[18]

Compared with the mechanical blending approach, the sol-gel preparation route is less time and energy consuming. Another notable advantage is the inorganic domain morphology is under better control. A small enough inorganic domain size ensures high transparency of composite materials, and the decisive factor of the optical clarity is the scale of phase separation in the composite. Macro-phase separation always renders opaque products. It is believed that strong interactions between inorganic domains and polymer phase can help avoid or 'delay' macro-phase separation. Transparent SiO_2-TiO_2-PDMS composite films have been successfully synthesized by Whang and coworkers via sol-gel process. Fujishima and coworkers mixed titanium tetrabutoxide (TBOT) and PDMS. TBOT is transformed into a TiO_2 network after PDMS is cured under UV irradiation.[17,19,20]

In another respect, sol-gel strategies suffer from some drawbacks. For example, the metal oxides generated are usually in the amorphous phases, which have lower refractive indices compared to those of crystalline phases. (TiO_2 prepared at low temperature by sol-gel methods is usually amorphous, with a refractive index between 2.0 and 2.2. Anatase TiO_2 has n= 2.45, and rutile TiO_2 has n= 2.70.)[3,21] For another example, it is hard to obtain thick and crack-free composite samples, because gel network shrinking and capillary action arising from solvent evaporation are more significant in thicker samples.

4.1.5 Objectives

The objective of this work is to prepare transparent silicone composites with high refractive index which are well suited for optical electronics. First, the strategy of mixing high refractive index particles and PDMS was evaluated. TiO_2 nanoparticles of average size 5-10 nm were modified with linear trimethylsilyl-terminated PDMS[22] and hydridosilanes[23] to make particles and PDMS matrices compatible. These ligand-anchored particles were mechanically dispersed into long chain PDMS with a high-shear mixer. In an alternative approach, ZrO_2 dispersions and SiO_2 dispersions were mixed with silicone in the presence of co-solvents, for the purpose of incorporating particles into silicone and avoiding phase separation.

Furthermore, the feasibility of generating the inorganic phase inside silicone by sol-gel processes was evaluated. TiO_2/PDMS composite was prepared by developing a TiO_2 gel network in the cross-linked PDMS. Polydibutyltitanate was mixed with short chain vinyl-terminated linear PDMS, hydrido group-containing PDMS and water to carry out a one-pot organic-inorganic synthesis. In addition, TiO_2 particles (polytitanate branched polymer) were synthesized from titanium butoxide,

and further immobilized inside silicone to yield a silicone hybrid film containing TiO_4 linkage groups.

Finally, the silicone building blocks and inorganic oxide content were tuned to obtain silicone composites of different molecular structures. Our goal was to accurately manipulate both the mechanical properties and refractive index of the silicone composite. Chemical structures of the silicone composite samples were elucidated by infrared spectra, while their thermal properties were assessed with the Thermogravimetric Analysis.

4.2 Experimental Section

4.2.1 Particle Modification and Dispersion

Titanium Oxide (Anatase phase, Average Size 5-10 nm) was purchased from Sun Innovation's Nanomaterial Store, Inc. Silica dispersion in methyl ethyl ketone (particle size 10-15nm) was obtained from Nissan Chemical. Zirconium n-propoxide, isobutanol and propionic acid were purchased from Gelest, Inc. and Acro Chemical, separately. Transparent zirconia sol was prepared by mixing reagents in a molar ratio of isobutanol/1-propanol/zirconium *n*-propoxide/propionic acid/deionized water = 22.5:5:1:2:4.5 and stirring the mixture at room temperature for one day.

1,3,5,7-tetramethylcyclotetrasiloxane (D_4^H), octamethylcyclotetrasiloxane (D_4), trimethylsiloxy-terminated polydimethylsiloxane (M_w~2000) were all obtained from Gelest, Inc. Hydroxyl-terminated polydimethylsiloxane (M_n~550) was purchased from Sigma-Aldrich. All the particles and chemicals were used as received. About 1g TiO_2 particles were wetted with 0.5 mL D_4^H, D_4, trimethylsiloxy or hydroxyl-terminated PDMS, sealed in a shlenk tube, and heated at 150 ^oC for 3 days.

After these particles were treated with vapor phase reaction , 6.7 wt% D_4^H, D_4 or trimethylsiloxy terminated PDMS (M_w~2000) - modified titania particles were mixed into trimethylsiloxy terminated PDMS (M_w~116 500) to prepared silicone composites. The component mixtures were vigorously mixed in a FlackTek Inc. DAC 150.1. FV speed mixer operating at 3500 rpm for 4 min. 5.9 wt% hydroxyl-terminated PDMS - modified titania particles were mixed into trimethylsiloxy-terminated PDMS (M_w~116 500) in the same fashion.

Vinyl-terminated PDMS samples (M_w~800), polymethylhydrosiloxane (PDMS-H, M_w~1800-2100), and platinum-divinyltetramethyldisiloxane complex (Karstedt's catalyst) were all purchase from Gelest, Inc. and used without any further purification. In one experiment, the two types of silicones were blended in a molar ratio of H: vinyl=15:1. Karstedt's catalyst was then added to the silicone mixture (172 ppm Pt based on silicone product mass). The three-component mixture was introduced into the freshly prepared zirconia sol to prepare a silicone composite containing 7.7 wt% ZrO_2. In another experiment, the three-component mixture was similarly prepared except that less Karstedt's catalyst was added (75 ppm Pt based on silicone product mass). This mixture was dissolved in ethanol to prepare a 0.582 g/mL silicone solution. Subsequently, this silicone-in-ethanol solution was mixed with a silica dispersion to form a silicone composite containing 38.2 wt% SiO_2. The final silicone composite products are transparent silicone composite films after thorough solvent evaporation for both experiments.

4.2.2 PDMS/TiO_2 Composite Preparation with Polydibutyltitanate

Vinyl-terminated PDMS samples (M_w~186) and polymethylhydrosiloxane (M_w~1800-2200) were mixed with a molar ratio of H: vinyl=15:1. Karstedt's catalyst

was then added to the silicone mixture (11 ppm Pt based on silicone product mass). Various quantities of titania precursor polydibutyltitanate and water were further stirred into the silicone mixture with a molar ratio of Ti: H_2O=1:1, and stirring continued for 5.5 h. These mixtures were cast on a glass or quartz slide. Cross-linked silicone hybrid films were obtained after the mixture cured at room temperature for 30 min.

4.2.3 PDMS/TiO_2 Composite Preparation with Titanium Butoxide

Anhydrous ethanol was purchased from Sigma-Aldrich. Titanium butoxide (TBOT) was purchased from Gelest, Inc. The ethanol was mixed with titanium butoxide in a molar ratio of EtOH: TBOT=7.5:1, and stirred for 30 min. In another container, ethanol and water were mixed in the molar ratio of EtOH: H_2O=7.5:1.25. In the following step, the aqueous ethanol solution was dripped into the TBOT in ethanol solution over 10 min. The overall reagents ratio is TBOT: H_2O: EtOH =1:1.25:15, which leads to the formation of a branched titanate oligomer.

Branched titanate oligomers were precipitated in an excess of acetone. These oligomers were dispersed into D_4^H, polymethylhydrosiloxane (M_w~2800) and hydroxyl-terminated polydimethylsiloxane (M_n~550) to prepare silicone composites of various titania loadings (25 wt% or 33 wt%).

4.2.4 Optical Property Characterization

Silicone composites were coated on quartz slides at a thickness of tens of micrometers. Optical transmittance spectra of these thin films were recorded on a Perkin Elmer UV WinLab 5.1.4.0630 over a wavelength range of 200-900 nm.

Refractive indices of the film samples were determined on a Spectronic Instruments refractometer.

4.2.5 Mechanical Property Characterization

Hydrido-rich silicone/TiO_2 composites prepared as described in 4.2.3 were cross-linked with two types of vinyl-containing PDMS: (1) Vinyl-terminated PDMS (PDMS-Vinyl, M_w~5000-7000, Gelest, Inc.) (2) vinylmethylsiloxane-dimethylsiloxane copolymer (7.0-8.0% vinylmethylsiloxane, M_w~28 000, Gelest, Inc.) The two components were mixed in a volume ratio of hydrido-rich composite: vinyl-containing PDMS = 1:2. Karstedt's catalyst was utilized to cross-link the two components (167 ppm Pt based on silicone product mass). The new composites were shaped into ~8 mm× 8 mm×0.3 mm sample bars and analyzed on a TA instruments 800 dynamic mechanical analyzer. The measurements were conducted in a film tension mode at 10 Hz and 20 ^oC.

4.2.6 Thermal Property and Chemical Structure Characterization

PDMS/TiO_2 composites prepared with titanium butoxide were characterized on a TA Instrument TGA Q50 for thermal properties. The samples were heated from room temperature to 900 ^oC at an air flow rate of 60 mL/min. The sample masses were plotted versus temperature. A Perkin Elmer 100 FT-IR spectrometer was used to study film chemical composition. Attenuated total reflection infrared spectroscopy (ATR-IR) data was recorded. X-ray photoelectron spectroscopy (XPS) spectra of the synthesized ZrO_2 and TiO_2 particles were collected on a Physical Electronics Quantum 2000.

4.3 Results and Discussion

4.3.1 Preparation of Silicone Composites by Mechanical Blending

Many researchers have reported successful attempts to develop transparent particle/PDMS composites and particle dispersions with the aid of mechanical mixing. Wong and coworker claimed that 5 wt% rutile TiO_2 nanoparticles (~10 nm) of high refractive index can be homogeneously dispersed into silicone resin after their surface modification with organic surfactants, so the silicone transparency is not compromised. It is noted that intense sonication is used to disperse the particles.[24] Gao's research in our group indicates Aeroxide® TiO_2 (P25, Degussa Corp.) can be well dispersed into N-methyl-2-pyrrolidone by sonication after the particles are modified with D_4^H. Moreover, the SpeedMixer DAC 150.1 FV recently has gained great popularity in research labs because of its advertised capability of dispersing 25% fumed silica into viscous silicones. Therefore, mechanical blending is the first approach we used to prepare transparent and high refractive index silicone composites.

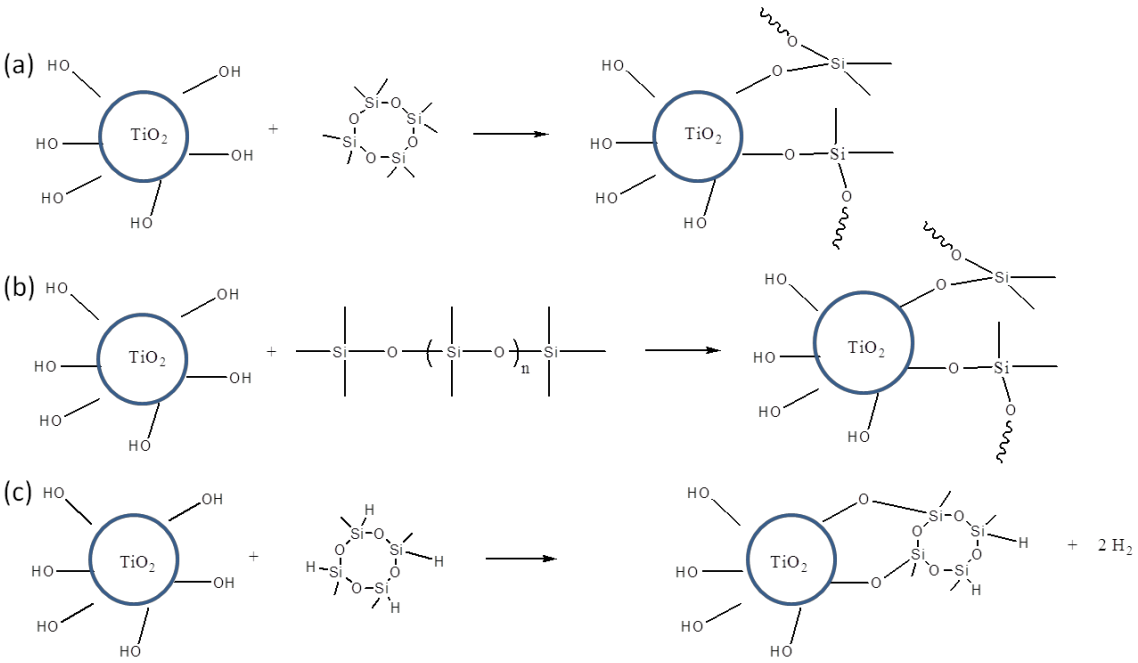

Figure 4-3 Titania particle (Sun Innovations, Inc. Anatase phase, 5-10 nm, >99%) surface modification with (a) D_4, (b) trimethylsiloxy-terminated polydimethylsiloxane (M_w~2000) and (c) D_4^H. Vapor phase reactions were carried out by adding 0.5 g silane or silicone to ~ 1.0 g titania particles, followed by heating the mixture at 150 ^oC for 3 days within a sealed vessel.

Figure 4-4 Image of 3.5 g trimethylsiloxy-terminated polydimethylsiloxane (M_w~116 500) mixed with ~ 0.25 g D_4^H, D_4 and trimethylsiloxy-terminated polydimethylsiloxane (M_w~2000) modified titania particles (left to right).

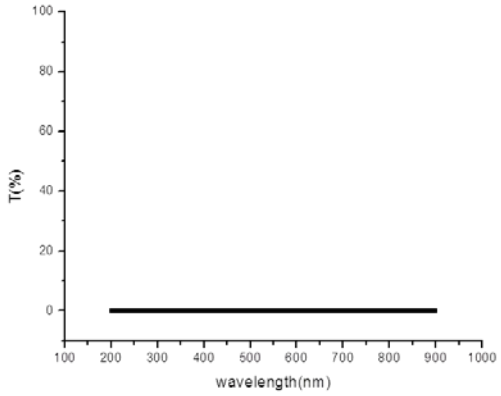

Figure 4-5 UV-Vis transmission of mixture of 6.7 wt% D_4^H modified titania in trimethylsiloxy terminated polydimethylsiloxane (M_w~116500). Sample transmission is measured in a standard cuvette.

Commercial anatase TiO_2 particles of diameter less than 10 nm were purchased to serve as inorganic fillers for silicone. The small particle size, which is well below the visible light wavelength, is crucial to ensure the composite transparency. Trimethylsiloxy-terminated PDMS is selected to modify TiO_2 surfaces, as we were inspired by Krumpfer's method to fabricate low hysteresis surfaces.[22] Silica, with an isoelectric point in water of 3,[25] hydrolyzes in water and is acidic. Krumpfer and coworkers claim that the silanol groups on silica and the siloxane bonds in PDMS can be equilibrated in the presence of silicic acid.[22] Titanol (Ti-OH) is more acidic than silanol (Si-OH) because the electronegativity of Si (1.9) is higher than that of Ti (1.54). The implication is that titania particles can be also modified by trimethylsiloxy-terminated PDMS due to the presence of acid catalyst (Figure 4-3(b)). It is shown in Figure 4-3(a) and (c) that D_4 and D_4^H are two other good reagents to modify TiO_2 particle surface. Ring opening reaction of D_4 can occur under acid catalyst,[26] so that linear siloxane ligands are grafted onto TiO_2 particles after vapor phase reaction (Figure 4-3(a)). D_4^H is selected because reaction of hydridosilanes and titania is documented as a simple method to treat titanium surfaces.[27]

All the modified TiO_2 nanoparticles were mechanically blended into trimethylsiloxy-terminated PDMS (M_w ~116 500) by using a SpeedMixer. It is observed from Figure 4-4 and Figure 4-5 that incorporation of a small amount of particles (6.7 wt% D_4^H-modified TiO_2) into trimethylsiloxy-terminated PDMS results in a sharp transparency loss compared to the pure PDMS. We also attempted to disperse the particles into silicone by using a probe sonicator operating at 20 kHz, 400 W and 100 % amplitude, yet no satisfactory results were achieved. The difficulties in dispersing particles may be ascribed to three reasons: 1) Dry particles are used in the experiments. It is always harder to disperse dry particles than wet particles. Drying leads to the formation of hard aggregates,[28] which are robust towards mechanical blending. The hard agglomerates reduce system optical clarity. 2) The small particle size (less than 10 nm) determines the tremendous attraction among particles, including Van der Waal's interaction and hydrogen bonding. 3) The particles are modified by a vapor phase reaction, which may not be an efficient way to obtain high ligand grafting density. Particle clusters that break up under mechanical shear force may re-agglomerate after shear forces are ceased.

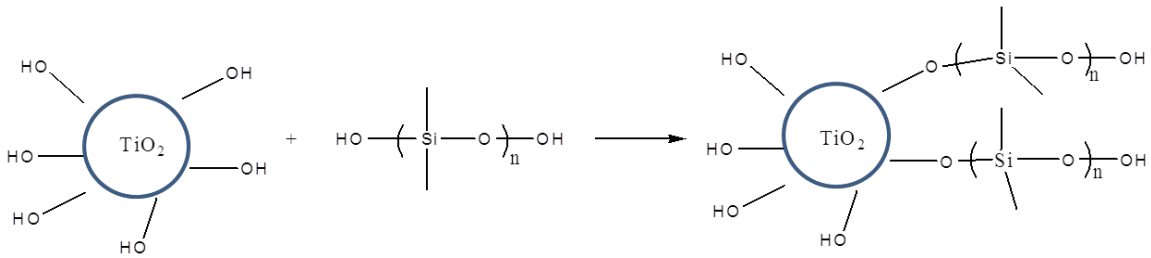

Figure 4-6 Titania particle (Sun Innovations, Inc. Anatase phase, 5-10 nm, >99%) surface modification with hydroxyl terminated polydimethylsiloxane (M_n~550, Sigma-Aldrich). Titania particles were modified with 8.3 vol% hydroxyl-terminated polydimethylsiloxane in heptane solution at 90 ^oC for 48 h.

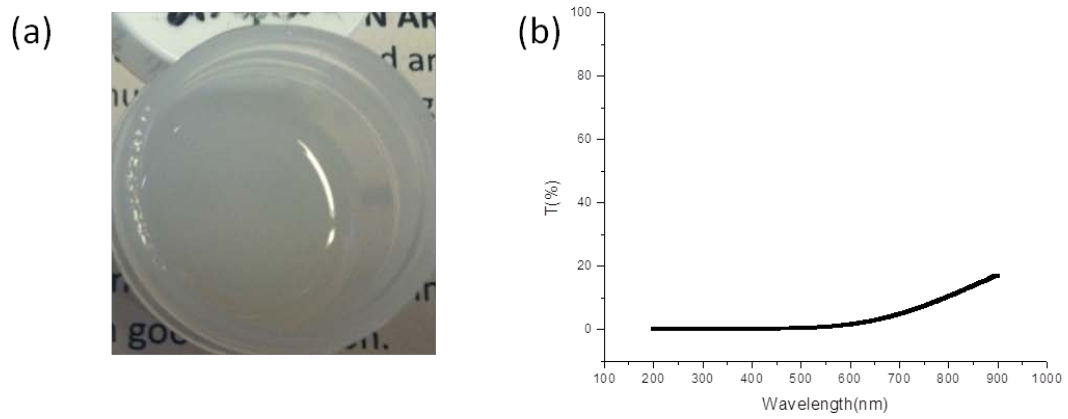

Figure 4-7 (a) Images and (b) UV-Vis transmission of mixture of 5.9 wt% hydroxyl-terminated polydimethylsiloxane-modified titania particles in trimethylsiloxy-terminated polydimethylsiloxane (M_w~116 500)

Hydroxyl-terminated PDMS was also utilized to modify TiO_2 particle surfaces, because of our recognition that dimethylsilanediol is a useful inorganic oxide surface modification reagent.[29] We made use of the condensation reaction between titanol and silanol to graft siloxane ligands to TiO_2 particles (Figure 4-6). The modified particles were washed with heptane, a good solvent for silicone. The supernantant was decanted and further mixed with silicone. In this case, the particle dispersion was mixed with silicone by a SpeedMixer, in order to fill 5.9 wt% TiO_2 particles into linear PDMS. After complete solvent evaporation, the resulting composite appears more transparent than the composites prepared by the previous approaches (Figure 4-3). The images and UV-vis spectra of the composites are both shown in Figure 4-7.

4.3.2 Preparation of Silicone Composite by Mixing Transparent Sol and Silicone

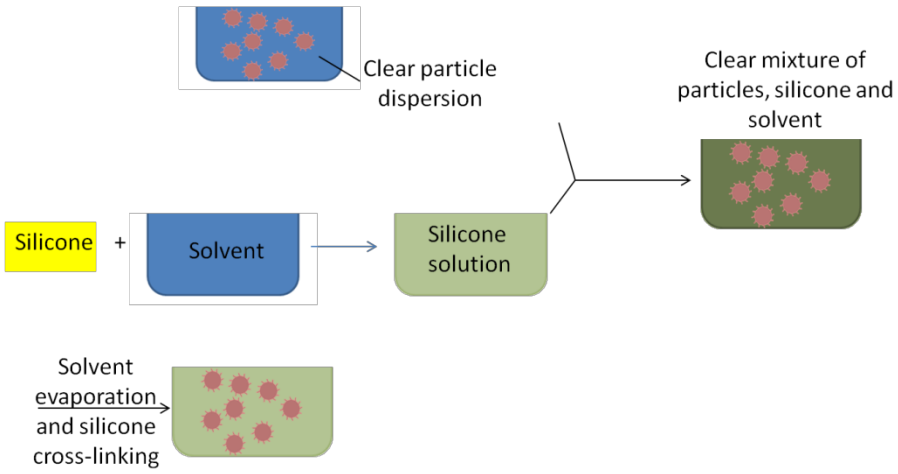

Figure 4-8 Dispersion strategy to prepare transparent silicone nanocomposites

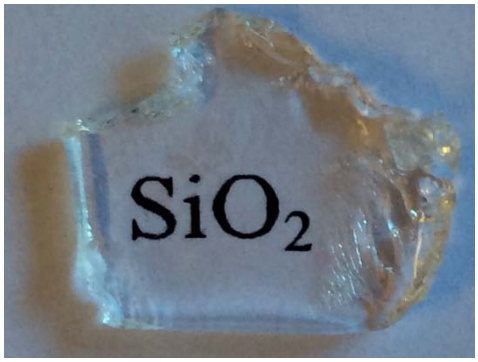

Figure 4-9 SiO_2/PDMS nanocomposite with 38.2 wt% SiO_2 content prepared by using co-solvent approach. Organosilicasol (30-31 wt% 10-15nm silica particles in methyl ethyl ketone (MEK)) was mixed with 0.582 g/mL silicone (PDMS-Vinyl (M_w~800), PDMS-H (M_w~1800-2100), H: vinyl=15:1, 75 ppm Pt) in ethanol solution.

In the work described next, our efforts were focused on mixing transparent inorganic oxide sol and silicone. This approach is advantageous because there are rarely hard agglomerates in transparent sols and the solvent can prevent the phase separation of inorganic oxide and silicone. As is depicted in Figure 4-8, clear particle

dispersion was either synthesized or purchased, while silicone was fully dissolved in a solvent. The silicone solution was slowly added to the particle dispersion under stirring or sonication to achieve a homogeneous mixture. The subsequent silicone cross-linking generates a siloxane network that immobilizes individual particles. Transparent hybrid material is developed after solvent evaporation. The feasibility of this approach was tested by mixing silica sol, PDMS-Vinyl (M_w~800), and PDMS-H in the mixed solvents of MEK and ethanol. Figure 4-9 is an image of a transparent silicone composite having a large colloidal particle loading (38.2 wt% SiO_2).

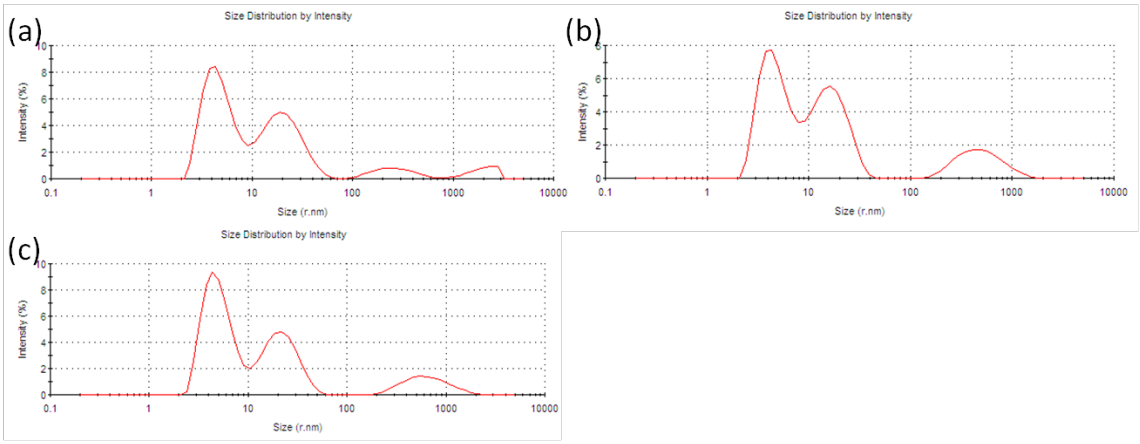

Figure 4-10 (a)(b)(c) Size distribution by intensity of ZrO_2 sol

Table 4-1 Z-Average size of ZrO_2 particles in ZrO_2 sol based on three measurements

peak	**Size (r, nm)**	**Intensity (%)**	**peak**	**Size (r, nm)**	**Intensity (%)**	**peak**	**Size (r, nm)**	**Intensity (%)**
1	5.227	53.5	1	4.838	49.6	1	4.686	44.0
2	22.23	33.7	2	20.96	39.3	2	16.41	40.7
3	692.8	12.7	3	275.8	6.4	3	522.6	15.3
Z-average size (r, nm)=7.654			Z-average size (r, nm)=7.496			Z-average size (r, nm)=7.725		
Average of Z-Average size (r, nm)=7.63 ± 0.12								

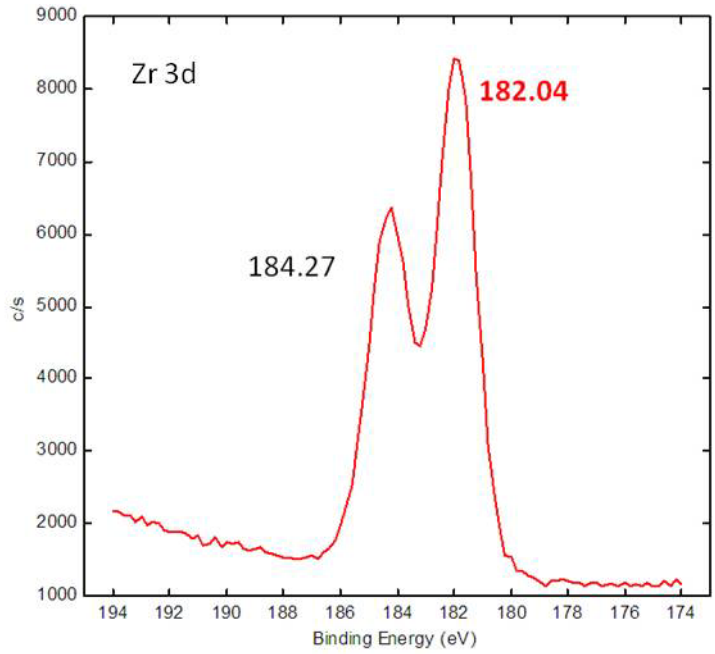

Figure 4-11 XPS characterization of ZrO_2 particles drop cast on a silicon wafer. The ZrO_2 nanoparticle dispersion was prepared by sol-gel synthesis (isobutanol/1-propanol/zirconium *n*-propoxide/propionic acid/H_2O =20:5:1:2:2.5).

A stable and transparent ZrO_2 nanoparticle dispersion was prepared by the sol-gel process($Zr(OC_3H_7)_4 + nC_3H_7COOH \rightarrow Zr(OC_3H_7)_{4-n}(OOCC_3H_7)_n + nC_3H_7OH$).[30] Figure 4-10 and Table 4-1 show the ZrO_2 particle size distribution information in the transparent sol obtained using a Malvern Nanozetasizer. In Figure 4-10, the peak located below 10 nm corresponds to the monomer, while the peak above 100 nm is assigned to branched macromolecules. The peak at around 20 nm is associated with low molecular weight polymer. The hydrodynamic radius of ZrO_2 particles is 7.63 nm based on three measurements of the same dispersion. This measurement is consistent with a value reported in the literature (8 nm-12 nm).[30] It is noted from XPS spectra (Figure 4-11) that there is a peak at 182.04eV (Zr $3d_{2/5}$ in ZrO_2), which reveals the existence of ZrO_2.

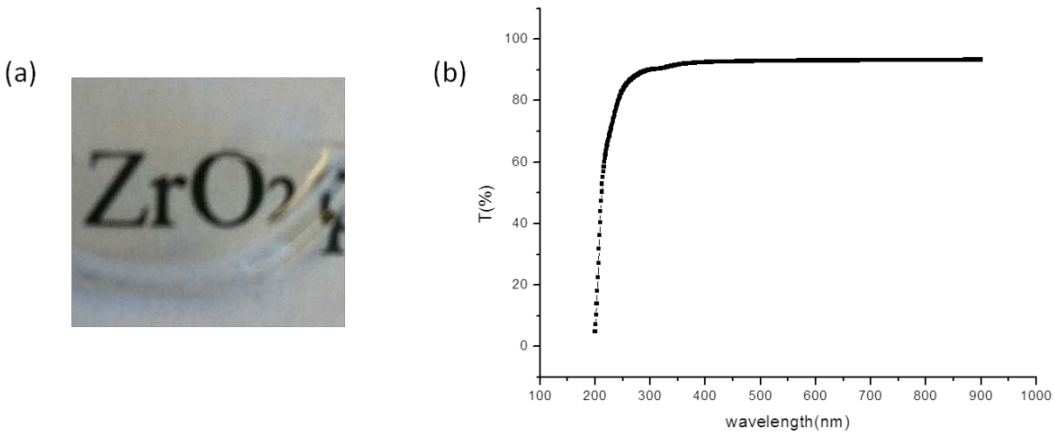

Figure 4-12 (a) Image of ZrO_2/PDMS nanocomposite and (b)UV-Vis transmission of ~10 µm thick ZrO_2/PDMS nanocomposite samples with 7.7 wt% ZrO_2 content. The composites with refractive index of 1.4221 were prepared by mixing 49.5 mg/mL ZrO_2 in isobutanol and propanol dispersion and silicone with refractive index of 1.4055 (PDMS-Vinyl (M_w~800), PDMS-H (M_w~1800-2100), H: vinyl=15:1, 172 ppm Pt).

Figure 4-12 shows the optical transmittance of a ZrO_2/PDMS composite. 7.7 wt% ZrO_2 is filled in PDMS by mixing transparent ZrO_2 sol with PDMS-Vinyl (M_w~800), PDMS-H and Platinum catalyst. The optical transmittance of the composite is above 90 % when the light wavelength is between 300 nm and 900 nm. It is implied from this result that ZrO_2 nanoparticles are uniformly embedded inside the cross-linked PDMS matrix.

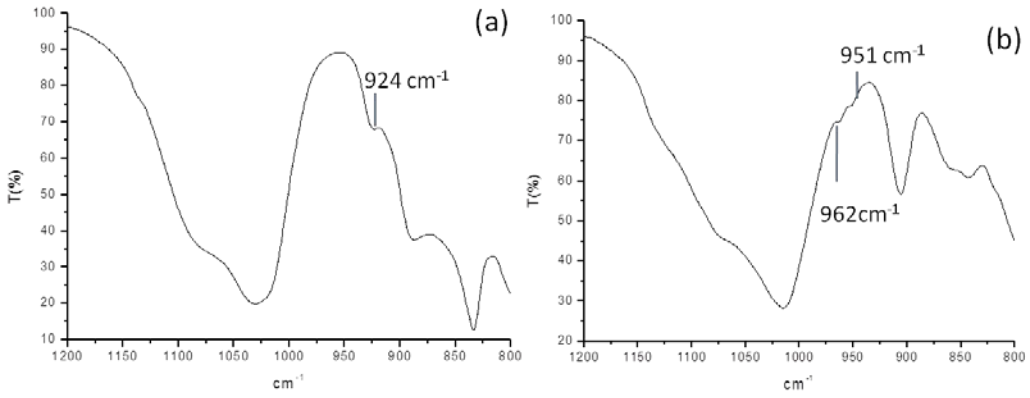

Figure 4-13 ATR-IR spectra of (a) pure PDMS and (b) ZrO_2/PDMS nanocomposite sample with 7.7 wt% ZrO_2 content.

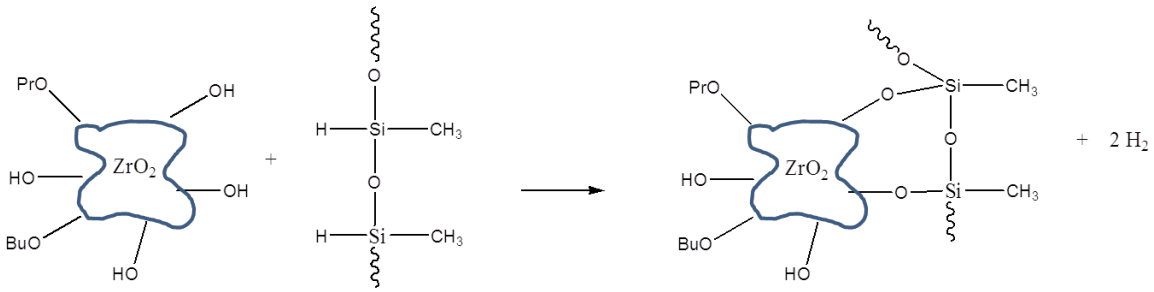

Figure 4-14 Reaction of zirconia surfaces with PDMS-H to form Zr-O-Si bonds.

ATR-IR spectra (Figure 4-13) were collected to investigate the molecular structure of the ZrO_2/PDMS nanocomposite. Pure PDMS is prepared with the same recipe as the ZrO_2/PDMS nanocomposite, except that there is no addition of ZrO_2 sol before silicone cross-linking. No adsorption peak is seen in the IR spectrum of pure PDMS at the wavenumber of 950-979 cm^{-1}. In comparison, absorption bands at 951 cm^{-1} and 962 cm^{-1} appear in the IR spectra of the ZrO_2/PDMS nanocomposite; these are associated with Si-O-Zr bond stretching.

IR results explain the excellent optical clarity of ZrO_2/PDMS composite indicating that hydridosilanes are reactive towards zirconia surfaces.[31] In our experiments, excess Si-H groups were applied to the silicone cross-linking (Si-H: Si-

Vinyl=15:1). Therefore, PDMS-H can react with ZrO_2 particles as soon as the sol and PDMS are mixed together. ZrO_2 may be 'corroded' and 'dissolved' in the PDMS-H matrix (Figure 4-14), in a similar fashion as 'SiO_2 participates in the cross-linked silicone synthesis' (Chapter 2).

4.3.3 Preparation of Silicone/TiO_2 Composites with Sol-gel Methods

Table 4-2 Refractive index (measured with refractometer) of TiO_2/PDMS nanocomposites prepared by one-pot syntheses. Silicone (PDMS-Vinyl (M_w~186), PDMS-H (M_w~1800-2100), H: vinyl=15:1, 11 ppm Pt), polydibutyltitanate, and water (Ti/H_2O=1:1) were stirred together at room temperature for 5.5 h. Then the samples were cured at room temperature for 30 min.

Titania content in silicone composites (wt%)	Refractive index
37	1.5254
32	1.5045
26	1.4902
19	1.4822
0	1.4093

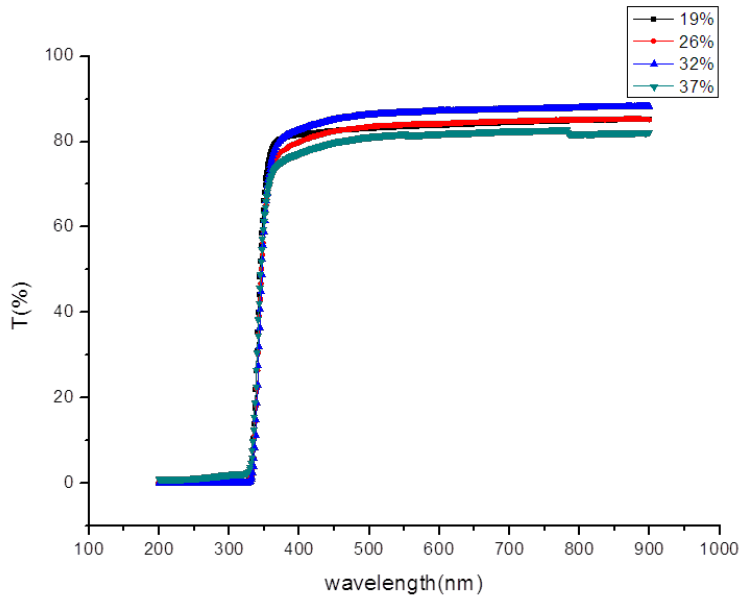

Figure 4-15 UV-Vis transmission of ~50 µm thick TiO_2/PDMS nanocomposite samples. TiO_2 contents are 37 wt% (green curve), 32 wt% (blue curve), 26 wt% (red curve), and 19 wt% (black curve).

Polydibutyltitanate is a commercial titania precursor. It is known from Flory-Huggins theory that miscibility of small molecules is better than the miscibility of small molecules and polymer. Thus, we selected low molecular weight silicones (PDMS-Vinyl (M_w~186) and PDMS-H (M_w~1800-2100)) to mix with polydibutyltitanate. The TiO_2 precursor is compatible with the two-component silicone over a range of mass ratios. Polydibutyltitanate is hydrolyzed inside the silicone to give PDMS/TiO_2 composites. It can be concluded from Table 4-2 that the refractive index of the composite is tunable by varying the titania precursor content. All of the composite films permit 80% light (wavelength >350 nm) transmission; the absorption by TiO_2 leads to the transmittance drop below 350 nm (Figure 4-15).

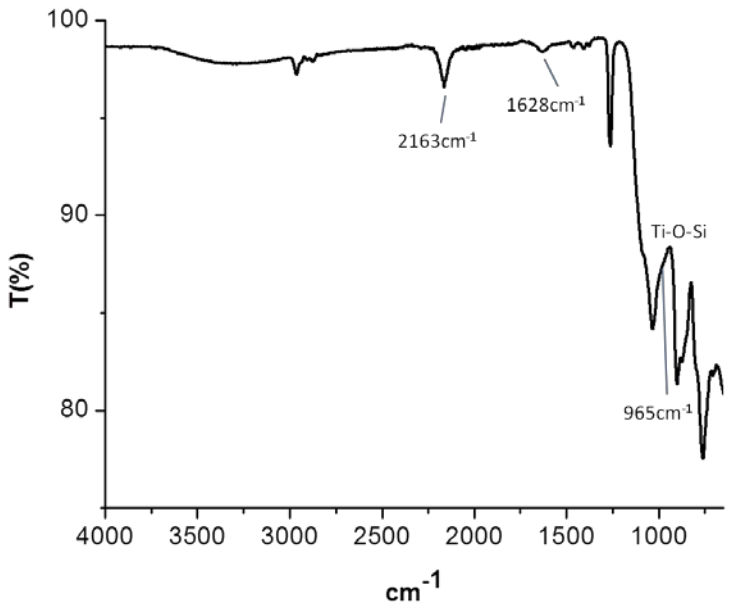

Figure 4-16 ATR-IR spectra of TiO_2/PDMS nanocomposite sample with 37 wt% TiO_2 content

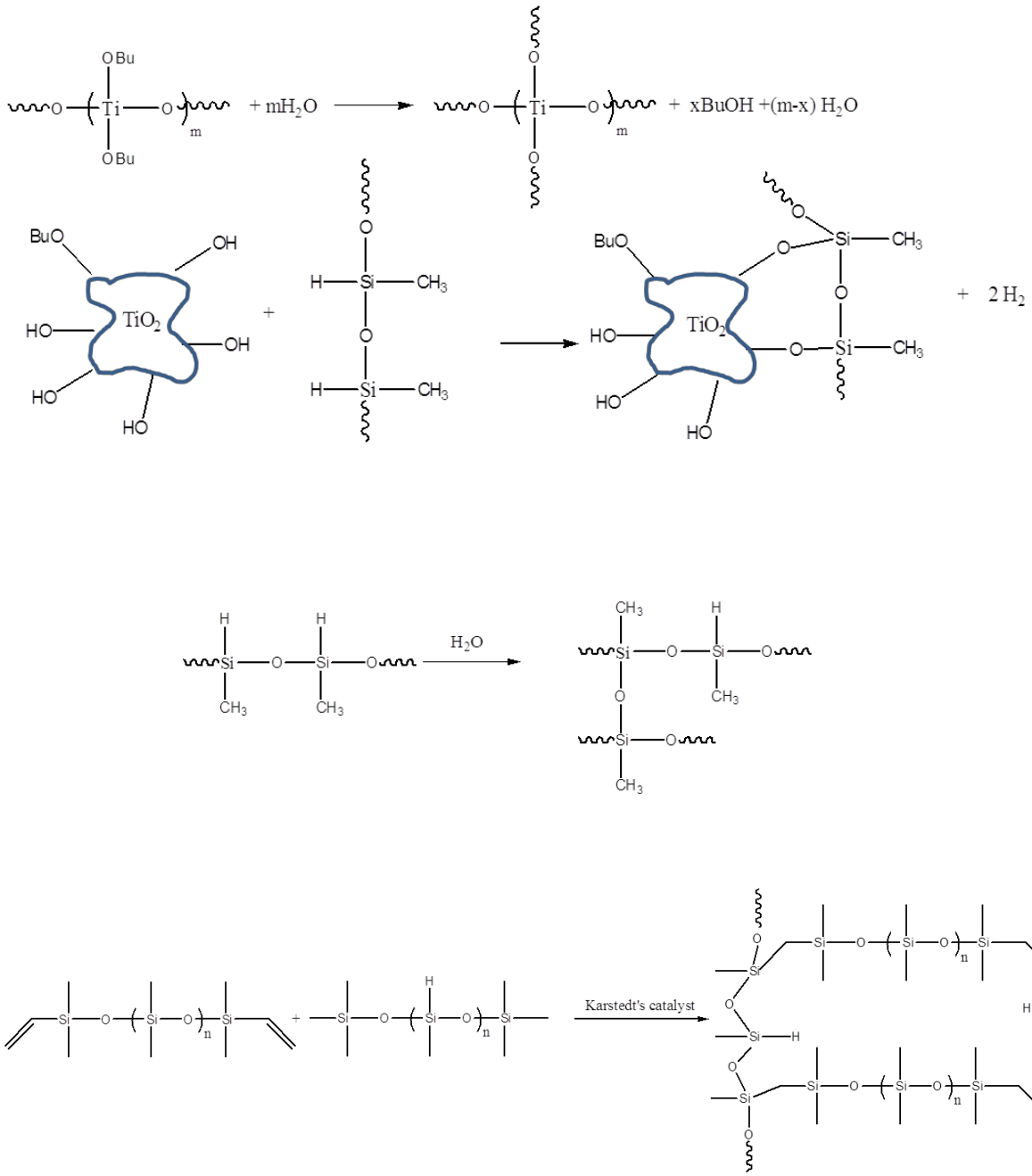

Figure 4-17 One-pot synthesis of H-DTQ' silicone resin

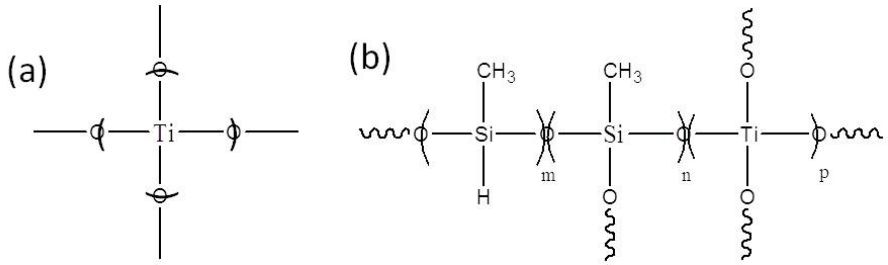

Figure 4-18 Molecular structure of (a) Q'; (b) H-DTQ' silicone resin.

IR spectra (Figure 4-16) of the PDMS/ TiO_2 composites indicate the presence of titania and present other molecular structural information. The absorption band at 1628 cm^{-1} is the absorption of Ti-O-Ti (asymmetrical stretching). The shoulder at 965 cm^{-1} is the characteristic absorption peak of Ti-O-Si. The peak at 2163 cm^{-1} indicates presence of Si-H bonds. The broad peak at 3100-3700 cm^{-1} is assigned to the Ti-OH and Si-OH. These absorption peaks reflect the molecular structure of PDMS/TiO_2 composite. In Figure 4-17, linear polydibutyltitanate is transformed into a branched polymer due to addition of water (Ti/H_2O=1:1). First, PDMS-H reacts with the branched polytitanate polymer, and leads to the formation of Ti-O-Si bonds. Second, PDMS-H can cross-link with each other in the presence of water, generating T silicone molecular structure. Third, PDMS-H can cross-link with PDMS-Vinyl via hydrosilylation, introducing D structures into the composites. Therefore, the overall product of all these reactions is a Si-H rich H-DTQ' silicone composite (Figure 4-18).

(a) $nTi(OBu)_4 + (4n + x - y)H_2O \rightarrow Ti_nO_{[2n-(x+y)/2]}(OH)_x(OBu)_y + (4n - y)Bu(OH)$

$Ti_nO_{[2n-(x+y)/2]}(OH)_x(OBu)_y \rightarrow nTiO_2 + xH_2O + yBu(OH)$

(b)

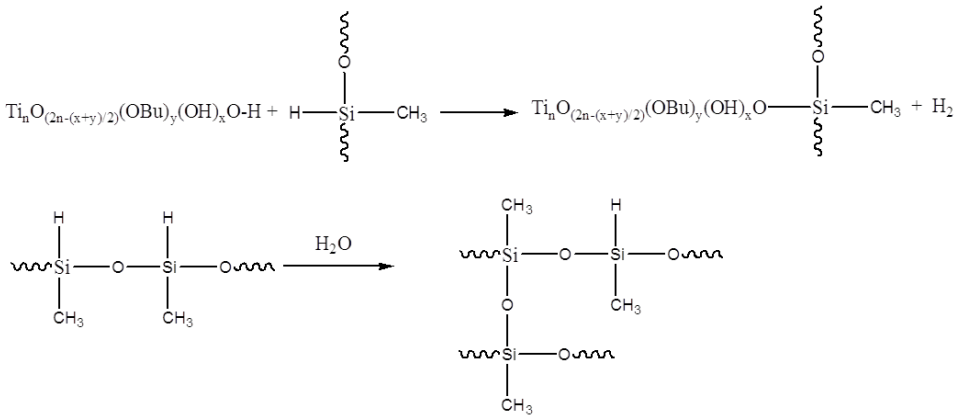

Figure 4-19 Synthesis of (a) TiO_2 sol and (b) H-DTQ' silicone resin

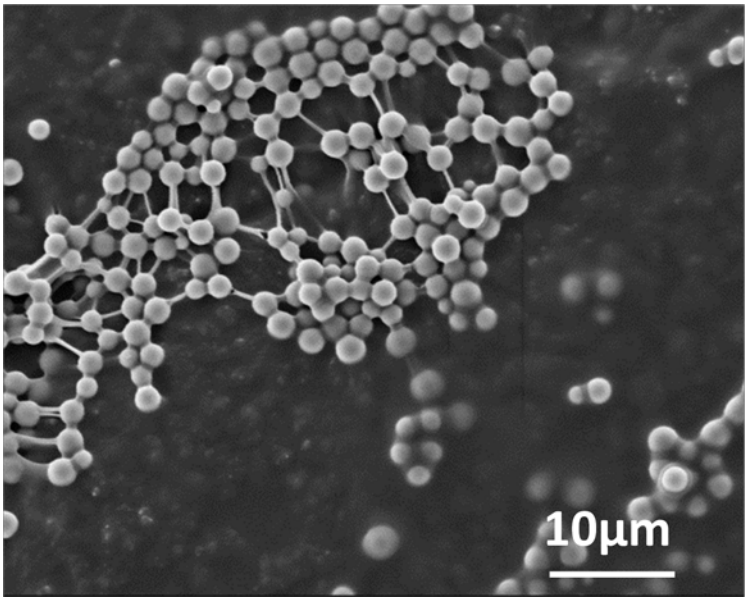

Figure 4-20 SEM image of TiO_2 particles prepared by sol-gel synthesis (titanium butoxide:H_2O:ethanol =1:1.25:15) and precipitation in acetone.

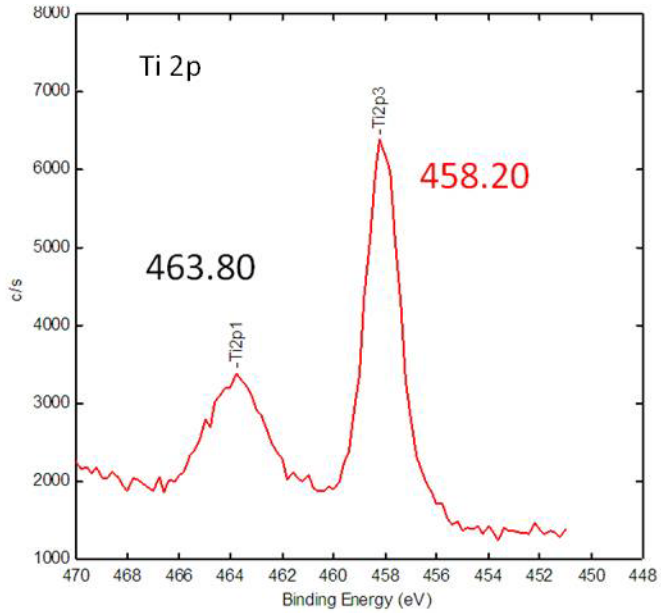

Figure 4-21 XPS characterization of TiO_2 particles drop casted on silicon wafer.

Since the aforementioned one-pot synthesis can only yield H-DTQ' silicone resin containing short D segments, the synthesis of Q' and H-DTQ' are separated in the experiments described next (Figure 4-19). In the first step, transparent TiO_2 sol in ethanol was prepared by hydrolysis of titanium butoxide following the literature recipe.[32] The particles (branched oligomers) were precipitated in acetone because the non-polar acetone solvent is an unfavorable solvent for the polar particles. As is shown in Figure 4-20, the precipitates have an interconnected spherical morphology. It is noted from XPS spectra (Figure 4-21) that there is a peak at 458.20 eV (Ti $2p_{3/2}$ in TiO_2), which reveals the existence of TiO_2.

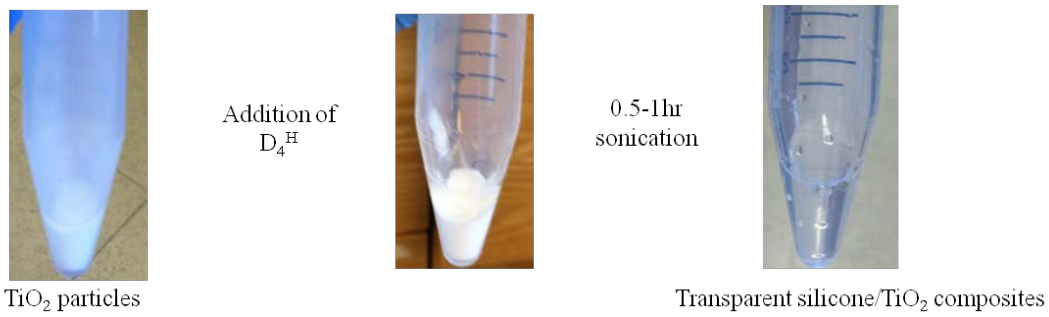

Figure 4-22 Synthesis of H-DTQ' silicone resin by mixing D_4^H and TiO_2 particles

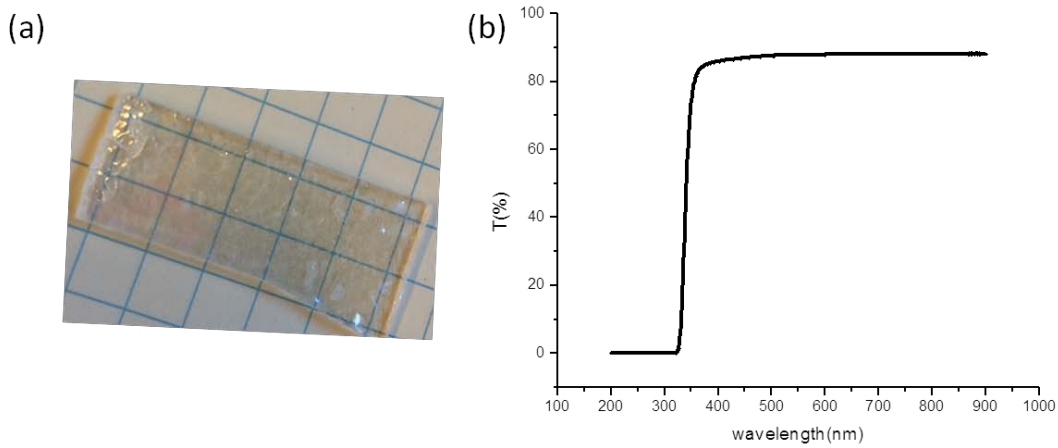

Figure 4-23 (a) Image and (b) UV-Vis transmission of H-DTQ' silicone resin with 33 wt% TiO_2 content on a quartz slide. H-DTQ' silicone resin is formed by mixing D_4^H and TiO_2 particles. (the H-DTQ' siilcone sample thickness is around 10 μm)

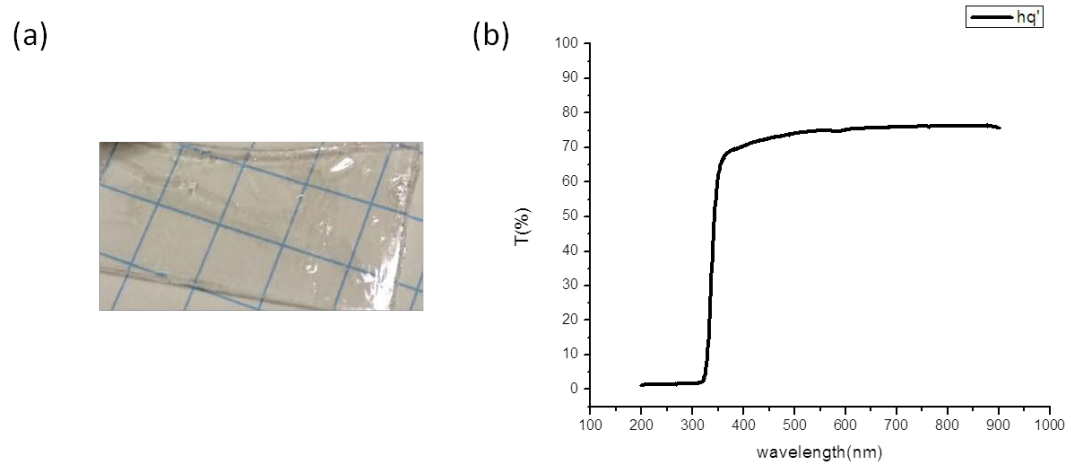

Figure 4-24 (a) Image and (b) UV-Vis transmission of H-DTQ' silicone resin with 25 wt% TiO_2 content on a quartz slide. H-DTQ' silicone resin is formed by mixing PDMS-H (M_w~1800-2100) and TiO_2 particles. (H-DTQ' silicone sample thickness is 3 μm)

In the following step, the precipitates were covered by D_4^H, and sonicated together until a transparent liquid composite was attained (Figure 4-22). The experimental process was similar when D_4^H was substituted with PDMS-H. PDMS-H can react with the branched polytitanate oligomers and give rise to H_2 byproduct. Hence, only thin film samples were prepared to allow hydrogen to escape. Exposure of the liquid composite film to air leads to further condensation between Ti-OH and Ti-OH, Si-H and Si-H, Ti-OH and Si-H. The final product is a cross-linked silicone network (solid H-DTQ' silicone resin). Figure 4-23 and Figure 4-24 display the excellent optical transparency of H-DTQ' having a TiO_2 loading of 33 wt% and 25 wt%, respectively. However, these thin films have poor fracture toughness, which is ascribed to their high T content. T silicone is more densely cross-linked, more brittle and harder than D silicone.

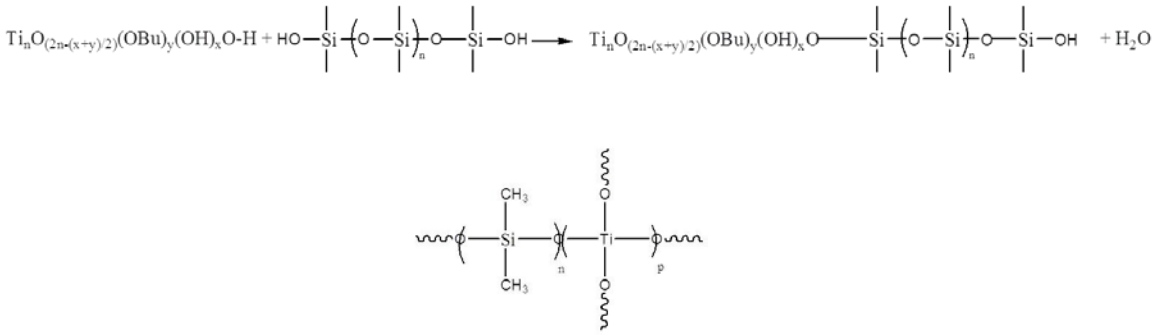

Figure 4-25 Synthesis and molecular structure of DQ' silicone resin

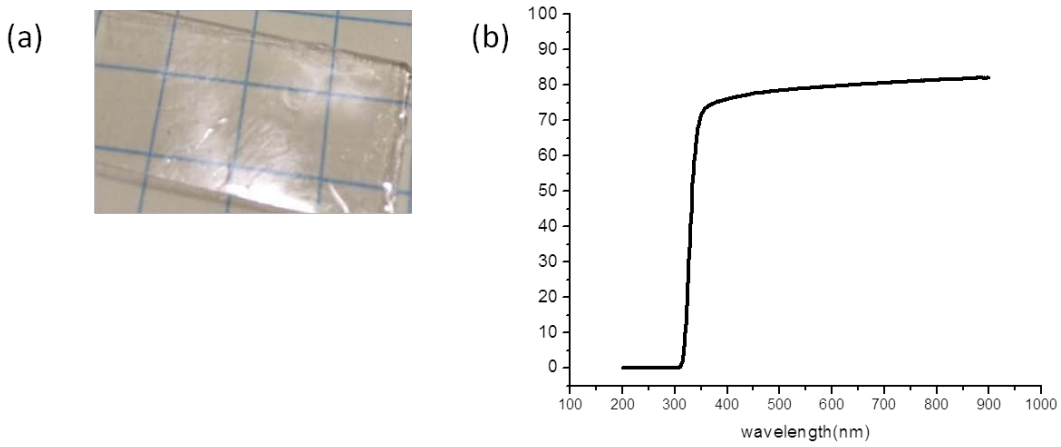

Figure 4-26 (a) Image and (b) UV-Vis transmission of DQ' silicone resin with 25 wt% TiO_2 content on a quartz slide. DQ' silicone resin is formed by mixing PDMS-OH (M_n~ 550) and TiO_2 particles. (DQ' silicone sample thickness is 19 μm)

In Figure 4-25, T silicone is eliminated from the silicone resin preparation recipe to acquire a mechanically robust (good resistance to fracture) silicone composite. Hydroxyl-terminated PDMS is utilized to react with branched titanate oligomer to yield DQ' silicone resin. This DQ' silicone resin is a liquid just after sonication. A transparent liquid thin film is casted on a quartz slide, and it gradually solidifies due to the further reactions among titanols. A close examination of digital image Figure 4-26(a) suggests that DQ' silicone resin is smooth, containing no mechanical failures after fully cross-linking and drying.

Table 4-3 Refractive indices (measured with refractometer) of TiO_2/PDMS nanocomposites containing different silicone molecular units and TiO_2 content.

Type of silicone composite	TiO_2 content in silicone composites (wt%)	Refractive index
H-DTQ' silicone formed with D_4^H	33	1.4660 (D_4^H: 1.3870)
H-DTQ' silicone formed with PDMS-H	25	1.4528 (PDMS-H: 1.3960)
DQ' silicone formed with PDMS-OH	25	1.4585 (PDMS-OH: 1.4060)

Table 4-4 Storage modulus measured at 20 ^oC by DMA, refractive index measured by refractometer and transparency measured by UV-vis for ~1 mm thick cross-linked PDMS samples. (TiO_2 content= 5.5 vol%) (a)H-DTQ' silicone resin is cross-linked with PDMS-Vinyl (M_w~5000-7000, 167 ppm Pt). (b) H-DTQ' silicone resin is cross-linked with PDMS-vinyl (7.0-8.0% vinylmethylsiloxane-dimethylsiloxane copolymer, M_w~28000, 167 ppm Pt). In both samples, H-DTQ: PDMS-Vinyl= 1:2 (volume ratio).

Sample	Storage modulus (MPa)	Refractive index	Transparency (wavelength> 400nm)
(a)	42	1.4478	60%
(b)	56	1.4498	80%

The refractive indices of silicone/TiO_2 composites containing different silicone molecular structures were determined using a refractometer. The data are presented in Table 4-3. A titania loading of 25 wt% can result in a refractive index increase of around 0.5 for silicone. A titania loading of 33 wt% can increase the refractive index of silicone by 0.6, such as in the case of H-DTQ' formed from D_4^H. These listed data might be underestimates of the real composite refractive index value, because the samples may contain remnant butanol when they are characterized.

Hydrido-rich silicone/TiO_2 composites were cross-linked with two types of vinyl-containing PDMS. The experimental procedure is described in section 4.2.5. Optical properties of the new composites are listed in Table 4-4. It is seen that both samples have excellent transparency and high refractive index (~1.45), yet their storage modulus at room temperature vary (56 MPa and 42 MPa). It is concluded that

H-DTQ' can function as one building block to yield transparent, high refractive index silicone composites. Mechanical properties of the new composites are adjustable by varying vinyl group density.

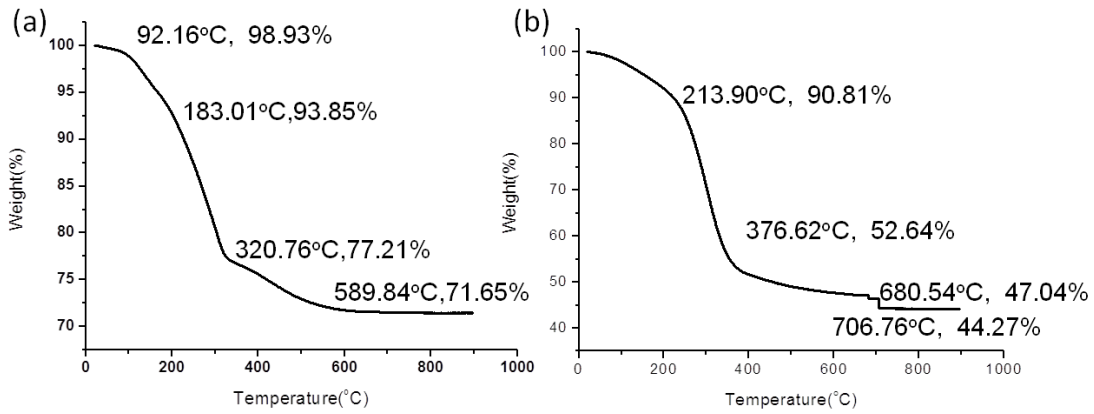

Figure 4-27 TGA curves of (a) H-DTQ' silicone resin with 25 wt% TiO_2 content formed by mixing PDMS-H (M_w~1800-2100) and TiO_2 particles ; (b) DQ' silicone resin with 25 wt% TiO_2 content formed by mixing PDMS-OH (M_n~ 550) and TiO_2 particles.

One problem with H-DTQ' silicone formed from D_4^H is that the mechanism of reaction between D_4^H and TiO_2 is scarcely discussed in literature. Tada's view about this reaction is that D_4^H rings can first react with TiO_2, forming lots of interfacial Ti-O-Si bonds. Then a second layer of D_4^H rings get absorbed and reacts with the first layer of D_4^H rings, giving rise to Si-O-Si bond. This reaction continues to build up multiple layers of D_4^H on TiO_2 Surfaces, which is equivalent to coating a SiO_x film on TiO_2.[23] However, it is hard to rule out the possibility that D_4^H rings open during the reaction.

Because of this complication, the other two composites in Table 4-3 attracted our interest in thermal property studies. Figure 4-27 show TGA analysis of the silicone composites in air. Two major mass loss stages are observed in the curves. The first mass loss step is below ~200 ^oC, which is caused by further condensation among

Ti-OH, Si-OH and Ti-OBu, evaporation of water and evaporation of butanol. The second step is from ~200 ^{o}C to 600 ^{o}C. This likely arises from the oxidation of organic moieties, such as methyl groups.[32] Comparing TGA results of two samples, it is evident that H-DTQ' is more thermally stable than DQ', probably because it has more cross-links in its structure. The poor thermal stability of our synthesized silicone/TiO_2 composites poses an obstacle for their real application as LED encapsulant materials.

4.4 Conclusions

In summary, we have demonstrated the preparation of transparent PDMS/SiO_2 and PDMS/ZrO_2 composites by mixing transparent sol and PDMS solution. Ligand molecules on particles along with silicone cross-linking reactions prevent phase separation of particles and polymer matrix. This dispersion strategy ensures good composite transparency. In contrast, it is quite difficult to disperse dry particles into silicone with mechanical blending.

Transparent PDMS/TiO_2 composites of high refractive index are prepared by sol-gel processes. A one-pot synthesis starting from polydibutyltitanate and silicone results in transparent silicone composites of varied refractive indices. In the two-step synthesis, branched titanate oligomers are achieved by partial hydrolysis and condensation of titanium butoxide. These oligomers (Q' structures) are 'miscible' with many functional silicones under sonication, so that they can be used to fabricate silicone composites of different molecular structure such as H-DTQ' and DQ'. TGA analysis reveals that the poor thermal stability of H-DTQ' and DQ' is one limitation for their application. These transparent, high refractive index silicone composites may

serve as good LED encapsulant materials that increase LED light-extraction efficiency.

4.5 References

1. Yang, X. F.; Shao, Q.; Yang, L. L.; Zhu, X. B.; Hua, X. L.; Zheng, Q. L.; Song, G. X.; Lai, G. Q., Preparation and performance of high refractive index silicone resin-type materials for the packaging of light-emitting diodes. *J Appl Polym Sci* **2013,** *127* (3), 1717-1724.

2. Sun, Y. P.; Gu, A. J.; Liang, G. Z.; Yuan, L., Preparation and Properties of Transparent Zinc Oxide/Silicone Nanocomposites for the Packaging of High-Power Light-Emitting Diodes. *J Appl Polym Sci* **2011,** *121* (4), 2018-2028.

3. Liu, J. G.; Nakamura, Y.; Ogura, T.; Shibasaki, Y.; Ando, S.; Ueda, M., Optically transparent sulfur-containing polyimide-TiO(2) nanocomposite films with high refractive index and negative pattern formation from poly(amic acid)-TiO(2) nanocomposite film. *Chem Mater* **2008,** *20* (1), 273-281.

4. Sato, H.; Iba, H.; Naganuma, T.; Kagawa, Y., Effects of the difference between the refractive indices of constituent materials on the light transmittance of glass-particle-dispersed epoxy-matrix optical composites. *Philos Mag B* **2002,** *82* (13), 1369-1386.

5. Li, Y. Q.; Fu, S. Y.; Yang, Y.; Mai, Y. W., Facile synthesis of highly transparent polymer nanocomposites by introduction of core-shell structured nanoparticles. *Chem Mater* **2008,** *20* (8), 2637-2643.

6. Wen, B.; Wang, F.; Zhang, S. M.; Ding, Y. F.; Yang, M. S., ZnO and ZnO-SiO2 core-shell structured fillers on properties of polycarbonate nanocomposites. *Plast Rubber Compos* **2010,** *39* (9), 419-424.

7. Godnjavec, J.; Znoj, B.; Vince, J.; Steinbucher, M.; Znidarsic, A.; Venturini, P., STABILIZATION OF RUTILE TiO2 NANOPARTICLES WITH GLYMO IN POLYACRYLIC CLEAR COATING. *Mater Tehnol* **2012,** *46* (1), 19-24.

8. Palkovits, R.; Althues, H.; Rumplecker, A.; Tesche, B.; Dreier, A.; Holle, U.; Fink, G.; Cheng, C. H.; Shantz, D. F.; Kaskel, S., Polymerization of w/o microemulsions for the preparation of transparent SiO2/PMMA nanocomposites. *Langmuir* **2005,** *21* (13), 6048-6053.

9. Lee, S.; Shin, H. J.; Yoon, S. M.; Yi, D. K.; Choi, J. Y.; Paik, U., Refractive index engineering of transparent ZrO2-polydimethylsiloxane nanocomposites. *J Mater Chem* **2008,** *18* (15), 1751-1755.

10. Nakayama, N.; Hayashi, T., Preparation and characterization of TiO2 and polymer nanocomposite films with high refractive index. *J Appl Polym Sci* **2007,** *105* (6), 3662-3672.

11. Schaer, E.; Guizani, S.; Choplin, L., Model development for the description of silica particles dispersion in silicone polymer. *Chem Eng Sci* **2006,** *61* (17), 5664-5677.

12. Tadros, T., Interparticle interactions in concentrated suspensions and their bulk (Rheological) properties. *Adv Colloid Interfac* **2011,** *168* (1-2), 263-277.

13. Hore, M. J. A.; Frischknecht, A. L.; Composto, R. J., Nanorod Assemblies in Polymer Films and Their Dispersion-Dependent Optical Properties. *Acs Macro Lett* **2012,** *1* (1), 115-121.

14. Lan, Q.; Francis, L. F.; Bates, F. S., Silica nanoparticle dispersions in homopolymer versus block copolymer. *J Polym Sci Pol Phys* **2007,** *45* (16), 2284-2299.

15. Vesaratchanon, J. S.; Nikolov, A.; Wasan, D. T., Sedimentation of concentrated monodisperse colloidal suspensions: Role of collective particle interaction forces. *J Colloid Interf Sci* **2008,** *322* (1), 180-189.

16. Alexandru, M.; Cristea, M.; Cazacu, M.; Ioanid, A.; Simionescu, B. C., Composite Materials Based on Polydimethylsiloxane and In Situ Generated Silica by Using the Sol Gel Technique. *Polym Composite* **2009,** *30* (6), 751-759.

17. Rajan, G. S.; Sur, G. S.; Mark, J. E.; Schaefer, D. W.; Beaucage, G., Preparation and characterization of some unusually transparent poly(dimethylsiloxane) nanocomposites. *J Polym Sci Pol Phys* **2003,** *41* (16), 1897-1901.

18. Chin Myung Whang, C. S. Y., and Yoo Hang Kim, Preparation and Characterization of Sol-Gel Derived SiO2-TiO2-PDMS Composite Films. *Bull. Korean Chem. Soc.* **2001,** *22*, 1366-1370.

19. Chan, C. K.; Peng, S. L.; Chu, I. M.; Ni, S. C., Effects of heat treatment on the properties of poly(methyl methacrylate)/silica hybrid materials prepared by sol-gel process. *Polymer* **2001,** *42* (9), 4189-4196.

20. Nakata, K.; Kimura, H.; Sakai, M.; Ochiai, T.; Sakai, H.; Murakami, T.; Abe, M.; Fujishima, A., UV/Thermally Driven Rewritable Wettability Patterns on TiO2-PDMS Composite Films. *Acs Appl Mater Inter* **2010,** *2* (9), 2485-2488.

21. Guan, C.; Lu, C. L.; Liu, Y. F.; Yang, B., Preparation and characterization of high refractive index thin films of TiO2/epoxy resin nanocomposites. *J Appl Polym Sci* **2006,** *102* (2), 1631-1636.

22. Krumpfer, J. W.; McCarthy, T. J., Rediscovering Silicones: "Unreactive" Silicones React with Inorganic Surfaces. *Langmuir* **2011,** *27* (18), 11514-11519.

23. Tada, H., Layer-by-Layer Construction of Siox Film on Oxide Semiconductors. *Langmuir* **1995,** *11* (9), 3281-3284.

24. Yan Liu, Z. L., Xueying Zhao, Kyoung-sik Moon, Sehoon Yoo, J Choi, C. P. Wong, High Refractive Index and Transparency Nanocomposites as Encapsulant for High Brightness LED packaging. *Electronic Components and Technology Conference* **2013**, 553-556.

25. Kosmulski, M., Chemical Properties of Material Surfaces. CRC Press: 2001.

26. Kantor, S. W.; Grubb, W. T.; Osthoff, R. C., The Mechanism of the Acid-Catalyzed and Base-Catalyzed Equilibration of Siloxanes. *J Am Chem Soc* **1954,** *76* (20), 5190-5197.

27. Fadeev, A. Y.; McCarthy, T. J., A new route to covalently attached monolayers: Reaction of hydridosilanes with titanium and other metal surfaces. *J Am Chem Soc* **1999,** *121* (51), 12184-12185.

28. Schaefer, D. W.; Kohls, D.; Feinblum, E., Morphology of Highly Dispersing Precipitated Silica: Impact of Drying and Sonication. *J Inorg Organomet P* **2012,** *22* (3), 617-623.

29. Lin, Y.; Wang, L. M.; Krumpfer, J. W.; Watkins, J. J.; McCarthy, T. J., Hydrophobization of Inorganic Oxide Surfaces Using Dimethylsilanediol. *Langmuir* **2013,** *29* (5), 1329-1332.

30. Schmidt, T.; Mennig, M.; Schmidt, H., New method for the preparation and stabilization of nanoparticulate t-ZrO2 by a combined sol-gel and solvothermal process. *J Am Ceram Soc* **2007,** *90* (5), 1401-1405.

31. Helmy, R.; Wenslow, R. W.; Fadeev, A. Y., Reaction of organosilicon hydrides with solid surfaces: An example of surface-catalyzed self-assembly. *J Am Chem Soc* **2004,** *126* (24), 7595-7600.

32. Xiang, H. P.; Ge, J. F.; Cheng, S. H.; Han, H. M.; Cui, S. W., Synthesis and characterization of titania/MQ silicone resin hybrid nanocomposite via sol-gel process. *J Sol-Gel Sci Techn* **2011,** *59* (3), 635-639.

CHAPTER 5
PERMEABILITY OF SILICONE THIN FILMS: MEASUREMENT AND CONTROL

5.1 Introduction

5.1.1 Concept, Theory and Influential Factors for Water Vapor Permeation

Gas permeation through polymer membranes is a research area with a long history. The first study dates back to 1892 by Thomas Graham.[1] There is an increasing research interest in gas, especially water vapor permeation through PDMS because PDMS is widely used in pervaporation.[2] Pervaporation is a liquid mixture separation process. Some of the permeant vaporizes, passes through the separation membrane, and gets removed from the mixture.[3] Industrial needs of the polymeric barrier layer have also promoted the studies on controlling moisture permeability.

Gas (such as water vapor) permeation through a polymer membrane involves three steps: adsorption of permeant by the polymer, diffusion of permeant through the polymer, and desorption of permeant from the other side of the polymer. The whole process can be described using Fick's diffusion law:[4,5]

$$J = -D\frac{\partial C}{\partial x} \qquad \text{Equation 5-1}$$

where J represents the permeation flux of the permeant, and D and C are the diffusion coefficient and permeant concentration, respectively. The film thickness, L, of the polymer membrane is usually small, so a steady state of permeant concentration profile is reached quickly. Integration of Equation 5-1 from x=0 (lower surface of the film) to x=L (upper surface) leads to another expression for flux.

$$J = \frac{D}{L}(C_0 - C_L) \qquad \text{Equation 5-2}$$

In Equation 5-2, C_0 and C_L denote permeant concentration at the lower surface and upper surface of the film, respectively. According to Henry's law, they can be related to the partial pressure of permeant at the two sides of the film, which we denote as p_0 and p_L. (Figure 5-1)

Solubility coefficient is,

$$K = \frac{C_0}{p_0} = \frac{C_L}{p_L} \qquad \text{Equation 5-3}$$

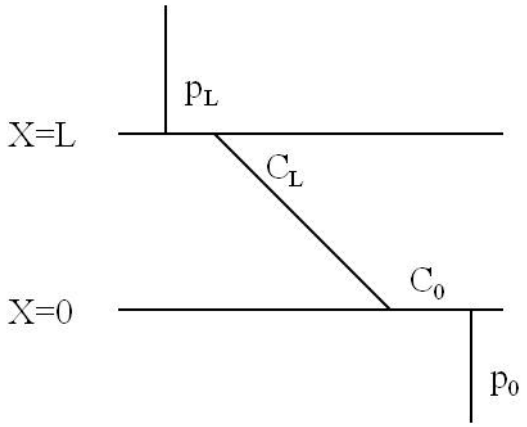

Figure 5-1 Pressure and concentration of permeant at two sides of polymer membrane

The permeability (coefficient) P is defined as the product of the diffusion coefficient and the solubility coefficient.

$$P = DK \qquad \text{Equation 5-4}$$

Therefore, the flux can be written in a third form.

$$J = \frac{DK}{L}(p_0 - p_L) = \frac{P}{L}(p_0 - p_L) \qquad \text{Equation 5-5}$$

For a polymer film with area A, the total amount of permeant penetrating through it after time Δt is $\Delta m = \frac{PA \cdot \Delta t}{L}(p_0 - p_L)$ Equation 5-6

So that permeability can be given as follows,

$$P = \frac{\Delta m}{\Delta t} \frac{L}{A(p_0 - p_L)} \qquad \text{Equation 5-7}$$

The unit for permeability recommended by Huglin and Zakaria is $\frac{cm^3 \cdot cm}{cm^2 \cdot s \cdot cmHg}$.[6]

Another parameter, the water vapor transmission rate, describes the amount of water transported through a certain area of a membrane within a given amount of time. It is commonly expressed in units of $g / m^2 \cdot 24h$.[7]

The permeability is a function of many variables. Important variables are permeant size, polymer characteristics, temperature and pressure.[8] Semicrystalline polymers contain both crystalline and amorphous components. The crystalline domains are impermeable and create longer pathways for permeant to diffuse through (tortuosity effect). Researchers used the following two equations to describe the solubility and the diffusivity of water in semicrystalline polymers,

$$S = S_a \phi_a \qquad \text{Equation 5-8}$$

$$D = D_a \phi_a^m \qquad \text{Equation 5-9}$$

where S_a and D_a are the solubility and the diffusivity for pure amorphous polymer, and ϕ_a is the amorphous part volume fraction. The value of m depends on the type of polymer, for example, it is 0.3 for polyethylene. Generally, higher crystallinity (smaller ϕ_a) indicates lower permeability. Other polymer characteristics impacting permeability include polymer polarity, orientation, degree of crosslinking, etc.

The effects of temperature on the permeability can be expressed in terms of an Arrhenius relationship,

$$P = P_0 \exp(-\frac{E_P}{RT}) \qquad \text{Equation 5-10}$$

Ep is the activation energy for permeation. The permeability usually increases with an increase of the temperature. The effect of pressure on permeability is more complicated. At pressures close to standard pressures where Henry's law is obeyed, permeability is considered as a material property, and is independent of pressure. At pressures where Henry's law no longer applies, the relationship between permeability and pressure can be very complex.

5.1.2 Water Vapor Permeability Measurement Methods

As early as 1969, O.C. Raspor summarized several convenient ways to measure water permeability of a test film.[9] He mentioned ASTM standard E96 (Figure 5-2). A cup containing either water or desiccant is sealed with the test film. The cup is maintained inside an environment with controlled humidity and temperature, and weight loss or weight gain of the setup is monitored. Both the water vapor transmission rate and the water vapor permeability can be obtained by this method.

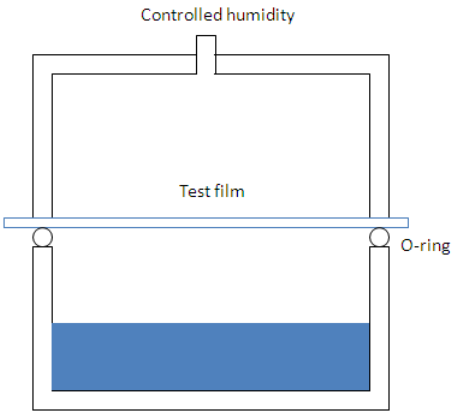

Figure 5-2 Scheme of apparatus for ASTM standard test method E96. The blue block represents water

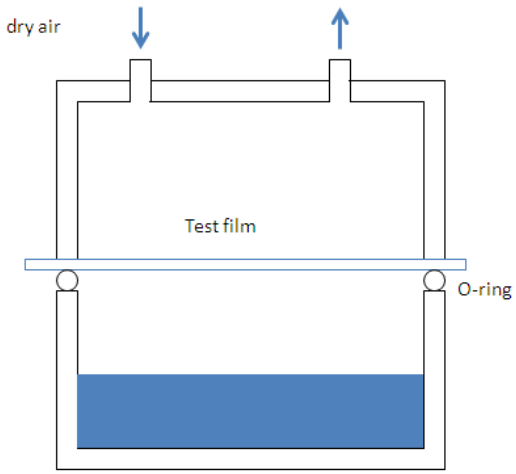

Figure 5-3 Scheme of apparatus for ASTM standard test method F1249. The blue block represents water

Many new methods have been developed to measure water permeability of a thin film. In test method ASTM standard F1249, a thin film is placed between a dry chamber and a wet chamber. Moisture penetrating through the thin film is carried away with sweeping dry air (Figure 5-3), and gets analyzed with an infrared energy sensor. The permeability of tested material can be back calculated with the infrared sensor signal.[7]

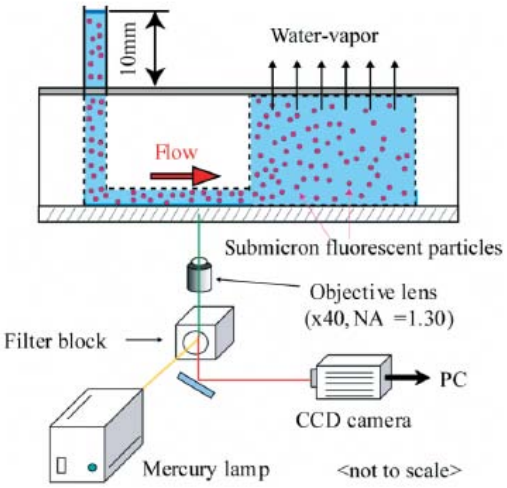

Figure 5-4 Scheme of microfluidic device to measure membrane permeability

Miki and coworkers designed a novel device to measure moisture transmission. The experimental setup is depicted in Figure 5-4. Volumetric flow comes into formation inside the microchannel with the evaporation of water vapor through polymer membrane. The flow velocity profile is recorded with the aid of a CCD camera. The permeation flux and the permeability coefficient can be derived from the velocity profile.[10]

5.1.3 Control of Water Permeability of Silicone Film

One strategy to modulate the permeability property of the membrane is through addition of particle fillers, which can either increase or decrease the permeability. When the particle incorporation leads to swelling of the membrane, the overall effect may be to enhance permeability by increasing the solubility K (Equation 5-3). Larsson and coworkers 'encapsulated' micron sized polymer powders Carbopol (Cross-linked polyacrylic acid) and Pemulen (copolymer of acrylic acid and C10-C30 alkyl acrylate) with room temperature vulcanized (RTV) silicone. Since hydrophilic

polymer fillers are used, water transmission becomes faster.[11] In addition to the hydrophilicity of fillers, the compatibility and adhesion between the membrane and fillers are also crucial for the effects of fillers on water transport:[5] Water vapor can penetrate through composite membranes via dual mechanisms, diffusion and capillarity. Nonselective voids are expected to exist at filler-polymer interface when their compatibility is poor. These voids can be considered as 'microcracks', and moisture transported through the microcracks would render a higher permeability value.[12] Furthermore, there is no direct correlation between hydrophilic fillers and improved permeability even if the non-ideal defects in filled polymer are completely eliminated. An example is the collagen/PDMS composite. Miki and coworkers introduced collagen powders to PDMS. Their measurements show reduced water permeability of PDMS.[10] The reason is that diffusivity of the water in collagen is quite low.[13]

Another strategy to alter water vapor transport through silicone film is coating a PDMS layer (structure layer) with a barrier layer. This 'multilayer film' approach to lower mass transport has shown its effectiveness in food packaging, such as jelly cups (PET-primer-LDPE-Appeel-polypropylene). [7]

5.1.4 Objectives

Encapsulants are used in electronic devices to prevent oxygen, water vapor and other gases from deteriorating the device substrate. Silicone shows great potential to serve as an encapsulant, because it contains low ionic impurities and tolerates a wide range of temperature and chemicals.[14] An objective of this research was to clarify that pure silicone has high water permeability to the scientific community. A customized permeability measurement setup was optimized to give repeatable and

accurate data. Adjusting and minimizing moisture transport through silicone film are some other primary interests of this research. The effect of cross-linking density and fillers on silicone water permeability was also systematically studied.

5.2 Experimental Section

5.2.1 Preparation of Cross-linked Silicone Thin Films

Clean glass slides were spin-coated with 1 wt% polyacrylic acid (PAA) aqueous solution at 500 rpm for 1 min after they were fully cleaned by oxygen plasma. Cross-linked silicone specimens were synthesized via hydrosilylation reaction in the presence of platinum-divinyltetramethyldisiloxane complex (Karstedt's catalyst) (Figure 5-5)[15] and anionic copolymerization (chapter 3). Vinyl-terminated PDMS samples (M_W~627 000 and 6000, Gelest, Inc.) were cross-linked with polymethylhydrosiloxane (M_W~2800, Gelest, Inc) to prepare elastomers of different cross-linking densities with a molar ratio of H: vinyl=15:1. 2 ppm Pt based on silicone product mass was added to the silicone mixture. Fillers, including amorphous octamethyltetrasiloxane-treated silica (Gelest, Inc.) and mica powders (Mineralite 3X, Mineral Mining Company, Inc), were dispersed into uncured silicone matrix by using a FlackTech Inc. SpeedMixer DAC 150.1. at 3500 rpm for 4 min. In order to reduce the mixture viscosity before spin-coating, hexane and Karstedt's catalyst were introduced into the mixture. Expanded polytetrafluoroethylene (PTFE) film Gore-Tex was fully soaked in the uncured silicone mixture, and then sandwiched between two glass slides before their placement in a heating oven at 105 ^{o}C for curing. PTFE was selected due to its much lower water vapor transmission rate (0.0045 $g \cdot mm / m^2 \cdot day$ at 20^{o}C) compared to that of silicone rubber (1.73-3.11 $g \cdot mm / m^2 \cdot day$).[7] GE Premium Waterproof Silicone and Dow Corning Sylgard 184 were purchased and

used as received. Sylgard 184 silicone elastomer was fabricated by mixing prepolymer with cross-linker in the weight ratio of 15:1. Fully cured thermoplastic silicone-polyimide block copolymer (PI-PDMS) was purchased from Gelest, Inc.

The silicone or silicone composite mixture was spin-coated on a PAA-coated glass slide at 300 rpm for 1 min. These coated slides were heated at ~105 ^{o}C for one day before the silicone films were floated on Deionized (DI) water. (Figure 5-6) Pinhole-free silicone thin films of uniform thickness were obtained. Optical profilometry (Zygo, NewView 7300, 10× lens) was used to determine film thickness information at five different spots of a single sample.

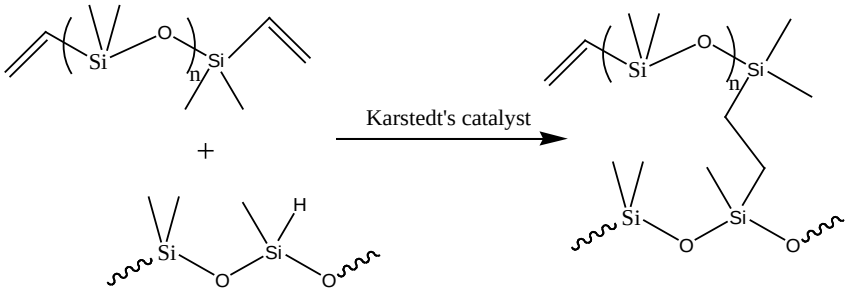

Figure 5-5 Platinum-catalyzed hydrosilylation reaction with Karstedt's catalyst

Figure 5-6 Schematic depiction of the silicone film floating on water

Extremely cross-linked silicone was prepared via the hydrosilylation reaction of 1,3,5,7-tetravinyl-1,3,5,7-tetramethylcyclotetrasiloxane (D_4^V, Dow Corning) and 1,3,5,7-tetramethylcyclotetrasiloxane (D_4^H, Gelest, Inc.) in the presence of Karstedt's catalyst (12 ppm Pt based on silicone mass) in a molar ratio of D_4^H : D_4^V=2:1. The

mixture was poured into a Petri dish to embed an o-ring, and heated at 60 ^{o}C overnight to obtain half-cured silicone. Fully-cured silicone was attained after the sample was further heated at 105 ^{o}C for two days. Thickness of D_4^H-D_4^V silicone samples was measured at three locations with a micrometer.

Scanning electron microscopy (SEM) was utilized to determine the filler dispersion in silicone matrix. Filled silicone samples were cryo-fractured in liquid nitrogen. SEM images were obtained using a JEOL NeoScope (JCM 5000).

Water solubility was evaluated with a Sartorius Ultramicrobalance (accuracy ±0.0001mg). Three pure silicone films were soaked in Milli-Q water for 38 days at room temperature, and their weights m_∞ were measured after they were gently wiped with soft absorbance paper and air-dried for around 15s. Then these films were fully dried inside JEOL NeoScope (JCM 5000), and their weights m_0 were immediately measured after they were taken out from the benchtop SEM. Solubility is calculated as $C = \frac{m_\infty - m_0}{m_0}$. Solubility coefficient can be further derived using the equation of $K = \frac{C}{p}$, where $p = 1\ atm$.

5.2.2 Water Permeability Measurements

An experimental setup to measure water permeability was constructed in our lab according to ASTM standard F1249, and the only difference from the ASTM standard is that dry nitrogen replaces dry air. (Figure 5-3) Tubes made of pyrex glass containing a lid and rubber O-ring joints were filled with water. The test film was placed between the lid and the bottom tube, and two separate chambers were formed.

The tube and lid were clamped tightly together in the presence of O-ring joints. The air gap between water and the silicone film was controlled below 1 cm. The upper chamber of the assembly was segregated from the environment but swept by dry nitrogen. The permeation cups were weighed after they were exposed in air for one day, to avoid errors from time lag.[16] The weight of the assembly was recorded with a balance at different time, and linear regression was applied to the plot of mass loss versus time to get the slope. Temperature during the measurement was controlled at 20 ^{o}C. Ultimately, water permeability of the test film can be estimated by using Equation 5-7. For each sample, at least three replicate films were prepared separately and measured, and the results were averaged.

5.2.3 Water Diffusivity Measurements with ATR-IR

Water diffusivity of silicone films were obtained using a PerkinElmer Spectrum 100 spectrometer equipped with ATR accessary (ZnSe crystal). A silicone film covered by a few overlaying filter papers was directly placed on the ZnSe crystal to record the spectra. 50 μL water was injected into the filter paper at the same time as data acquisition started. Spectra was acquired at 40s time intervals until the water absorption peak intensity in the range of 3700-3000 cm^{-1} remained constant.

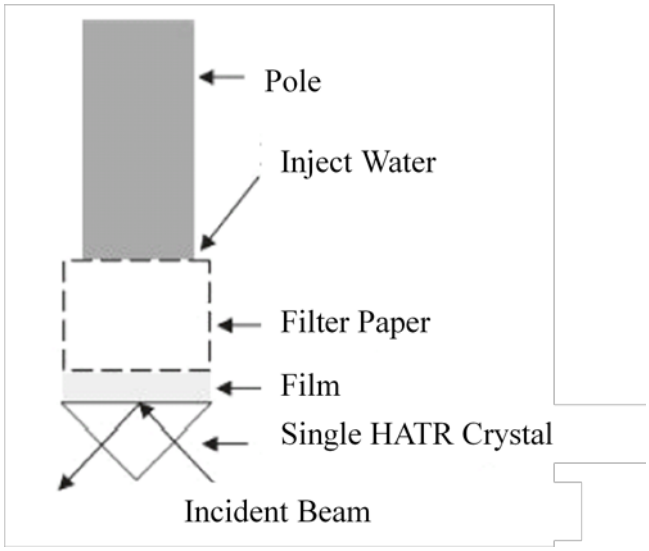

Figure 5-7 ATR-FTIR Experimental Configuration

Equation 5-11 was used to estimate the water diffusion coefficient D in polymer based on the ATR-IR spectra. In the equation, A_t is the water band absorbance at time t, A_∞ is the band absorbance at equilibrium, and γ represents the reciprocal of the penetration depth of the evanescent wave. λ is the wavelength of the infrared beam in the ATR element, θ is the incidence angle of radiation at the polymer/element interface, and n_{21} is the ratio of the refractive index of polymer to that of the element. The diffusion coefficient is derived from a nonlinear $\frac{A_t}{A_\infty} \sim t$ curve fitting.

$$\frac{A_t}{A_\infty} = 1 - \frac{8\gamma}{\pi[1-\exp(-2\gamma L)]}\sum_{n=0}^{\infty}\left[\frac{\exp(g)[f\exp(-2\gamma L)+(-1)^n(2\gamma)]}{(2n+1)(4\gamma^2+f^2)}\right]$$

$$g = \frac{-D(2n+1)^2\pi^2 t}{4L^2},\ f = \frac{(2n+1)\pi}{2L},\ \gamma = \frac{2\pi n_1(\sin^2\theta - n_{21}^{\ 2})^{1/2}}{\lambda} \qquad \text{Equation 5-11}$$

5.3 Results and Discussion

5.3.1 Literature Studies

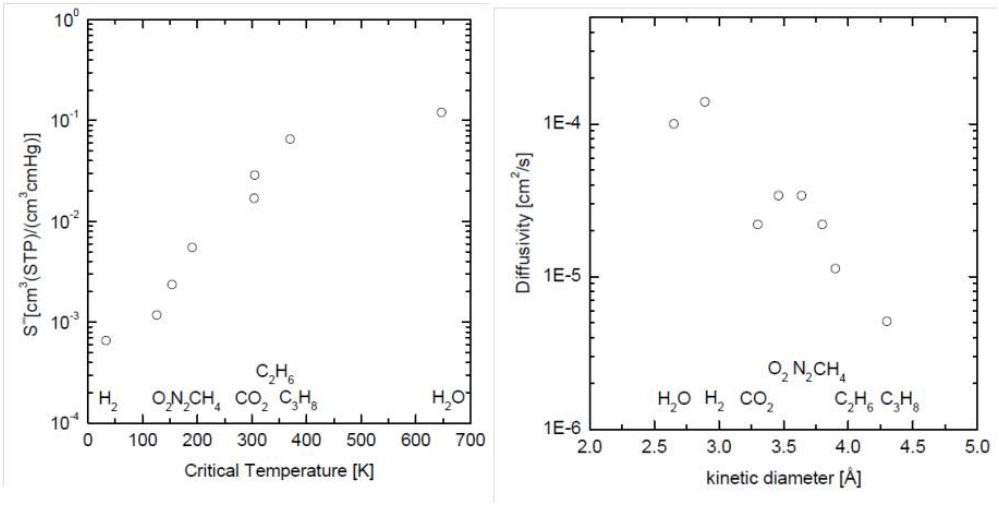

Figure 5-8 Solubility coefficient and diffusion coefficient at infinite dilution at 35 °C. Data reproduced from Merkel et. al. and water from Barriel.[17]

Water transport in silicone arouses lots of interest in both industry and academia. Some researchers are still 'mistakenly' using silicone as water sealant for permeation cells to carry out water vapor transport measurements,[18,19] and some other researchers neglect water permeability of silicone in microfluidic device studies.[20] Even in the studies where hydrophobic silicone was recognized as highly water permeable, [21] ambiguity still exists - the authors do not cite any references,[22] or they refer to literature about filled silicone instead of unfilled silicone.[23,24] There is also no convincing explanation about why silicone is more water permeable than many other polymeric materials. Metz claims in his PhD thesis[25] that water solubility and diffusivity are both high for PDMS compared with other gas penetrants, yet his argument is derived from the data comparison of two separate papers (Figure 5-8). In his plot, permeability of various gases through PDMS were characterized with a 'constant pressure' methodology,[26] whereas water vapor permeability was determined

under pressure changes.[17] Therefore, it is worthwhile to systematically investigate water permeability of pure silicones.

5.3.2 Water Permeability of Pure Silicone

Figure 5-9 gives direct contrast of water permeabilities through vegetable oils and silicone oil. Water sealed by a thin layer of silicone oil appears to permeate much faster than water sealed by vegetable oils. The more than 1 cm water level drop (Figure 5-9(e)) after 6 days of water evaporation clearly differentiates the siloxane polymer from the carbon-based oils.

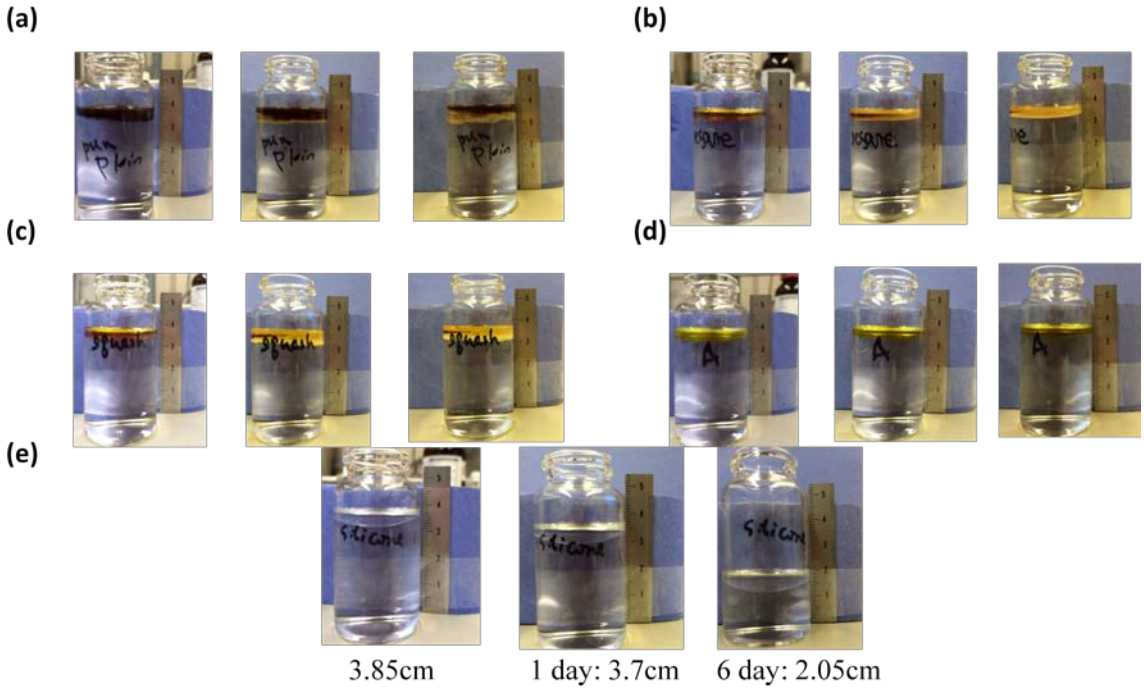

Figure 5-9 Water level changes with time when 17 mL water was covered by 1 mL (a) Pumpkin seed oil, (b) Sesame oil, (c) Squash oil, (d) Avocado oil, (e) Silicone oil (trimethylsiloxy-terminated polydimethylsiloxane, viscosity=350 cSt)

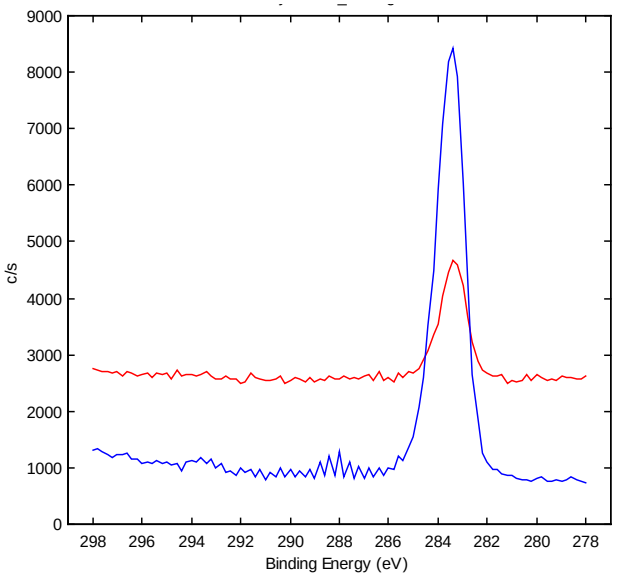

Figure 5-10 XPS spectra of silicone film surface. (red curve, 15^{o} take-off angle; blue curve, 75^{o} take-off angle)

From the X-ray photoelectron spectroscopy data (Figure 5-10), it is concluded silicone film fabricated with spin-coating and film floating contains no residual PAA on the sample surface. The absence of a C peak at a binding energy above 288eV implies the absence of carboxyl groups. The peak at 283eV corresponds to carbon bonded to silicon.

Table 5-1 Water permeability of saran wrap (Saran wrap:Poly(vinylidene chloride-co-acrylonitrile). Unit of permeability is $\times 10^{-9} \frac{cm^3 \cdot cm}{cm^2 \cdot s \cdot cmHg}$

Saran Wrap	
Measured permeability	8.4

Table 5-2 Measured water permeability of Sylgard 184 with different measurement time. Unit of permeability is $\times 10^{-9} \frac{cm^3 \cdot cm}{cm^2 \cdot s \cdot cmHg}$.

Sylgard 184			
Measurement time (min)	8000	14000	17000
Permeability	3304±462	3222±441	3185±425

Accuracy and repeatability of customized cup method were tested prior to all other measurements. The measurement result of Saran wrap in Table 5-1 is 8.4 $\times 10^{-9} \frac{cm^3 \cdot cm}{cm^2 \cdot s \cdot cmHg}$. It is in agreement with the reported literature value of 5.3 $\times 10^{-9} \frac{cm^3 \cdot cm}{cm^2 \cdot s \cdot cmHg}$. [27] Furthermore, this water resistant saran layer was coated on the silicone film to decrease its water permeability, and the silicone permeability value was sharply reduced from 4756±576 to $79 \pm 7 \times 10^{-9} \frac{cm^3 \cdot cm}{cm^2 \cdot s \cdot cmHg}$.

It is shown in Table 5-2 that the measured Sylgard 184 water permeability value is almost constant a different measurement times (different air gap between water level and film). All the data in Table 5-1 and Table 5-2 reflect the fact that our customized cup method produces accurate and reproducible characterization results. The measurement time was controlled under 17 000 min for all experiments reported in this chapter to prevent formation of a stagnation air layer beneath the film, ensuring good contact of saturated water vapor and silicone film.

Table 5-3 Water permeability and diffusivity in silicones of different molecular structure

Unit of permeability is $\times 10^{-9} \frac{cm^3 \cdot cm}{cm^2 \cdot s \cdot cmHg}$, and unit of diffusivity is $\times 10^{-8} cm^2 / s$.

(Pure silicone (62 700): PDMS-Vinyl (M_w~62 700), PDMS-H (M_w~1800-2100), H: vinyl=15:1, 2 ppm Pt. Living silicone: D_4 and bis-D_4 copolymerized by 0.2 wt% tetramethylammonium disiloxnolate; PI-PDMS: fully cured thermoplastic silicone-polyimide block copolymer).

	Pure silicone (62 700)	**GE one component RTV**	**Sylgard 184**	**Living silicone**	**PI-PDMS**

			silicone		
Permeability	4756±576	2371±317	3185±425	7000±1132	377±150
Diffusivity	81.4	5.37	78	313	

The reproducible measurement results of water permeability and diffusivity for various silicones are summarized in Table 5-3. Both water diffusivity and permeability values bring into our attention to the significant water transport rate in silicone. Our measured diffusivity result of pure silicone (M_w~62 700) (81.4 $\times 10^{-8} cm^2 / s$) is smaller than other researchers' measurement results ($10^{-4} \sim 10^{-5} cm^2 / s$)[28]. However, this water diffusivity data is still higher than the diffusivity of most other types of polymer, according to the Polymer Handbook.[29] It is also confirmed by the data in Table 5-3 that pure silicone, two types of commercial silicone and living silicone all exhibit very high water permeability (~$4000 \times 10^{-9} \frac{cm^3 \cdot cm}{cm^2 \cdot s \cdot cmHg}$) value.

The measured water solubility of pure silicone (62 700) is 158±93 mol/m^3. This compares with a literature value of 40 mol/m^3.[28] The literature value does not include error analysis and so it is difficult to compare with our obviously imprecise value. After unit conversion, our measured solubility coefficient of pure silicone is 2.9±1.7 $\times 10^{-8} Pa^{-1}$(On the other hand, the solubility value is estimated based on the measured permeability and measured diffusivity, which gives a value of 4.4 $\times 10^{-3} Pa^{-1}$). This measured silicone water solubility coefficient of 2.9±1.7 $\times 10^{-8} Pa^{-1}$ is small compared with water solubility of many other polymers in the Polymer Handbook.[29]

These uncommon water transport properties for a water repellent polymer are probably due to the special structural features of the siloxane polymer: 1) Silicone has high free volume resulting from the large rotational and vibrational degree of freedom

of the polysiloxane chain. 2) O-H bond length is smaller than the Si-C or Si-O bond lengths, so the water molecule appears even smaller in comparison with the siloxane polymer free volume. 3) The Si–O bond is actually 51% ionic,[30,31] and the polar backbone can attract water on its vicinity. Free rotation of methyl side groups can fully expose the macromolecule backbone to water, which aids to the transport of water across silicone film.

The very high gas diffusivity and permeability limits the application of silicone as an encapsulant material.[7] A careful examination of water permeability values for different types of silicone in Table 5-3 implies additives and special functional groups can drastically affect the water transport rate. Commercial silicones contain a large quantity of additives, and they can decrease water permeability to certain extents. The decreased water permeability of PI-PDMS in comparison with pure silicone may be the result of the less water-permeable PI block. On the contrary, living silicone maintains higher permeability, which might be ascribed to the 'water carrier' tetramethylammonium cation. The variation trend of diffusivities is shown to closely correlate with that of permeability.

5.3.3 Water Permeability Control of Silicone

In some engineering applications, silicone water permeability requires careful control. For instance, water permeating through electronic devices can corrode electronics, producing unwanted chemicals. In the case of silicone light emitting diodes (LEDs) encapsulants, moisture absorbed by phosphors can alter light output. Therefore, an understanding and implementation of silicone permeability control is beneficial for its application in electronics.

The effect of filler addition on the rubbery polymer permeability has always been controversial in the literature. The traditional view about nonporous filler-filled polymer is that these fillers can increase the diffusion path length, and decrease both diffusion coefficient and permeability.[32] However, dewetting of polymer chains on particle surfaces results in defects, and it complicates the transport issue.[33] Enhanced permeability was attained for some polymer systems, for example, Sylgard 184 filled with chlorodimethylsilane-modified fume silica is reported to be of higher water permeability and diffusivity compared with its unfilled counterpart.[34] Li and coworkers incorporated titanate nanotubes in PDMS. They noticed increased fractional free volume of the membranes, which accounts for the enhanced membrane permeability and selectivity.[35]

Table 5-4 Water permeability and diffusivity of silicones containing different fillers

Unit of permeability is $\times 10^{-9} \frac{cm^3 \cdot cm}{cm^2 \cdot s \cdot cmHg}$, and unit of diffusivity is $\times 10^{-8} cm^2 / s$.

(CAB-O-SIL® TS-720: PDMS modified amorphous silica; D_4-SiO_2: octamethylcyclotetrasiloxane modified amorphous silica; Gor-Tex film: stretched polytetrafluoroethylene film).

	Pure silicone (62 700)	**Silicone filled with 20 wt% D_4-SiO_2**	**Silicone filled with 1 wt% D_4-SiO_2**	**Silicone filled with 1wt% TS-720**	**Silicone filled with Gor-Tex film**	**Silicone filled with 0.03 wt% mica powders**
Permeability	4756±576	1988±306	3283±147	3364±493	4665±38	4077
Diffusivity	81.4	8.14				

We explored how silanized silica affects the transport properties of cross-linked silicone thin films. Table 5-4 presents water permeability of silicone containing 0 wt%, 1 wt% and 20 wt% hydrophobized silica, as well as silicone/Gor-tex composites and silicone/mica composites. Morphologies of all the fillers are shown in

Figure 5-11. A small quantity (1 wt%) of spherical-shaped, hydrophobized silica can slightly decrease water permeability, while a large amount of the silica (20 wt%) is capable of dramatically decreasing the water permeability (around 50% of the pure silicone permeability value). Addition of hydrophobic Gor-Tex film or small amount of mica powder does not adjust permeability value much.

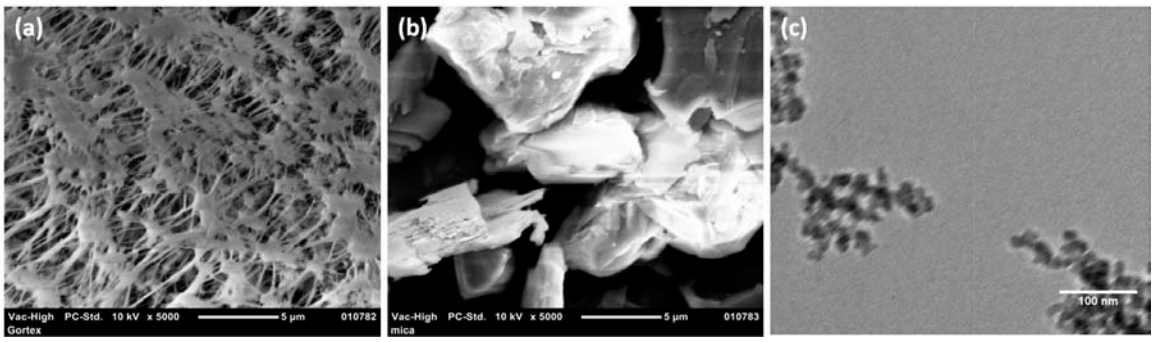

Figure 5-11 Morphologies of different fillers: (a) Gor-Tex film, (b) mica powder, (c) octamethylcyclotetrasiloxane modified amorphous silica.

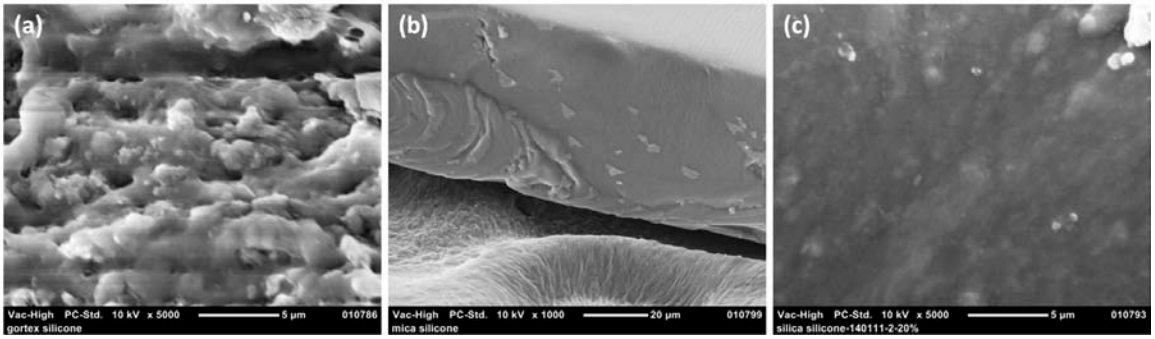

Figure 5-12 Morphologies of different filler-filled silicone samples: (a) Gor-Tex film, (b) 0.03 wt% mica powder, (c) 20 wt% octamethylcyclotetrasiloxane-modified amorphous silica.

Cross-sectional SEM images of silicone composites are shown in Figure 5-12. It is observed that lots of cavities are present in the silicone composite containing Gor-Tex film (Figure 5-12(a)), which is due to the dewetting of silicone from Teflon. These cavities can increase water permeability, yet Teflon can reduce the overall water permeability. Gor-Tex film-filled silicone has a similar water permeability

value as pure silicone, suggesting that the above two factors counterbalance each other. Figure 5-12(b) reveals limited amounts of mica powders do not alter the film morphology much, and this explains the composite's similarity to pure silicone in permeability. It is displayed in Figure 5-12(c) that silica nanoparticles compactly stack in the composites. The noticeable decrease in water permeability for silicone filled with silica compared with pure silicone, may result from the tortuous pathway generated by the particles.

Table 5-5 Water permeability and diffusivity of silicones of different cross-linking density

Unit of permeability is $\times 10^{-9} \frac{cm^3 \cdot cm}{cm^2 \cdot s \cdot cmHg}$, and unit of diffusivity is $\times 10^{-8} cm^2 / s$.

(Pure silicone(62 700): PDMS-Vinyl(M_w~62 700), PDMS-H(M_w~1800-2100), H: vinyl=15:1, 2 ppm Pt; Pure silicone(6000):PDMS-Vinyl(M_w~6000), PDMS-H(M_w~1800-2100), H: vinyl=15:1, 2 ppm Pt; D_4^H-D_4^V (partially cured): H: vinyl=2:1, 12 ppm Pt, cured at 60 ^oC overnight; D_4^H-D_4^V (fully cured): H: vinyl=2:1, 12 ppm Pt, cured at 60 ^oC for 1day, and then 105 ^oC for 2 days)

	Pure silicone (62 700)	**Pure silicone (6000)**	**D_4^H-D_4^V (partially cured)**	**D_4^H-D_4^V (fully cured)**
Permeability	4756±576	3667±501	1827±382	687±76
Diffusivity	81.4	15.8		

Data in Table 5-5 display the effect of cross-linking density on silicone permeability. Pure silicone (62 700), pure silicone (6000) and D_4^H-D_4^V are selected to represent lightly cross-linked silicone, medium cross-linked silicone and highly cross-linked silicone, respectively. It is observed water permeability decreases with increased silicone cross-linking density, probably because there is stronger disturbance for water transport when there are more cross-links.

5.4 Conclusions

The high water transport rate in pure silicone is not a clear concept in the literature. The ineffectiveness of silicone oil in sealing water vapor compared to vegetable oils was demonstrated as a visual proof that silicone is quite water permeable. Silicone or silicone composite films of uniform thickness were successfully attained by using spin-coating. Pure silicone films prepared by hydrosilylation and anionic copolymerization, along with two types of commercial silicone films all exhibited high water permeability and diffusivity values, which is likely due to the special structure features (i.e. large free volume) of siloxane polymer. Introduction of more water resistant polyimide blocks, silanized silica particles and saran coating layers can decrease water permeability of silicone. The permeability of silicone also decreases with increased cross-link density. Overall, the high water permeability of pure silicone was accurately measured, and several successful approaches to control this high permeability value were developed.

5.5 References

1. Stannett, V., The transport of gases in synthetic polymeric membranes-an historic perspective. *J Membrane Sci* **1978,** *3* (2), 97-115.

2. Dobrak, A.; Figoli, A.; Chovau, S.; Galiano, F.; Simone, S.; Vankelecom, I. F. J.; Drioli, E.; Van der Bruggen, B., Performance of PDMS membranes in pervaporation: Effect of silicalite fillers and comparison with SBS membranes. *J Colloid Interf Sci* **2010,** *346* (1), 254-264.

3. Shao, P.; Huang, R. Y. M., Polymeric membrane pervaporation. *J Membrane Sci* **2007,** *287* (2), 162-179.

4. Topcuoglu, O.; Altinkaya, S. A.; Balkose, D., Characterization of waterborne acrylic based paint films and measurement of their water vapor permeabilities. *Prog Org Coat* **2006,** *56* (4), 269-278.

5. Comyn, J., *Polymer Permeability*. Elsevier Applied Science Publishers LTD: 1985.

6. Huglin, M. B.; Zakaria, M. B., Comments on Expressing the Permeability of Polymers to Gases. *Angew Makromol Chem* **1983,** *117* (Nov), 1-13.

7. Massey, L. K., *Permeability properties of plastics and elastomers- a guide to packaging and barrier materials*. Plastics Design Library/ Willam Andrew Publishing: 2003.

8. Suloff, E. C. Virginia Tech.

9. W.R.R.Park, *Plastics film technology*. Reinhold Book Corporation: 1969.

10. Zhang, Y. H.; Ishida, M.; Kazoe, Y.; Sato, Y.; Miki, N., Water-Vapor Permeability Control of PDMS by the Dispersion of Collagen Powder. *Ieej T Electr Electr* **2009,** *4* (3), 442-449.

11. Borde, A.; Larsson, M.; Odelberg, Y.; Hagman, J.; Lowenhielm, P.; Larsson, A., Increased water transport in PDMS silicone films by addition of excipients. *Acta Biomater* **2012,** *8* (2), 579-588.

12. Shirazi, Y.; Ghadimi, A.; Mohammadi, T., Recovery of alcohols from water using polydimethylsiloxane-silica nanocomposite membranes: Characterization and pervaporation performance. *J Appl Polym Sci* **2012,** *124* (4), 2871-2882.

13. J. Chen, S. S., W. Liu, M. Scott, L. Lacy, S. Allen, S. A. Wickline, X. Yu, Contributions of Collagen Matrix to Restricted Water Diffusion in Post-infarct Rat Heart. *Proc. Intl. Soc. Mag. Reson. Med* **2003,** *11*, 887.

14. Nakata, K.; Kimura, H.; Sakai, M.; Ochiai, T.; Sakai, H.; Murakami, T.; Abe, M.; Fujishima, A., UV/Thermally Driven Rewritable Wettability Patterns on TiO2-PDMS Composite Films. *Acs Appl Mater Inter* **2010,** *2* (9), 2485-2488.

15. Speier, J. L.; Webster, J. A.; Barnes, G. H., The Addition of Silicon Hydrides to Olefinic Double Bonds .2. The Use of Group-Viii Metal Catalysts. *J Am Chem Soc* **1957,** *79* (4), 974-979.

16. J, C., Mathematics of diffusion. 2nd Edition ed.; Oxford University Press: 1975.

17. Barrie, J. A.; Machin, D., Sorption and Diffusion of Water in Silicone Rubbers .1. Unfilled Rubbers. *J Macromol Sci Phys* **1969,** *B 3* (4), 645-&.

18. Wan, V. C. H.; Kim, M. S.; Lee, S. Y., Water vapor permeability and mechanical properties of soy protein isolate edible films composed of different plasticizer combinations. *J Food Sci* **2005,** *70* (6), E387-E391.

19. Mchugh, T. H.; Avenabustillos, R.; Krochta, J. M., Hydrophilic Edible Films - Modified Procedure for Water-Vapor Permeability and Explanation of Thickness Effects. *J Food Sci* **1993,** *58* (4), 899-903.

20. Randall, G. C.; Doyle, P. S., Permeation-driven flow in poly(dimethylsiloxane) microfluidic devices. *P Natl Acad Sci USA* **2005,** *102* (31), 10813-10818.

21. Lenick, A., The Silicone Conundrum - Silicone Spectator. 2008.

22. Wright, P. S., Soft lining materials: their status and prospects. *J Dent* **1976,** *4*, 246-256.

23. Liu, R. X.; Qiao, X. Y.; Chung, T. S., The development of high performance P84 co-polyimide hollow fibers for pervaporation dehydration of isopropanol. *Chem Eng Sci* **2005,** *60* (23), 6674-6686.

24. Polymer Data Handbook. Mark, J. E., Ed. Oxford University Press, Inc: 1999.

25. S.J.Metz. Water Vapor and Gas Transport Through Polymeric Membranes. Universiteit Twente, Enschede, 2003.

26. Merkel, T. C.; Bondar, V.; Nagai, K.; Freeman, B. D.; Yampolskii, Y. P., Gas sorption, diffusion, and permeation in poly(2,2-bis(trifluoromethyl)-4,5-difluoro-1,3-dioxole-co-tetrafluoroethylene). *Macromolecules* **1999,** *32* (25), 8427-8440.

27. Oleg Roussak, H. D. G., Applied Chemistry: A Textbook for Engineers and Technologists. second ed.; Springer.

28. Watson, J. M.; Baron, M. G., The behaviour of water in poly(dimethylsiloxane). *J Membrane Sci* **1996,** *110* (1), 47-57.

29. J. Brandrup , E. H. I., E. A. Grulke Polymer Handbook. 4 ed.; John Wiley & Sons, Inc: 1999.

30. Rochow, E. G., *Introduction to the Chemistry of Silicones*. Wiley: 1953.

31. Pauling, L., The Nature of Silicon-Oxygen Bonds. *Am Mineral* **1980,** *65* (3-4), 321-323.

32. Merkel, T. C.; Freeman, B. D.; Spontak, R. J.; He, Z.; Pinnau, I.; Meakin, P.; Hill, A. J., Sorption, transport, and structural evidence for enhanced free volume in poly(4-methyl-2-pentyne)/fumed silica nanocomposite membranes. *Chem Mater* **2003,** *15* (1), 109-123.

33. Suer, M. G.; Bac, N.; Yilmaz, L., Gas Permeation Characteristics of Polymer-Zeolite Mixed Matrix Membranes. *J Membrane Sci* **1994,** *91* (1-2), 77-86.

34. Nisola, G. M.; Beltran, A. B.; Sim, D. M.; Lee, D.; Jung, B.; Chung, W. J., Dimethyl silane-modified silica in polydimethylsiloxane as gas permeation mixed matrix membrane. *J Polym Res* **2011,** *18* (6), 2415-2424.

35. Li, B.; Xu, D.; Zhang, X. F.; Jiang, Z. Y.; Wang, Y.; Ma, J.; Dong, X. A.; Wu, H., Rubbery Polymer-Inorganic Nanocomposite Membranes: Free Volume

Characteristics on Separation Property. *Ind Eng Chem Res* **2010,** *49* (24), 12444-12451.

CHAPTER 6
DIP-COATING DEPOSITION ON CHEMICALLY PATTERNED SURFACES: A MECHANISTIC ANALYSIS AND COMPARISON WITH TOPOGRAPHICALLY PATTERNED SURFACES

6.1 Introduction

6.1.1 Background

There have been several recent reports of studies using pillar-containing "superhydrophobic" surfaces as substrates for the preparation of patterned arrays of substances.[1-6] Hatton and Aizenberg[1] demonstrated that calcium carbonate deposits from a supersaturated aqueous solution selectively onto the tips of a nanopost array that was hydrophobized using a perfluoroalkyl-containing trifunctional silane. These workers also showed that polyvinyl alcohol and poly(L-lysine)[1,2] selectively adsorb to and that colloidal particles can be attached to these post tops. Jiang's group[3] described a technique involving "clinging microdroplets" and showed that when puddles of solutions or suspensions were evaporated between parallel surfaces, one of which is a micropost-containing surface, also hydrophobized with a perfluoroalkyl-containing trifunctional silane, an array of microdroplets remained attached to the micropost tops. This technique was used to prepare arrays of NaCl crystals as well as protein, microsphere, and nanoparticle aggregates. Senez et al.[4] described the distribution of a nonvolatile optical adhesive and particles (that were dispersed in water) on post tops relative to the direction of the receding contact line. They used a perfluoroalkyl-containing trifunctional silane to lyophobize an overhanging post (reentrant geometry) - containing PDMS surface and were able to visualize the receding contact line of the cured optical adhesive using scanning electron microscopy. Our group reported studies similar to these,[5,6] that involved withdrawing superhydrophobic surfaces, containing posts modified with a monofunctional perfluoralkyl-containing silane, from aqueous NaCl and ionic liquid (with negligible vapor pressure) solutions to form controlled

size individual crystals or controlled volume (in the femtoliter range) sessile drops. Wang et al.[7] characterized these depositions on pillar arrays as "air-grid" surface patterning and pointed out a connection between these studies and those of Levkin's group[8-10] that used "superhydrophobic-superhydrophilic micropatterns" on porous materials to support arrays of sessile drops of aqueous solutions.

Wang's paper[7] optimistically discusses the impact and potential impact of patterned arrays of various materials and gives leading references to both applications and preparative methods. The authors identify two main factors required of a patterned substrate for supporting/seeding/nucle-ating/docking a patterned array of materials: the repeating unit and the separating barrier. They express "excitement" concerning the "unprecedented" reports of using air as a "gas-phase separating barrier." Their analysis is insightful, but we suggest an additional perspective on these preparative methods that we have found useful, that expands their arguments, and that may further justify their excitement.

6.1.2 Objectives

In contrast to the few recent reports[1-6] of gas-phase separated pillars, there is a significant literature that addresses the use of chemically patterned surfaces for formation of patterned arrays of various materials.[8-34] This chemical approach is arguably simpler, more generally accessible, and would be more easily scaled to larger areas and production applications than approaches that require the preparation of arrays of pillars. Photolithography and microcontact printing are now widely available, inexpensive tools and are logical choices for creating "repeating units" and "separating barriers." In this chapter we aim to compare these two approaches and address a key difference between smooth-chemically-patterned and post-containing surfaces as substrates for dip-coating deposition. Our perspective is that of the dewetting dynamics of bulk liquid during formation of sessile

drops/puddles on patterned surfaces. This perspective focuses on the events that occur at the receding contact line and clearly differentiates *tensile capillary bridge failure* (normal to the surface), with surfaces containing gas-phase separated posts, and *sessile capillary bridge failure* (parallel to the surface), that occurs with chemically patterned surfaces.

6.2 Experimental Section

Silicon wafers (100 mm diameter) were obtained from International Wafer Service (100 orientation, P/B doped, resistivity from 20 to 40 Ω·cm). Photolithography masks were prepared using AutoCAD and printed on polyester film by CAD/Art Services, Inc. Shipley S1813 photoresist and Microposit MF-321 developer were obtained from Microchem Corp. UV exposure was carried out using a 500 W (365 nm) OAI UV lamp. Tridecafluoro-1,1,2,2-tetrahydrooctyldimethylchlorosilane (R^FSiMe_2Cl – Gelest), sodium chloride (Fisher Scientific), potassium chloride (EM Science), *n*-hexadecane (Acros Organics), hexanes (Fisher) and bis(hydroxyethyl)dimethylammonium methanesulfonate (N^+S^- – Evonik) were used without further purification. 7,14-bis(triisopropylsilylethynyl)dibenzo[b,def]chrysene (TIPS-DBC) was prepared using a literature method[35] and recrystallized from hexane. Water was deionized using a Millipore Milli-Q® system that involves reverse osmosis and filtering steps (18 MΩ). Scanning electron microscopy (SEM) images were recorded using a JEOL Neoscope and optical microscopy images were acquired with an Olympus BX60 system. Viscosity measurements were conducted using an Advanced Rheometry AR2000 parallel plate rheometer.

Sections of silicon wafers (~1 cm x ~3 cm) were cleaned using a Harrick plasma cleaner operated at 300 mTorr (O_2) and 30 W for 15 min prior to being spin-coated with S1813 photoresist (4000 rpm for 60 sec.) After heating at 115 °C for ~90 sec to remove solvents (soft bake), the wafers were exposed to UV through a photolithography mask for 12

sec. Development comprised submersion in MF-321 developer for 50 sec, rinsing with deionized water for 1 min and drying in a nitrogen stream. The wafer was then treated with oxygen plasma (300 mTorr, 30 W, 5 min) to remove contaminants from the developed areas before being allowed to react with R^FSiMe_2Cl vapor in a closed container at 80 °C for 72 h. After this surface modification reaction, the remaining photoresist was removed by rinsing with toluene, acetone and water (in this order).

Dip-coating deposition involved carefully withdrawing silicon wafer sections from solutions using hand-held stainless steel tweezers. Sections were held near the center of a particular edge (defining the direction of withdrawal relative to the photolithography pattern), positioned so that the plane of the wafer was perpendicular to the liquid-vapor interface, and withdrawn straight up at a rate of ~1 cm/sec. Although simple and unsophisticated, this method is easily performed reproducibly. Aqueous solutions of NaCl and N^+S^- as well as neat N^+S^- liquid samples were prepared and used in 40 mL polystyrene vials (Fisher Scientific). Hexane and hexadecane solutions of TIPS-DBC (0.16 mg/mL) were prepared and used in 20 mL glass scintillation vials (Fisher Scientific).

6.3 Results and Discussion

The results that we report in this chapter concern dip-coating deposition onto smooth, flat, chemically patterned surfaces. We present these first with brief analysis and compare them, in this section, with results that were recently obtained using superhydrophobic surfaces containing pillars.[5,6] An important initial objective in undertaking this work was to develop chemically patterned alternatives to the post-containing surfaces. In light of the obvious advantages noted in the introduction, if chemically patterned substrates can be prepared that are functionally equivalent to those based on pillar arrays, the chemical approach would be the obvious choice of most any research or development group. In the

course of this work it became clear that there are aspects of the mechanism of this process (dip-coating deposition) that have not been addressed, analyzed or (perhaps even) considered. The discussion of these mechanistic aspects is the important substance of this chapter. The preparative aspects of the chemically patterned surfaces used are neither novel nor particularly impressive in quality, but they were required for and are sufficiently reproducible for direct comparison with the pillar-containing substrates. Others have demonstrated[8-34] that chemical pattern approaches for dip-coating deposition are functional and useful, at least for demonstrations with specific systems, and some used more sophisticated and more refined lithography than that which we report. The mechanistic analysis that we present, however, identifies rational approaches for controlling process variables that can readily be implemented, should certainly be considered, and that should make chemically patterned dip-coating deposition more general and more practical.

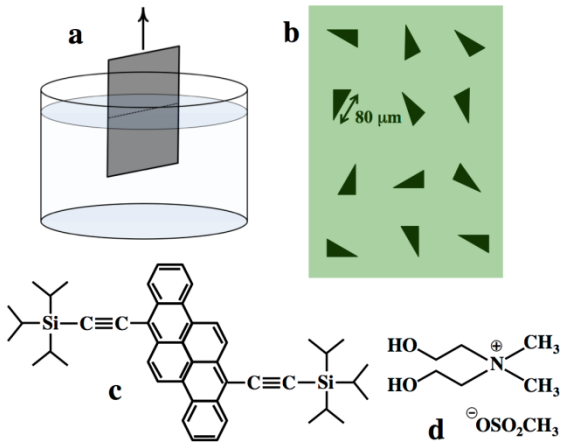

Figure 6-1 (a) Schematic depiction of the dip-coating deposition procedure. An initially submerged silicon wafer section is withdrawn from the liquid (using tweezers) with the surface of the wafer perpendicular to the liquid-vapor interface. (b) The pattern of Si/SiO_2 features (30°/60°/90° triangular spots) on a perfluoroalkyl monolayer background. Wafer sections containing this pattern were withdrawn in the direction pointing up in the figure for all experiments reported using this pattern. (c) The structure of TIPS-DBC. (d) The structure of N^+S^-.

We report results from five different types of experiment. Four of these involve dip-coating deposition of either bis(hydroxyethyl)dimethylammonium methanesulfonate (N^+S^-)

or sodium chloride (NaCl) onto a patterned array of features that was chosen (arrived at) by carrying out hundreds of preliminary experiments. The size scale, shape, separation and orientation (relative to the liquid-vapor interface) of the features, the concentration of the solutions, as well as the rate of withdrawal were all addressed as variables in initial experiments. Figure 6-1 shows the structure of N^+S^-, the chemical pattern of the features on the silicon substrates that were used for the first four experiment types that we describe, and a schematic of the simple dip-coating procedure. N^+S^- and NaCl were chosen for comparison with reported data.[5,6] N^+S^- was used for dip-coating either as a neat liquid or as a 25 vol% aqueous solution. Aqueous NaCl (0.5M) was used with two experimental protocols. One involved no control of the evaporation rate, and this method generated data that varied significantly with the ambient relative humidity. This fact was not appreciated during initial experimentation. The other method, that is simple in retrospect, but took many months to adopt, involved humidity control and staged evaporation. All reported data involved withdrawing the silicon wafer section by hand, using tweezers at a rate of ~1 cm/sec, at orientations of <10° from those reported (this is a conservative estimate that is irrelevant for most of the data). The photolithography was carried out in standard preparative labs (not a clean room) using procedures that we have reported.[36] The background surface chemical structure of all wafer surfaces consisted of a covalently attached R^FSiMe_2Cl-derived monolayer. The 30°/60°/90° triangular spots were Si/SiO_2 surfaces that had been cleaned of the photoresist using toluene, acetone and purified water. The background perfluoroalkyl monolayer exhibited water contact angles of θ_A/θ_R = 114°/106° and the triangular Si/SiO_2 features exhibited θ_A/θ_R = 40°/<10° (these values were determined using a wafer sample that was developed with no UV exposure). The 12-triangle array with variably oriented triangles was chosen to test the importance of the feature orientation relative to the withdrawal (dip-coating) direction.

The 5th set of experiments that we report used organic solvents (hexane and hexadecane) and a crystalline organic compound (TIPS-DBC)[196] that was available in our department during the time this research was carried out. The structure of TIPS-DBC is shown in Figure 6-1. A different patterned silicon substrate (not shown) was used for these studies and consisted of an array of 2500 (25 x 100) 50 μm diameter circular features of Si/SiO_2 on a background of R^FSiMe_2Cl-derived monolayer. This set of experiments was not carried out with as much experimental rigor as the other four, but demonstrates that high surface tension liquids are not required and helps emphasize that control of evaporation rate is important.

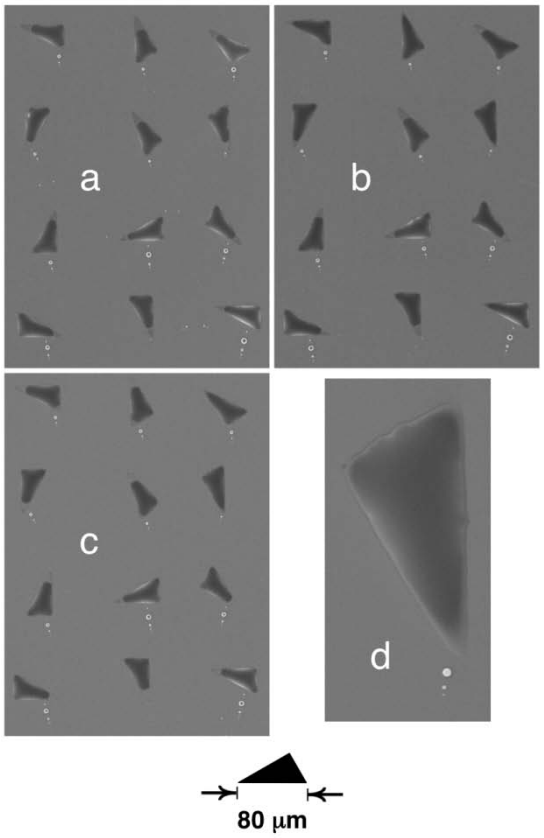

Figure 6-2 (a,b,c) SEM images of three chemically-patterned arrays that were dip-coated with neat N^+S^-. (d) A magnified image of one triangular spot. The withdrawal direction was toward the top of the figure in each case.

The room temperature ionic liquid, bis(hydroxyethyl)dimethylammonium methanesulfonate (N^+S^- - structure in Figure 6-1) is a non-volatile liquid that exhibits the highest surface tension (66.4 dyn/cm)[37] of any ionic liquid that we have studied. We used this liquid with our post-containing surfaces,[5] thus it was chosen for the comparative studies described here. Dip-coating silicon wafer sections containing the 12-triangle chemically patterned array described above, using neat N^+S^-, produced samples that rendered the images shown in Figure 6-2. The SEM images labeled a, b and c are from 3 different experiments involving 3 different patterned array samples that were withdrawn in the direction pointing "up" in the figure and were not coated with gold or treated in any other way. We acknowledge the redundancy of these data, but include all 3 of these images to emphasize the reproducibility of the experiment and to note that our photolithography technique, although rather crude, produces features that render reproducible dip-coating results. Each triangular feature contains a "puddle" of N^+S^- that does not completely wet the triangle. The puddles appear to have receded away from the vertices of almost every feature, particularly from the sharp points of the 30° angles. The triangular Si/SiO_2 spots themselves show contrast with the R^FSiMe_2Cl-derived background in the SEM images due to differential charging and it is not possible to define an obvious 3-phase contact line using these microscopy data. Higher magnification images are difficult to obtain and do not provide more lucid data. Both N^+S^- and the R^FSiMe_2Cl-derived monolayer apparently react with the electron beam or exhibit dynamic differential charging and the puddle shape can change. Although the 36 triangles shown in Figure 6-2(a)(b)(c) differ slightly in shape due to photolithography development defects and differ in orientation relative to the withdrawal direction, most of the 36 puddles appear quite similar in volume and shape. Figure 6-2(d) is a magnified image of one triangular spot. A notable feature of the images in Figure 6-2 is that droplets of N^+S^- are

"spattered" in places on the R^FSiMe_2Cl-derived monolayer background. The locations and the reproducibility of these droplet locations are addressed below in this section.

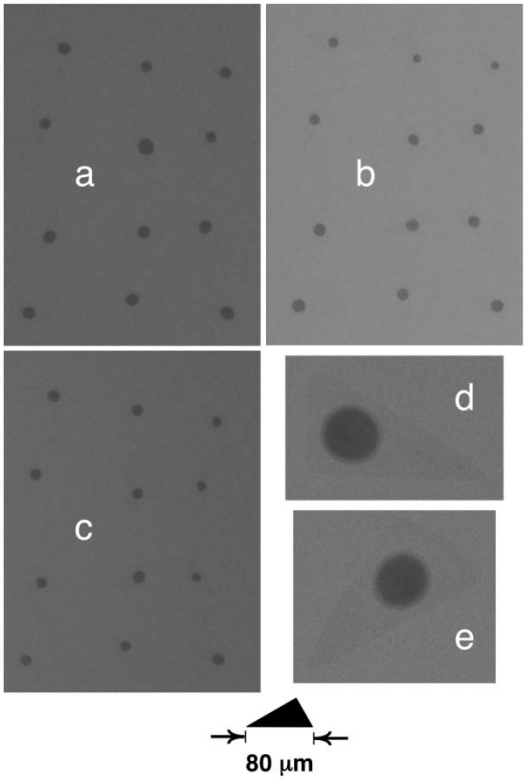

Figure 6-3 (a,b,c) SEM images of three 12-triangle arrays that were dip-coated with 25% aqueous N^+S^-. (d,e) Magnified images of individual features. The withdrawal direction was toward the top of the figure in each case.

Figure 6-3 shows SEM results, presented in the same format as those just discussed (Figure 6-2), for dip-coating samples containing the same chemical pattern with a 25 vol% solution of N^+S^- in water. Again, the redundant SEM images labeled a, b and c are of samples from 3 different, but identical experiments that involved withdrawing the substrates in the direction pointing "up" in the figure. After dip-coating, these samples were allowed to "dry" at room temperature for at least 3 hours prior to analysis with the primary objective of not introducing volatile liquids into the electron microscope. In all 36 cases, the nonvolatile N^+S^- residue appears as a nearly circular puddle near the center of the triangular feature. This suggests that the orientation of the triangles (or withdrawal direction) is not important in

these experiments and that the evaporation of water induces dewetting from the triangle vertices and recession of the contact lines to form spherical-cap-shaped puddles. The variability in the puddle diameter is obvious, but this variance is not so pronounced as to affect our interpretation of the data or to warrant further analysis. There is no correlation between the puddle diameter and the triangle orientation or the position of the feature in the 3 x 4 array. The variability in puddle diameter can be rationalized by several issues: We do not know the height of the spherical caps, the contact angles may vary, and thus the volume of the puddles may be less variable than the diameter. The recession of the initially triangular-shaped puddles occurs at contact lines with contact angles that we measured (with water sessile drops) as θ_R = <10°. Slight differences in receding contact angles at particular locations of the demonstrably "unclean" Si/SiO_2 triangles would affect the diameter of the puddle and the location of the puddle in the triangle. We emphasize that there are no apparent "spattered" droplets of N^+S^- of the sort that were observed (Figure 6-2) in experiments with neat N^+S^-.

Figure 6-3(d)(e) shows two magnified images of spherical-cap-shaped puddles of N^+S^- on individual triangular features. All such images exhibit puddles with a ring of intermediate contrast near the contact line. We focus attention on this ring for two reasons. First, we do not imply that its presence in these data reflects puddle structure rather than differential charging of uncoated SEM samples and second, because we used these data to estimate[38] the volume of liquid in these puddles in attempts to measure the volume and thickness of the 25% aqueous N^+S^- that was dip-coated. One 12-triangle array exhibited puddles with diameters (including this ring) that range from 16.3 to 25.5 μm (average 22.2 μm). Assuming that these puddles are spherical caps with contact angles of <10°, the average height of the spherical cap was <0.97 μm, the volume of 25% aqueous N^+S^- that was dip-coated was <750 μm^3, and the average initial puddle thickness before evaporation and

recession was <0.54 μm. This calculation[38] suggests that a very thin film (less than ~0.5 μm) of aqueous N^+S^- is applied during dip-coating to the triangular features that have sides of 40, 69 and 80 μm. Optical microscopy confirms that the deposited films are thin and further suggests that the estimate obtained from SEM data is high. Figure 6-4 shows two optical micrographs of a 12-triangle array that was withdrawn from 25% aqueous N^+S^-. Figure 6-4(a) shows the sample ~30 sec after it was withdrawn and Figure 6-4(b) shows the same sample ~200 min later (no additional changes were observed over the previous ~100 min). Analysis[39] of the interference rings indicates that the puddles in Figure 6-4(a) have heights of 200 - 400 nm (2 or 3 destructive interference rings) and that those in Figure 6-4(b) are 600 – 800 nm deep (11 features have either 4 or 5 destructive interference rings and one has 3 rings).

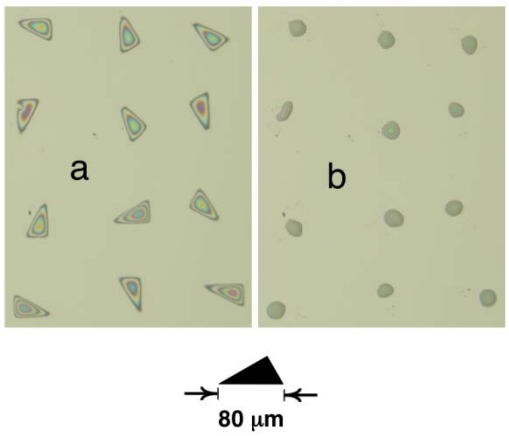

Figure 6-4 Optical micrographs of a 12-triangle chemically patterned array that was dip-coated with 25% aqueous N^+S^-. (a) ~30 sec after withdrawal. (b) ~ 200 min after withdrawal.

We began our studies with chemically patterned substrates using aqueous NaCl solutions as our "test solution" and carried out hundreds of dip-coating experiments using arrays of spots with different feature sizes, shapes and orientation as well as solutions with a range of concentrations. We were attempting to duplicate results that could be obtained[6] easily and reproducibly using post-containing surfaces: in these cases, individual crystalline particles of NaCl readily formed on millions of posts. Our results with chemically patterned

surfaces varied, but in general we did not obtain arrays of individual crystals, and we initially ascribed these failures to our photolithography technique, blaming the multiple crystal deposition on defects in the developed patterns.

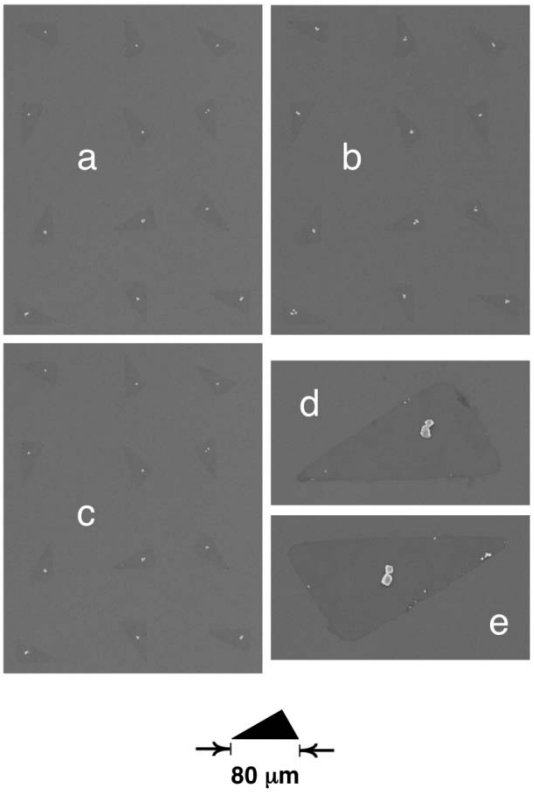

Figure 6-5 (a,b,c) SEM images of three 12-triangle arrays that were dip-coated with 0.5 M aq. NaCl. (d,e) Magnified images of individual features. The withdrawal direction was toward the top of the figure in each case.

Figure 6-5 shows SEM data, in the same style as previous figures, for dip-coating experiments performed using 0.5 M NaCl. The samples imaged in Figure 6-5(a)(b)(c) were withdrawn in a direction "up" in the figure. NaCl is confined to the triangular spots, but there are, in most of the 36 cases shown, multiple crystals in clusters near the center of the triangles. The uniform location of these clusters suggests that circular puddles formed and receded in much the same way that the N^+S^- solutions evaporated. Close inspection of the triangular spots and Figure 6-5(d)(e) (these were chosen for emphasis) show that there are often smaller crystals as well within the triangular regions and that these tend to be near the intersection of

the Si/SiO_2 spot and the R^FSiMe_2Cl-derived monolayer background, suggesting that photolithography defects are the cause of the small crystal deposition. We note again that in these initial studies we did not take any particular care in the drying (water evaporation) of dipped samples. After removal from the dipping solution, substrates were simply exposed to the ambient laboratory environment before analysis using SEM. On a particularly humid day, a dip-coated sample was examined using optical microscopy after drying and sessile drops of saturated NaCl, rather than crystals, were observed. The humidity was sufficiently high for NaCl to exhibit deliquescence. This sample was placed in a desiccated container and a pattern of individual crystals formed. This experiment led us to examine the "drying" step of dip-coating deposition as an evaporation/ condensation equilibrium that can be controlled by adjusting the vapor pressure of the evaporating solvent.

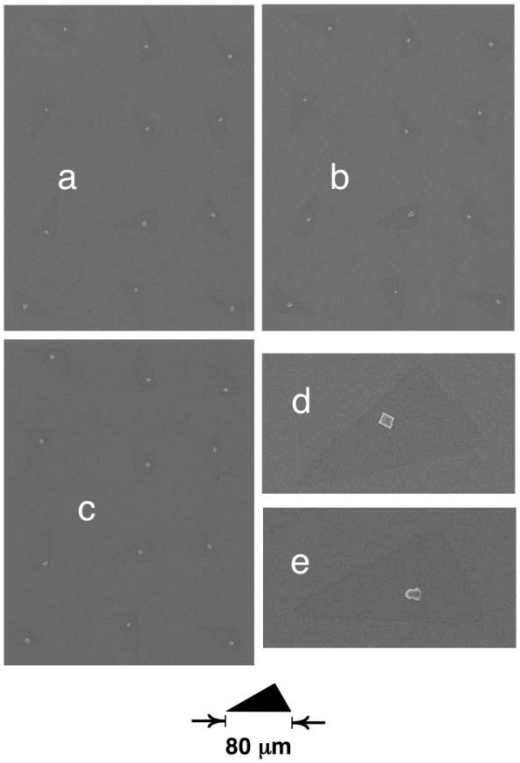

Figure 6-6 (a,b,c) SEM images of three 12-triangle arrays that were dip-coated with 0.5 M aq. NaCl at ~80% relative humidity, equilibrated in this atmosphere for 2 h and then dried in a dessicated vessel. (d,e) Magnified images of individual features. The withdrawal direction was toward the top of the figure in each case.

Based on the conditions of the fortuitous experiment just described, a procedure was implemented that involved dip-coating samples in a glove bag in which relative humidity was controlled to ~80% at room temperature. The samples were allowed to equilibrate in this environment for 2 h before being placed in a Petri dish containing dessicant. This staged drying procedure reproducibly produced results that replicated those of the humid day experiment. Sessile drops of saturated NaCl form by equilibration and crystallization/complete drying is induced after decreasing water vapor pressure using a dessicant. Figure 6-6 displays results (SEM) of three identical experiments, shown in the same style as previous figures, for samples dip-coated with 0.5 M NaCl and worked up with this equilibration/staged drying protocol. Individual crystals are present on all 36 triangles, in marked contrast to the results shown in Figure 6-5 where drying was not controlled with elevated humidity, clusters of crystals were the norm, and smaller crystals were present near the photolithography intersections. The substrates used in the experiments described in Figure 6--6 were prepared using exactly the same photolithography procedure that was used for the experiments reported in Figure 6-5. The differences between these two sets of experiments and the role of the equilibration and staged drying are discussed below in the Discussion section. This procedure was used to examine NaCl concentration effects and SEM data from experiments performed with both lower and higher concentrations (0.1 M and 4 M) yield data (not shown) that indicate as expected, the size of the crystals can be controlled by concentration.

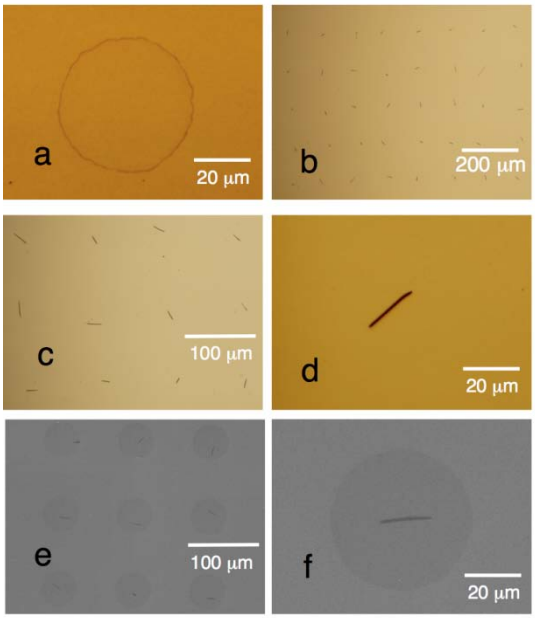

Figure 6-7 (a) Optical microscopy images of TIPS-DBC that was dip-coated onto an array of 2500 50 μm diameter circular features from hexane solution. The image in (a) indicates that most of the material is confined to a "coffee ring" structure at the perimeter of the circular feature. Optical (b,c,d) and scanning (e,f) electron micrographs of TIPS-DBC that was dip-coated onto the same substrate from *n*-hexadecane solution.

The 5th and last set of results that we report involves dip-coating deposition of TIPS-DBC (Figure 6-1(c)) from alkane solutions onto arrays of 2500 50 μm diameter circular features. The chemistry of the features and background are identical to those described for the 12-triangle arrays above (Si/SiO_2 spots on a background of R^FSiMe_2Cl-derived monolayer). TIPS-DBC was purified by recrystallization from hexane and this was the first solvent investigated for dip-coating. Figure 6-7(a) shows the result of an experiment that was followed using optical microscopy. "Coffee ring" structures formed on all of the circular features due to the pinning of the drop and rapid drying (b.p. = 69 °C). This compound crystallizes as needles and close inspection of the coffee rings reveals that they are composed of many small crystals. Rather than use a hexane-rich atmosphere, by analogy with the NaCl experiments described above, *n*-hexadecane (b.p. = 287 °C) was tested because it was available as a purified liquid (a common contact angle probe fluid in our lab). This solvent, that evaporates much more slowly, rendered arrays of individual needles on the circular

features. Figure 6-7(b)-(f) shows optical and scanning electron microscopy images of the TIPS-DBC needles.

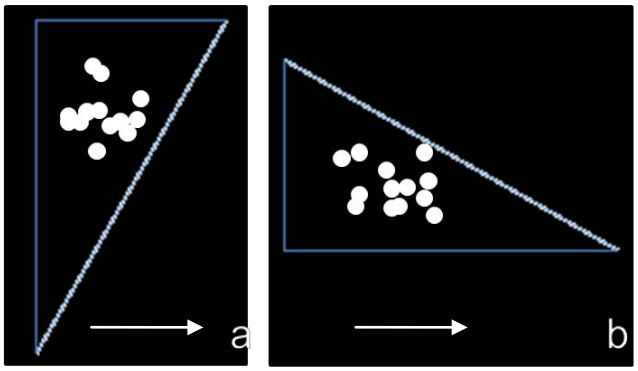

Figure 6-8 Depiction of crystal locations within 30^o-60^o-90^o triangle regions after the chemically patterned surfaces are withdrawn from 0.1M NaCl. White dots represent the NaCl crystals. Blue lines represent the hydrophilic domain boundaries, and the arrowheads represent the pulling direction of the surface.

Results in Figure 6-6 prove to be quite reproducible. More than 10 hydrophilic triangle arrays like that in Figure 6-1(b) are patterned on the R^FSiMe_2Cl-derived background, and the substrate is withdrawn from 0.1M NaCl. SEM images of each triangle array appear very similar to that in Figure 6-6 (a), indicating more than 120 individual NaCl crystals are arranged into ordered arrays on a single piece of substrate. To improve our understanding about the crystallization dependence on the hydrophilic feature orientation, locations of NaCl crystals within the triangle region are all marked with white dots. It is surprising that all the crystal deposition positions are around the triangle centroid, irrespective of the triangle region orientation. (Figure 6-8). It indicates that the hydrophilic region orientation does not significantly influence our dip-coating crystallization results, at least for this specific design of triangle arrays.

In order to capture the process that bulk liquid depins from the chemically patterned surfaces, 12-triangle silica arrays are patterned on a R^FSiMe_2Cl-modified background. This

pattern (Figure 6-9(a)) is different from that in Figure 6-1(b) in the aspect that its longest side measures 200 μm. A large water droplet covers this patterned surface lying horizontally. Then the water droplet is permitted to retract to the left. It is observed from Figure 6-9(b) that the water receding contact line is pinned by rows of triangles. The water exhibits a 'stick and slip' motion. It also implies that shear capillary bridge rupture occurs between the bulk liquid and the hydrophilic silica features.

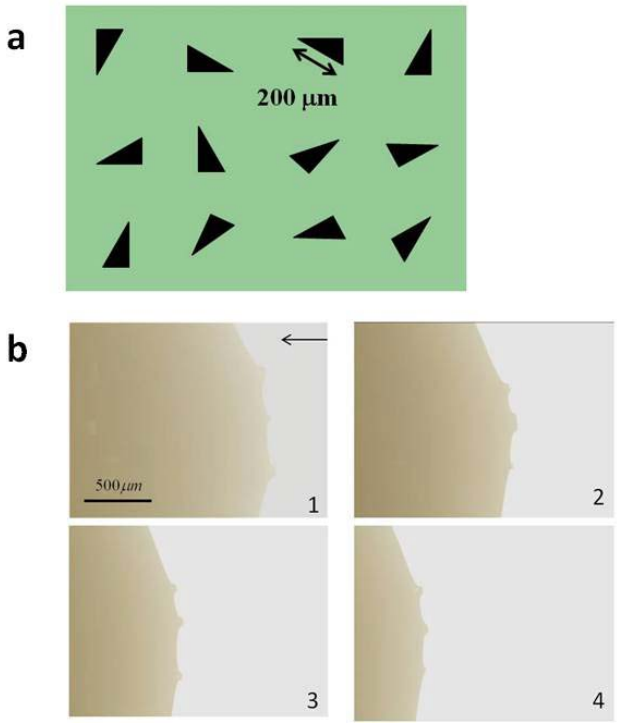

Figure 6-9 (a) Pattern of Si/SiO_2 features (30°/60°/90° triangular spots) on a perfluoroalkyl monolayer background. (b) In-situ observation of a large water drop receding on the chemically patterned surface. The arrowhead indicates the water drop retraction direction.

We undertook this study in an effort to compare chemically patterned substrates with post-containing (superhydrophobic) substrates in regard to their utility in dip-coating deposition. Wang[7] has made this comparison, identifying the "repeating units" and the "separating barriers" as the two main differentiating factors and describing the post-

containing surfaces as “air-grid patterned.” We extend these arguments with focus on the events that occur at the receding contact line both during withdrawal of the substrate from the dip-coating solution and during evaporation of the applied liquid on the “repeating unit” of the substrate.

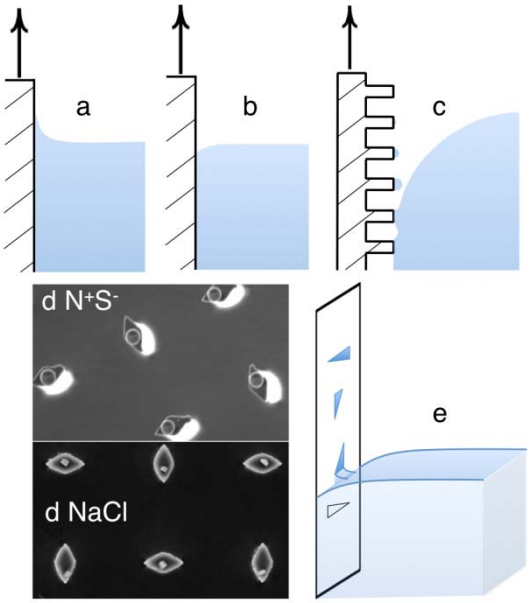

Figure 6-10 2D representations of hydrophilic (a, θ_R ~ 10°), hydrophobic (b, θ_R ~ 106°) and superhydrophobic (c, θ_R ~ 156°) surfaces being withdrawn from water. d: SEM images of N^+S^- droplets and NaCl crystals that were dip-coated on a post-containing superlyophobic surface. The dimensions of the rhombus-shaped post tops are 3 x 6 μm. e: The withdrawal from water of a chemically patterned surface containing hydrophilic triangles (θ_R ~ 10°) on a hydrophobic background (θ_R ~ 106°).

When a solid object with a uniform surface is withdrawn from water into air (perpendicular to the air/liquid interface – Figure 6-1(a)), a discrete and reproducible contact angle is maintained at the solid/liquid/vapor (3-phase) contact line. This contact angle is the receding contact angle (θ_R) of water on the surface of the solid object being withdrawn. Figure 6-10(a)(b) shows 2D cross sections depicting this angle (θ_R) for two solid objects, one with θ_R = ~10° and one with θ_R = ~106°. These values were chosen as examples because they are the values for the “repeat unit” and “separating barrier” materials in the samples described in the Results section above, and they are appropriate for displaying surfaces that

would generally be characterized as "hydrophobic" ($\theta_R \sim 106°$) and "hydrophilic" ($\theta_R \sim 10°$). Surfaces with these values for receding water contact angles will also exhibit advancing contact angles ($\theta_A \sim 114°$, 40° for the surfaces described here), but the θ_A values are not important to this discussion nor to dip-coating deposition. We note that with the exception of our papers,[5,6] receding contact angles were not reported for any of the "repeating units" or "barriers" used for dip-coating depositions reported in the literature. Figure 6-10(c) depicts a 2D cross section of a superhydrophobic surface containing posts being withdrawn from water. We have reported[5,6] this experiment using both neat N^+S^- and aqueous solutions ofNaCl and N^+S^- as the liquid and a substrate containing 3 x 6 μm staggered rhombus shaped posts. Data from these studies for neat N^+S^- and 1 M aqueous NaCl are displayed in Figure 6-10(d). We make three points regarding these post-containing substrates before discussing the dip-coating process: (a) The surfaces are photolithography-patterned and etched silicon wafers that were modified with tridecafluoro-1,1,2,2-tetrahydrooctyldimethylchlorosilane (R^FSiMe_2Cl), a monofunctional silane that can only form a monolayer with Si/SiO_2 surfaces. The trifunctional silanes used in the reports[1-4] reviewed above in the Introduction form oligolayers containing residual silanols with thickness, structure and receding contact angles that depend on reaction conditions.[40] In particular, both the thickness of the layer and the silanol content (potential pinning sites) increase with increasing adventitious water concentration and the receding water contact angle decreases. (b) The R^FSiMe_2Cl-derived surface exhibits (macroscopic) water contact angles of $\theta_A/\theta_R = 169°/156°$[6] and N^+S^- contact angles of $\theta_A/\theta_R = 164°/152°$.[5] (c) The tops of the posts are smooth (the same topography as the virgin silicon wafer containing its native oxide), as they were protected by photoresist during etching, and exhibit (local) water contact angles of $\theta_A/\theta_R = 117°/109°$ and N^+S^- contact angles of $\theta_A/\theta_R = 100°/85°$.[41]

When this surface is withdrawn from either water or N^+S^- (Figure 6-10(c)), the meniscus formed by a receding contact angle of θ_R >150° ends at a 3-phase contact line that is >2 mm (a function of the capillary length of the liquid[39]) beneath the surface of the liquid. This contact line does not recede continuously with respect to the surface during withdrawal (as in Figure 6-10(a)(b) because the macroscopic contact angle (θ_R = 156° or 152°) is much higher than the receding contact angle of the post tops, θ_R = 109° for water or θ_R = 85° for N^+S^-. Instead the contact line is pinned by the post tops, capillary bridges form between the post tops and the bulk liquid and these bridges fail via a Plateau-Rayleigh instability. Sessile drops and a new contact line form. The femtoliter scale (10^{-15} L) liquid drops form on the micrometer scale post tops that are millimeters beneath the surface of the liquid in the dip-coating vessel. The drops are not visible when water is used as the liquid as they evaporate rapidly and the substrate emerges dry from the dip-coating solution. The electron micrographs reported by Senez et al.,[4] of an optical adhesive (with lower surface tension and lower contact angles) that was cured on an inclined post-containing surface, offer snapshots of this process both immediately prior to and subsequent to capillary bridge failure. We emphasize two distinguishing elements of this (topographically patterned) dip-coating deposition process: (1) The drops are deposited on the surface features by the failure of capillary bridges in tension between the substrate and the dip-coating solution; we refer to this as *tensile capillary bridge failure*. This failure occurs in a direction nearly normal to the surface. (2) The features that pin the capillary bridges, that the drops are deposited on (and evaporate from in the case of water), and upon which NaCl is crystallized/deposited, have very low surface energy. They exhibit water contact angles of θ_A/θ_R = 117°/109° and N^+S^- contact angles of θ_A/θ_R = 100°/85°. These liquid pinning features exhibit wettability that would generally be referred to as hydrophobic and/or lyophobic.

The chemically patterned substrates that are discussed above in the Results section use the same monofunctional R^FSiMe_2Cl-derived surface that coated the post top features, but in this case as the separating barrier between hydrophilic features. We measured slightly lower water contact angles (θ_A/θ_R = 114°/106°) than we have reported for this surface previously (θ_A/θ_R = 117°/109°) and rationalize these differences as due to exposure to photolithography reagents and rinse solvents in the multistep preparation. The previously reported values are from surfaces that could be cleaned vigorously with oxygen plasma and chemically derivatized with one (final step) vapor phase reaction. The hydrophilic features were bare Si/SiO_2 formed by removing the photoresist with a series of solvent rinses. These features exhibit water contact angles of θ_A/θ_R = 40°/<10°. Figure 6-10(e) shows a depiction of a column of four hydrophilic features in a hydrophobic (separating barrier) background being withdrawn from water. This is meant to depict the experiments described in the Results section. As the surface is withdrawn and a triangular hydrophilic feature encounters the contact line, it lifts the water by pinning the contact line at its uppermost boundary. Adjacent to the feature (to the left and right), the contact line continues to recede and a sessile capillary bridge forms between the triangular feature and the bulk liquid in the vessel. There are discontinuities in contact angle at the left-most and right-most points of the triangular features. This bridge ruptures at some separation distance between the pinned portion of the contact line and the portions of the line that have receded adjacent to the feature, leaving a puddle of water on the feature and a stable receding contact line on the hydrophobic separating barrier.

There are multiple points concerning the results described above that warrant discussion, particularly in regard to the events that are depicted in Figure 6-10(e). We emphasize that the events at the receding 3-phase contact line on chemically patterned surfaces (Figure 6-10(e)) are fundamentally different than those that occur at topographically

patterned hydrophobic surfaces (Figure 6-10(c)). Sessile, rather than tensile, capillary bridges form between the hydrophilic features and the bulk liquid, leaving puddles on hydrophilic surface regions (rather than droplets on hydrophobic posts). The capillary bridges fail parallel with the surface. These differences, that are shown schematically in Figure 6-11, are pronounced and extend the arguments made by Wang[7] that distinguish air as a special "separating barrier." These differences also suggest that the experiments of Levkin[8-10] that used superhydrophobic/superhydrophilic micropatterned surfaces are more connected with chemical patterning than topography patterning as they involve sessile capillary bridge failure and puddles on hydrophilic regions.

We have observed these sessile capillary bridges and their rupture using optical microscopy by dragging droplets across surfaces, but were not successful in recording useful movies. The obtuse receding contact angle of the hydrophobic background (θ_R = 106°) obscures the contact line. We did discern that the individual puddles observed on each feature are due to failures of capillary bridges between individual features and the bulk liquid, and that multiple feature - spanning larger puddles do not form and break into feature-confined smaller puddles. This is consistent with the recent report of Nakajima et al.[42] that includes movies of chemically patterned triangle arrays being withdrawn from water. These movies do not (nor did our attempts at recording movies) give insight into the structure (shape) of the capillary bridges as the contact line rapidly "snaps" from feature-to-feature. We have recently reported[43] the shear distortion and failure of millimeter-sized capillary bridges between individual hydrophilic features on hydrophobic backgrounds and could clearly distinguished tensile and sessile failure. In these experiments it was possible to observe in detail (at controllable rate) the thinning of sessile capillary bridges and the redistribution of water that depend on the shape and orientation of the surface features. Maintaining uniform mean curvature (Laplace pressure) of the air-liquid interface during distortion was the key element

controlling the capillary bridge shape. In the experiments described above that involved low viscosity liquids (aqueous solutions of N^+S^- or NaCl) very thin (sub-micron) films of solution were applied to the features as they were lifted out of the liquid. Estimates of the thickness of the puddles are made above. Minimizing the departure from uniform curvature (zero curvature of the flat liquid/vapor interface in the vessel) at this complex interface (with contact angle discontinuities) controls the volume of liquid applied to the features.

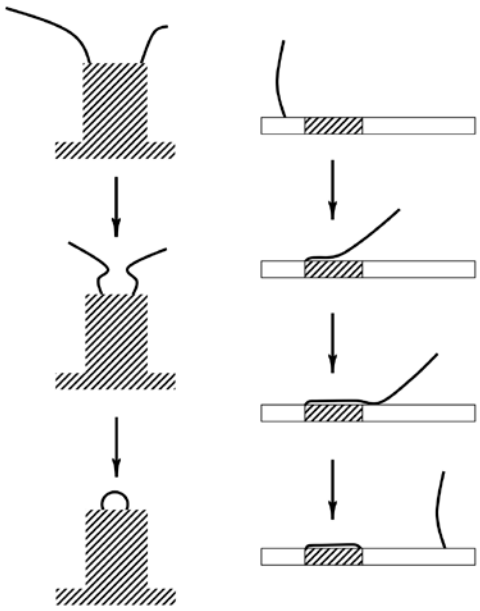

Figure 6-11 Schematic depictions of tensile (left) and sessile (right) capillary bridge failure.

The experiments described in Figure 6-2 that used the high viscosity liquid (neat N^+S^-) and the 12-triangle pattern (4 rows and 3 columns, Figure 6-1(b)) offer insight into details of this process. The pattern differs in several respects from the single row of features in Figure 6-10(e) and is not, in other respects, a good model for an array of features with many rows and many columns. The viscosity of neat N^+S^- (~1200 cP)[44] is anomalously high relative to the other solutions used in the studies reported here. Close inspection of Figure 6-2(a)(b)(c) reveals that the "spattered drops" observed are replicated in both position and volume in the 3

experiments pictured. The reproducibility is remarkable and suggests that they are not "spattered", but due to the process of dip-coating deposition.

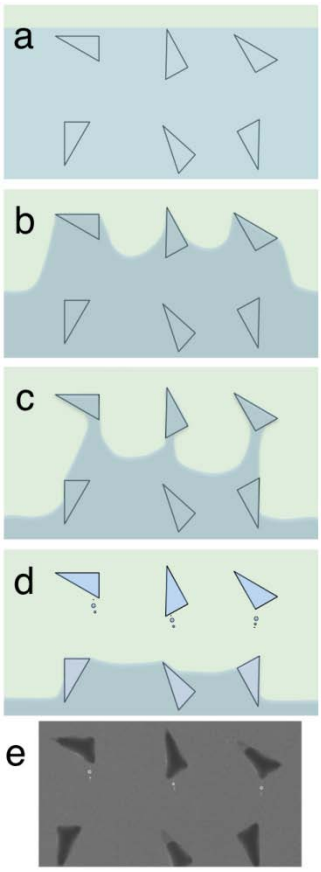

Figure 6-12 Proposed mechanism for dip-coating deposition of neat $N^{+}S^{-}$ onto the 12-triangle array. As the substrate is lifted through the liquid/air interface the initially straight miniscus (a) is lifted by the first row of triangular features (b) forming sessile capillary bridges (c) that break (d) forming small droplets that reveal the capillary bridge orientation. e is the upper section of Figure 6-2(b).

Figure 6-12 describes a plausible mechanism for the process that leads to the regular reproducible structures observed in Figure 6-2. The initially linear receding meniscus (Figure 6-12(a)) makes a complex and dynamic intersection with the solid surface as the first row of the 12-triangle array passes through the liquid-vapor interface (Figure 6-12(b)). The 3 triangles in the row entrain liquid upward and there are discontinuities in contact angle at both the left boundary and the right boundary and also discontinuities at the internal edges of

the features of both outer triangles and at both edges of the features of the inner triangle. We confidently make the conjecture that receding events on either side of the array move the contact line to a lower position on the sample than the meniscus contact points between triangular features (as is depicted in Figure 6-12(b)). The three sessile capillary bridges that form in each row (Figure 6-12(c)) will most certainly not rupture in a concerted event. One or another of the three will rupture first leaving liquid pinned by two features, and after the second one breaks, only one feature in the row will remain pinned. The durations between the first and second and the second third capillary bridge failures will affect the length and structure of each capillary bridge as the meniscus on either side of the array will have moved, as the sample is withdrawn at constant rate. The sequence of failures in a row (all 4 of which are different) may depend on the triangle orientation and their relative orientation, the separation of the features in rows and columns (array density) as well as their array pattern (square versus hexagonal, for instance) and this sequence, in addition to the physical features, may affect the capillary bridge structure and thus the volume of liquid deposited. The sessile capillary bridges fail with a sessile Plateau-Rayleigh instability (Figure 6-12(d)) and leave sessile droplets in patterns that reveal the direction of the capillary bridges and their failure. This mechanism argues that the capillary bridges formed from features in the outer columns should rupture before those involving the interior column. The assumption of variable dynamics of sequential events argues that both the rate of substrate withdrawal and liquid viscosity should be important. We note that the lowest interior triangle of each array pictured in Figure 6-2 does not have small droplets associated with it and is likely the last feature coated.

The drying (solvent evaporation) process, after withdrawal of the dip-coated samples, is also central to dip-coating deposition and there is obvious contrast between the events that occur on chemically patterned versus topographically patterned surfaces. This issue has

proved to be central to "coffee ring" formation and has been analyzed in significant detail recently by Mugele et al.[45,46] who reported that electrowetting can inhibit coffee ring formation. Coffee rings tend to not form on high contact angle, low energy surfaces, but generally form on low contact angle, high energy surfaces. The post tops of the topographically patterned surfaces consist of low surface energy perfluoroalkyl groups that exhibit receding water contact angles of θ_R = ~109°. These surfaces are unlikely to be fouled by adventitious impurities. The droplets form millimeters below the surface of the liquid (due to the meniscus at the superhydrophobic surface) in the dip-coating process and evaporate in this high vapor pressure environment. In contrast, the hydrophilic patterns on the chemically patterned surfaces consist of Si/SiO_2 that contact angle analysis demonstrates is fouled by impurities. This fouling is important and required; if the receding contact angle were θ_R = 0°, then the puddle would pin at the feature perimeters and structures due to this pinning would always occur. The receding angles of the features are θ_R = ~10° or less and experiments indicate that pinning does occur when the solvent evaporates quickly. This is shown in Figure 6-5 for aqueous NaCl and Figure 6-7(a) for TIPS-DBC/hexane. The importance of regarding evaporation as a condensation/vaporization equilibrium and slowing the process so that vapor concentration of evaporating solvent is high and that receding events are not pinned, permits concentration of solutions before crystallization occurs. This is shown in Figure 6-6 for aqueous NaCl and Figure 6-7(b)-(f) for TIPS-DBC/hexadecane.

6.4 Conclusions

There are significant mechanistic differences between dip-coating deposition using chemically patterned and topographically patterned surfaces. The most notable difference is that liquid is deposited by tensile capillary bridge failure, normal to the surface, with topographically patterned surfaces and by sessile capillary bridge failure, parallel to the

surface, with chemically patterned surfaces. Topographic patterning permits the use of low surface energy features that are generally clean surfaces for concentration and crystallization. Chemical patterning requires relatively high surface energy features that are generally less clean. Using slow solvent evaporation so that the vapor pressure of evaporating solvent is high is useful for concentrating solutions for preparing individual crystals of crystalline substances.

6.5 References

1. Hatton, B. D.; Aizenberg, J., Writing on Superhydrophobic Nanopost Arrays: Topographic Design for Bottom-up Assembly. *Nano Lett* **2012**, *12* (9), 4551-4557.

2. Mishchenko, L.; Khan, M.; Aizenberg, J.; Hatton, B. D., Spatial Control of Condensation and Freezing on Superhydrophobic Surfaces with Hydrophilic Patches. *Adv Funct Mater* **2013**, *23* (36), 4577-4584.

3. Su, B.; Wang, S. T.; Ma, J.; Song, Y. L.; Jiang, L., "Clinging-Microdroplet" Patterning Upon High-Adhesion, Pillar-Structured Silicon Substrates. *Adv Funct Mater* **2011**, *21* (17), 3297-3307.

4. Dufour, R.; Brunet, P.; Harnois, M.; Boukherroub, R.; Thomy, V.; Senez, V., Zipping Effect on Omniphobic Surfaces for Controlled Deposition of Minute Amounts of Fluid or Colloids. *Small* **2012**, *8* (8), 1229-1236.

5. Krumpfer, J. W.; Bian, P.; Zheng, P. W.; Gao, L. C.; McCarthy, T. J., Contact Angle Hysteresis on Superhydrophobic Surfaces: An Ionic Liquid Probe Fluid Offers Mechanistic Insight. *Langmuir* **2011**, *27* (6), 2166-2169.

6. Krumpfer, J. W.; McCarthy, T. J., Dip-Coating Crystallization on a Superhydrophobic Surface: A Million Mounted Crystals in a 1 cm(2) Array. *J Am Chem Soc* **2011**, *133* (15), 5764-5766.

7. Chen, L.; Yang, G.; Wang, S. T., Air-Grid Surface Patterning Provided by Superhydrophobic Surfaces. *Small* **2012**, *8* (7), 962-965.

8. Geyer, F. L.; Ueda, E.; Liebel, U.; Grau, N.; Levkin, P. A., Superhydrophobic-Superhydrophilic Micropatterning: Towards Genome-on-a-Chip Cell Microarrays. *Angew Chem Int Edit* **2011**, *50* (36), 8424-8427.

9. Li, J. S. S.; Ueda, E.; Nallapaneni, A.; Li, L. X. X.; Levkin, P. A., Printable Superhydrophilic-Superhydrophobic Micropatterns Based on Supported Lipid Layers. *Langmuir* **2012**, *28* (22), 8286-8291.

10. Ueda, E.; Levkin, P. A., Emerging Applications of Superhydrophilic-Superhydrophobic Micropatterns. *Adv Mater* **2013**, *25* (9), 1234-1247.

11. Kumar, A.; Biebuyck, H. A.; Whitesides, G. M., Patterning Self-Assembled Monolayers - Applications in Materials Science. *Langmuir* **1994**, *10* (5), 1498-1511.

12. Koh, S. J., Strategies for controlled placement of nanoscale building blocks. *Nanoscale Res Lett* **2007**, *2* (11), 519-545.

13. Qin, D.; Xia, Y. N.; Xu, B.; Yang, H.; Zhu, C.; Whitesides, G. M., Fabrication of ordered two-dimensional arrays of micro- and nanoparticles using patterned self-assembled monolayers as templates. *Adv Mater* **1999**, *11* (17), 1433-1437.

14. Lu, G.; Li, W.; Yao, J. M.; Zhang, G.; Yang, B.; Shen, J. C., Fabricating ordered two-dimensional arrays of polymer rings with submicrometer-sized features on patterned self-assembled monolayers by dewetting. *Adv Mater* **2002**, *14* (15), 1049-+.

15. Xue, L. J.; Han, Y. C., Pattern formation by dewetting of polymer thin film. *Prog Polym Sci* **2011**, *36* (2), 269-293.

16. Li, H.; Zhang, J.; Zhou, X. Z.; Lu, G.; Yin, Z. Y.; Li, G. P.; Wu, T.; Boey, F.; Venkatraman, S. S.; Zhang, H., Aminosilane Micropatterns on Hydroxyl-Terminated Substrates: Fabrication and Applications. *Langmuir* **2010,** *26* (8), 5603-5609.

17. Jie, Y. N.; Niskala, J. R.; Johnston-Peck, A. C.; Krommenhoek, P. J.; Tracy, J. B.; Fan, H. Q.; You, W., Laterally patterned magnetic nanoparticles. *J Mater Chem* **2012**, *22* (5), 1962-1968.

18. Thalladi, V. R.; Whitesides, G. M., Crystals of crystals: Fabrication of encapsulated and ordered two-dimensional arrays of microcrystals. *J Am Chem Soc* **2002**, *124* (14), 3520-3521.

19. Suh, K. Y.; Khademhosseini, A.; Eng, G.; Langer, R., Single nanocrystal arrays on patterned poly(ethylene glycol) copolymer microstructures using selective wetting and drying. *Langmuir* **2004**, *20* (15), 6080-6084.

20. Barton, J. E.; Odom, T. W., Mass-limited growth in zeptoliter beakers: A general approach for the synthesis of nanocrystals. *Nano Lett* **2004**, *4* (8), 1525-1528.

21. Choi, S.; Stassi, S.; Pisano, A. P.; Zohdi, T. I., Coffee-Ring Effect-Based Three Dimensional Patterning of Micro/Nanoparticle Assembly with a Single Droplet. *Langmuir* **2010**, *26* (14), 11690-11698.

22. Brasjen, B. J.; van Cuijk, A. W.; Darhuber, A. A., Dip-coating of chemically patterned surfaces. *Chem Eng Process* **2011**, *50* (5-6), 565-568.

23. Nidetz, R.; Kim, J., Directed self-assembly of nanogold using a chemically modified nanopatterned surface. *Nanotechnology* **2012**, *23* (4).

24. Fustin, C. A.; Glasser, G.; Spiess, H. W.; Jonas, U., Site-selective growth of colloidal crystals with photonic properties on chemically patterned surfaces. Adv Mater 2003, 15 (12), 1025-+.

25. Maury, P.; Escalante, M.; Reinhoudt, D. N.; Huskens, J., Directed assembly of nanoparticles onto polymer-imprinted or chemically patterned templates fabricated by nanoimprint lithography. *Adv Mater* **2005**, *17* (22), 2718-+.

26. Bao, R. R.; Zhang, C. Y.; Zhang, X. J.; Ou, X. M.; Lee, C. S.; Jie, J. S.; Zhang, X. H., Self-Assembly and Hierarchical Patterning of Aligned Organic Nanowire Arrays by Solvent Evaporation on Substrates with Patterned Wettability. *Acs Appl Mater Inter* **2013**, *5* (12), 5757-5762.

27. Gentili, D.; Foschi, G.; Valle, F.; Cavallini, M.; Biscarini, F., Applications of dewetting in micro and nanotechnology. *Chem Soc Rev* **2012**, *41* (12), 4430-4443.

28. Tian, D. L.; Song, Y. L.; Jiang, L., Patterning of controllable surface wettability for printing techniques. *Chem Soc Rev* **2013**, *42* (12), 5184-5209.

29. Darhuber, A. A.; Troian, S. M.; Davis, J. M.; Miller, S. M.; Wagner, S., Selective dip-coating of chemically micropatterned surfaces. *J Appl Phys* **2000**, *88* (9), 5119-5126.

30. Riskin, A.; De Dobbelaere, C.; Shan, L.; Boyen, H. G.; D'Haen, J.; Hardy, A.; van Bael, M. K., Dewetting of Patterned Silicon Substrates Leading to a Selective Deposition of Micellar-Based Nanoparticles. *J Phys Chem C* **2012**, *116* (19), 10743-10752.

31. Aizenberg, J.; Braun, P. V.; Wiltzius, P., Patterned colloidal deposition controlled by electrostatic and capillary forces. *Phys Rev Lett* **2000**, *84* (13), 2997-3000.

32. Briseno, A. L.; Aizenberg, J.; Han, Y. J.; Penkala, R. A.; Moon, H.; Lovinger, A. J.; Kloc, C.; Bao, Z. A., Patterned growth of large oriented organic semiconductor single crystals on self-assembled monolayer templates. *J Am Chem Soc* **2005**, *127* (35), 12164-12165.

33. Briseno, A. L.; Mannsfeld, S. C. B.; Ling, M. M.; Liu, S. H.; Tseng, R. J.; Reese, C.; Roberts, M. E.; Yang, Y.; Wudl, F.; Bao, Z. N., Patterning organic single-crystal transistor arrays. *Nature* **2006**, *444* (7121), 913-917.

34. Briseno, A. L.; Roberts, M.; Ling, M. M.; Moon, H.; Nemanick, E. J.; Bao, Z. N., Patterning organic semiconductors using "dry" poly(dimethylsiloxane) elastomeric stamps for thin film transistors. *J Am Chem Soc* **2006**, *128* (12), 3880-3881.

35. Winzenberg, K. N.; Kemppinen, P.; Fanchini, G.; Bown, M.; Collis, G. E.; Forsyth, C. M.; Hegedus, K.; Singh, T. B.; Watkins, S. E., Dibenzo[b,def]chrysene Derivatives: Solution-Processable Small Molecules that Deliver High Power-Conversion Efficiencies in Bulk Heterojunction Solar Cells. *Chem Mater* **2009**, *21* (24), 5701-5703.

36. Cheng, D. F.; McCarthy, T. J., Using the Fact that Wetting Is Contact Line Dependent. *Langmuir* **2011**, *27* (7), 3693-3697.

37. Gao, L. C.; McCarthy, T. J., Ionic liquid marbles. *Langmuir* **2007**, *23* (21), 10445-10447.

38. The volume of liquid in the puddles was determined by calculating the height, h, of the circular puddle, assuming that it has a spherical cap: $h = \frac{r}{\sin\theta}(1-\cos\theta)$, θ is the contact angle of N^+S^- on silica, and r is the average radius of the puddles. The average volume of the N^+S^- puddle is $V_{IL} = \frac{1}{6}\pi h(3r^2 + h^2)$ and the average volume of 25% aqueous N^+S^- that was dip-coated is $V = 4V_{IL}$.

39. deGennes, P. G. B.-W., F, Capillary and Wetting Phenomena. Springer: 2004.

40. Fadeev, A. Y.; McCarthy, T. J., Self-assembly is not the only reaction possible between alkyltrichlorosilanes and surfaces: Monomolecular and oligomeric covalently attached layers of dichloro- and trichloroalkylsilanes on silicon. *Langmuir* **2000**, *16* (18), 7268-7274.

41. Gao, L. C.; McCarthy, T. J., Ionic liquids are useful contact angle probe fluids. *J Am Chem Soc* **2007**, *129* (13), 3804-+.

42. Nakajima, A.; Nakagawa, Y.; Furuta, T.; Sakai, M.; Isobe, T.; Matsushita, S., Sliding of Water Droplets on Smooth Hydrophobic Silane Coatings with Regular Triangle Hydrophilic Regions. *Langmuir* **2013**, *29* (29), 9269-9275.

43. Wang, L. M.; McCarthy, T. J., Shear Distortion and Failure of Capillary Bridges. Wetting Information Beyond Contact Angle Analysis. *Langmuir* **2013**, *29* (25), 7776-7781.

44. We measured viscosity values of N^+S^- between 1100 and 1229 cP (4 measurements) using a parallel plate rheometer. 25% aq. N^+S^- exhibited a viscosity of ~2 cP. For comparison, water and glycerol exhibited 1.1 and 1002 cP with this instrument.

45. Mampallil, D.; Eral, H. B.; van den Ende, D.; Mugele, F., Control of evaporating complex fluids through electrowetting. *Soft Matter* **2012**, *8* (41), 10614-10617.

46. Eral, H. B.; van den Ende, D.; Mugele, F., Say goodbye to coffee stains. *Phys World* **2012**, *25* (4), 33-37.

APPENDIX

PDMS/POLY(*P*-XYLYLENE) (PPX) COMPOSITES

The chemical vapor deposition (CVD) of poly(*p*-xylylene) (PPX) prepared from sublimation and pyrolysis of [2.2]paracyclophane leads to conformal coatings on the substrates with three dimensional topology. The resulting linear polymer PPX is crystalline, and the coating is of uniform thickness.[1] PPX is chemically inert, thermally stable (even at 220 ^{o}C), UV resistant and corrosion resistant. It is of low permeability to gases including water vapor. It is of low friction coefficient and exhibits special dielectric properties. It can inhibit bacterial growth as well.[2] Therefore, PPX coatings can serve as moisture barrier layer, corrosion resistance layer, biopassivation layer and components in microelectrical mechanical systems. Enormous research interests have focused on the mechanism of the gas phase reaction, the chemical structure, and the patterned growth of PPX. Jensen and coworkers claimed transition metals, metal salts, and organometallic complexes all inhibit the PPX deposition because the absorbed *p*-xylylene can be deactivated by these substances. Vasenkov used molecular dynamic simulation to elucidate the mechanism of adhesion of metal atoms to parylene, aiming at providing insight into the *p*-xylylene deactivation mechanism.[3] Although the mechanism of the inhibition remains unclear, using transition metal patterns to inhibit PPX growth is a promising method to pattern electrodes of micron sizes.

One important application of PDMS elastomer involves casting on photoresist patterns to make devices such as microcontact printing stamps, in which the precise replication of the molds is important. The adhesion between the mold and the

elastomer should be minimized to ensure the success of the molding process. Hansen and coworkers coated masters with parylene C (prepared from monochloro-[2.2]paracyclophane), which is a transparent, inert and hydrophobic polymer coating. It was demonstrated that the coated masters readily produced PDMS features of high precision.[4]

Wrinkling instability is the response of a membrane under low compressive strain. The membrane buckles out of the plane, and the wrinkling morphology is established. Examples of wrinkling are ubiquitous in daily life, ranging from imperfectly cured coatings to the aging of skin. The reasons for wrinkling involve mechanical compression, thermal expansion, swelling, shrinkage, etc.[5] PDMS is frequently used as the substrate to induce wrinkles, and the first publication regarding wrinkles on PDMS is from Whitesides' group. PDMS was coated with thin metal films by electron beam evaporation. The PDMS is heated during the coating process, and then the modified PDMS is cooled to ambient temperature. Wrinkling of the metal layer is formed due to the thermal contraction of the PDMS substrate.[6]

Wrinkling morphologies were observed on PPX thin film coated PDMS. A former group member, Kevin Wier deposited PPX on unconstrained PDMS and the PDMS under tension separately. He discovered that wrinkling develops on both samples.[7] However, the wrinkling instability was not studied from the perspective of wrinkling mechanics in his work, and the interfacial structure between PPX and PDMS remains unclear.

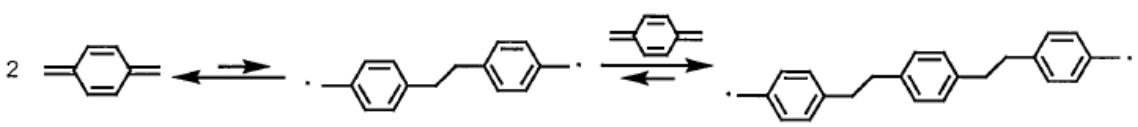

Figure A-1 Initiation reaction for the polymerization of PPX [8]

In this work, PPX coatings were synthesized following the Gorham's method. [2.2] paracyclophane (Sigma-Aldrich) was sublimed at around 200 ^{o}C by using a heating tape surrounding a Pyrex vessel. The volatile dimer was pyrolyzed in a tube furnace (Thermolyne 79300) at 650 ^{o}C to cleave into two *p*-xylylene monomers. Various cross-linked PDMS samples were placed in a deposition chamber which was kept at 10 ^{o}C. On the PDMS samples, two monomers first combine to form a dimer diradical, which can either decompose into two monomers, or react with another monomer to form a trimer diradical. The trimer diradical is a more energetically favorable state, and can initiate further polymerization (Figure A-1).[8]

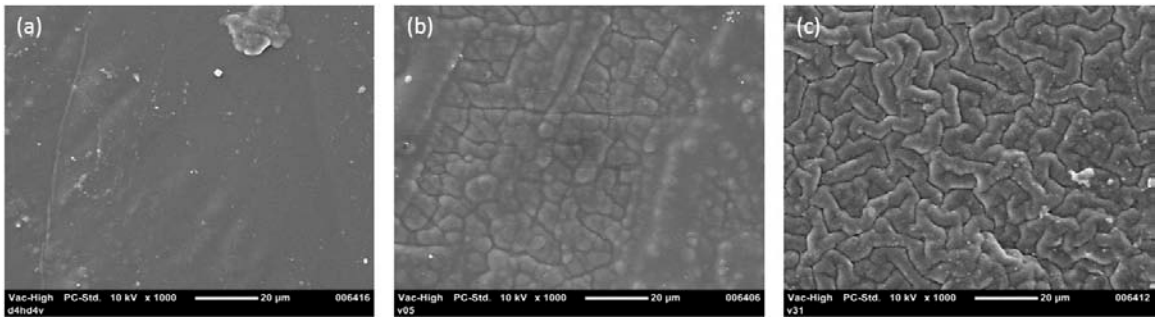

Figure A-2 SEM images of surfaces of PPX coated silicone samples (a) D_4^H-D_4^V, H: vinyl=15:1, 12 ppm Pt; (b) PDMS-Vinyl (M_w~800), PDMS-H (M_w~1800-2100), H:Vinyl=15:1, 3 ppm Pt; (c) PDMS-Vinyl (M_w~28 000), PDMS-H (M_w~1800-2100), H: Vinyl=15:1, 9 ppm Pt.

Table A-1 Wavelength of wrinkles of PPX coated silicone films calculated by using Image J. Wavelength results are based on at least 5 point measurements.

	D_4^H-D_4^V silicone	**Pure silicone (800)**	**Pure silicone (28 000)**
Wavelength of wrinkles (μm)	0	4.32	5.48

Cross-linked PDMS of different modulus and cross-linking density were prepared. Vinyl-terminated PDMS of two different molecular weights ('PDMS-Vinyl', M_w~28 000 g/mol and M_w~800 g/mol) were cross-linked with

polymethylhydridosiloxane ('PDMS-H', M_w~1800-2100 g/mol) in the presence of Karstedt's catalyst, and PDMS-H and PDMS-Vinyl were mixed with a molar ratio of H: vinyl=15:1. The hydrosilylation reaction between PDMS-Vinyl (M_w~28000 g/mol) and PDMS-H was catalyzed by 9 ppm Pt catalyst (based on silicone product mass), while hydrosilylation reaction between PDMS-Vinyl (M_w~800 g/mol) and PDMS-H was catalyzed by 3 ppm Pt catalyst. D_4^H and D_4^V were cross-linked with a molar ratio of H: vinyl=2: 1, and the reaction was catalyzed by 12 ppm Pt catalyst. These silicone samples are named as pure silicone (28 000), pure silicone (800) and D_4^H-D_4^V silicone, which represent lowly cross-linked silicone, medium cross-linked silicone and highly cross-linked silicone, respectively.

Different surface morphologies are observed on the PPX-coated silicone samples. It is shown in Figure A-2(a) that a smooth PPX thin film coats on D_4^H-D_4^V silicone, while wrinkling instabilities are generated on both the pure silicone (800) and pure silicone (28 000) (Figure A-2(b)(c)). One possible explanation for the wrinkling morphology is that the monomers can diffuse into the cross-linked silicones, swelling the upper part of the silicone. The lower part of the silicone exerts the compressive force to the 'swollen' part, so that wrinkles appear on the surface. In contrast, D_4^H-D_4^V silicone has a very compact network structure which does not allow the passage of *p*-xylylene monomer. The PPX coating may have a clear interface with D_4^H-D_4^V silicone, maintaining a smooth surface morphology.

Wavelengths of wrinkling instability on three types of PPX-coated silicone, which are listed in Table A-1, are calculated with the software Image J. It is seen that the pure silicone (28 000) has the largest wrinkle wavelength (5.48 μm), whereas the

D_4^H-D_4^V silicone has the smallest wavelength (0). The wavelengths of the wrinkles on PPX-coated silicone decrease with increasing silicone cross-linking density.

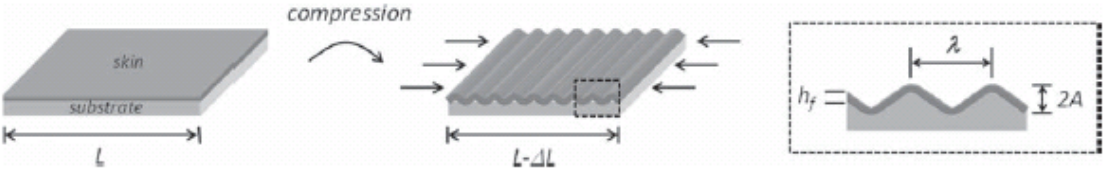

Figure A-3 Schematic of the wrinkling of a structure comprised of a stiff skin adhered to a soft substrate [9]

We are interested in finding an explanation for the trend of wrinkling wavelengths. Some researchers already conducted theoretical studies of the wrinkling mechanics. The model system is depicted in Figure A-3. A soft substrate is covered by a stiff skin, and the surface wrinkles under compression. The classic equation for film bending is:

$$E_f I \frac{d^4 z}{dx^4} + F \frac{d^2 z}{dx^2} + kz = 0 \qquad \text{Equation A-1}$$

In Equation A-1, E_f and F denote the plane-strain modulus of the stiff skin and the applied load, respectively. I is the moment of inertia. k is the wrinkle's modulus. Under the assumption that the wrinkling morphology follows sinusoidal form,

$$z(x) = A\sin\frac{2\pi x}{\lambda} \qquad \text{Equation A-2}$$

Equation A-1 and Equation A-2 together lead to the expression for applied force:

$$F = 4E_f I(\frac{\pi}{\lambda})^2 + \frac{E_S w}{4}(\frac{\pi}{\lambda})^{-1} \qquad \text{Equation A-3}$$

where w is the width of the film, λ is the wavelength of the wrinkles, and E_S is the modulus of the substrate.

To minimize the applied force, the first order derivative of F with respect to wavelength λ should be set as 0. This yields to the equation of the wavelength,

$$\lambda = 2\pi h(\frac{E_f}{3E_s})^{\frac{1}{3}} \qquad \text{Equation A-4}$$

In Equation A-4, h is the thickness of the stiff skin.[9] The PPX film is reported to have a modulus of 2.4 GPa.[10] The D_4^H-D_4^V silicone substrate is reported to have a modulus of 1.69 GPa, similar to that of PPX film.[11] The pure silicone (28 000) and pure silicone (800) substrates have a modulus at the scale of MPa (10^{-3} GPa), which is much smaller than that of PPX films, so their wrinkling wavelengths λ are large. It can be also concluded from Equation A-4 that λ increases when E_S decrease. This explains why the low cross-linked silicone (pure silicone (28 000)) has the largest λ value in Table A-1.

The PPX-coated pure silicone (62 700) was etched in a mixture of potassium hydroxide (KOH, Fisher Scientific, Inc.) and isopropanol (Fisher Scientific, Inc.). It is noted that PDMS-Vinyl has a M_w of 62 700 in this particular experiment. The PDMS phase can be completely etched by base, yet PPX has good resistance to base etching. As is shown in Figure A-3, PPX morphology at the air/PPX interface is the positive replica of the wrinkling morphology, while PPX morphology at silicone/PPX interface is the negative replica of the wrinkling morphology. These morphologies are displayed in SEM images, including the positive replica (Figure A-4(a)(b)) and

negative replica (Figure A-4(c)(d)). It might be interesting to take a closer examination of the silicone/PPX interface and learn some information about *p*-xylylene monomer dissolution in PDMS.

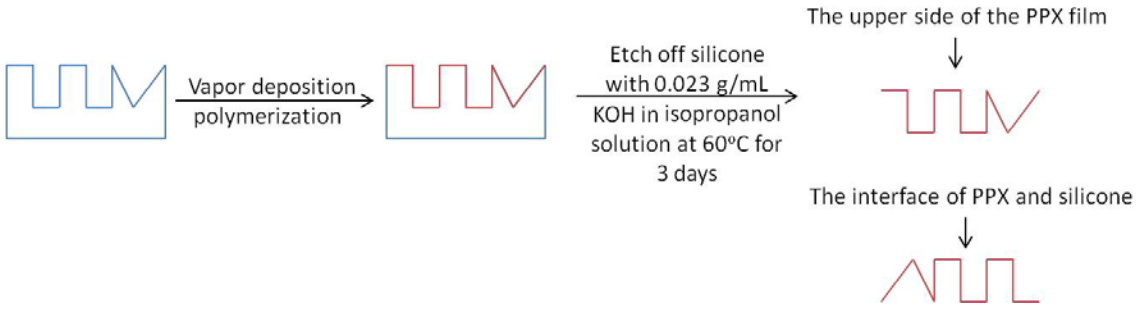

Figure A-3 Etching of silicone to observe PPX. Blue block represents cross-linked silicone and red curve represents PPX thin film.

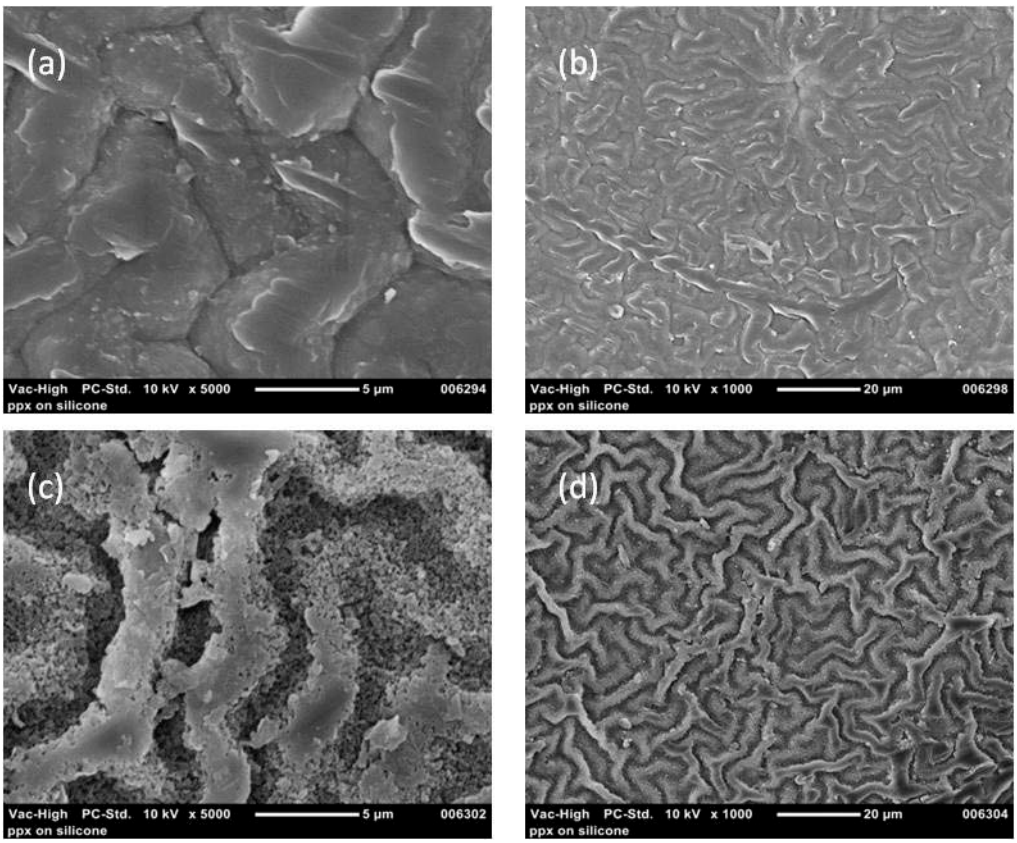

Figure A-4 SEM images of (a, b) The upper side of the PPX film; (c, d) The interface of PPX and silicone (PDMS-Vinyl (M_w~62 700), PDMS-H (M_w~1800-2100), H: vinyl=15:1, 2 ppm Pt)

References

1. Alf, M. E.; Asatekin, A.; Barr, M. C.; Baxamusa, S. H.; Chelawat, H.; Ozaydin-Ince, G.; Petruczok, C. D.; Sreenivasan, R.; Tenhaeff, W. E.; Trujillo, N. J.; Vaddiraju, S.; Xu, J. J.; Gleason, K. K., Chemical Vapor Deposition of Conformal, Functional, and Responsive Polymer Films. *Adv Mater* **2010,** *22* (18), 1993-2027.

2. Hopf, H., [2.2]Paracyclophanes in Polymer Chemistry and Materials Science. *Angew Chem Int Edit* **2008,** *47* (51), 9808-9812.

3. Vaeth, K. M.; Jensen, K. F., Transition metals for selective chemical vapor deposition of parylene-based polymers. *Chem Mater* **2000,** *12* (5), 1305-1313.

4. Heyries, K. A.; Hansen, C. L., Parylene C coating for high-performance replica molding. *Lab Chip* **2011,** *11* (23), 4122-4125.

5. Schweikart, A.; Fery, A., Controlled wrinkling as a novel method for the fabrication of patterned surfaces. *Microchim Acta* **2009,** *165* (3-4), 249-263.

6. Bowden, N.; Brittain, S.; Evans, A. G.; Hutchinson, J. W.; Whitesides, G. M., Spontaneous formation of ordered structures in thin films of metals supported on an elastomeric polymer. *Nature* **1998,** *393* (6681), 146-149.

7. Wier, K. A., COMPOSITE POLYMER COATINGS PREPARED IN SUPERCRITICAL CARBON DIOXIDE *phD thesis* **2006**.

8. Herrera-Alonso, M., Surface chemistry of poly(p-xylylene) and nylon. *phD thesis* **2005**.

9. Chung, J. Y.; Nolte, A. J.; Stafford, C. M., Surface Wrinkling: A Versatile Platform for Measuring Thin-Film Properties. *Adv Mater* **2011,** *23* (3), 349-368.

10. Beach, W. F. L., C.; Bassett, D. R.; Austin, T. M.; Olson, R. In, Encyclopedia of Polymer Science and Engineering. 2nd ed.; Wiley: 1989.

11. Zheng, P. W.; McCarthy, T. J., Rediscovering silicones, part 1, extremely crosslinked PDMS: A low surface energy, unfilled, UV/vis-transparent, thermally stable, molecularly smooth, hard, and elastic material. *Abstr Pap Am Chem S* **2011,** *241*.

BIBLIOGRAPHY

Abbasi, F.; Mirzadeh, H.; Katbab, A. A., Modification of polysiloxane polymers for biomedical applications: a review. *Polym Int* **2001,** *50* (12), 1279-1287.

Abbasi, F.; Mirzadeh, H.; Katbab, A. A., Bulk and surface modification of silicone rubber for biomedical applications. *Polym Int* **2002,** *51* (10), 882-888.

Aizenberg, J.; Braun, P. V.; Wiltzius, P., Patterned colloidal deposition controlled by electrostatic and capillary forces. *Phys Rev Lett* **2000,** *84* (13), 2997-3000.

Alexandru, M.; Cristea, M.; Cazacu, M.; Ioanid, A.; Simionescu, B. C., Composite Materials Based on Polydimethylsiloxane and In Situ Generated Silica by Using the Sol Gel Technique. *Polym Composite* **2009,** *30* (6), 751-759.

Alf, M. E.; Asatekin, A.; Barr, M. C.; Baxamusa, S. H.; Chelawat, H.; Ozaydin-Ince, G.; Petruczok, C. D.; Sreenivasan, R.; Tenhaeff, W. E.; Trujillo, N. J.; Vaddiraju, S.; Xu, J. J.; Gleason, K. K., Chemical Vapor Deposition of Conformal, Functional, and Responsive Polymer Films. *Adv Mater* **2010,** *22* (18), 1993-2027.

Aoki, T., Macromolecular design of permselective membranes. *Prog Polym Sci* **1999,** *24* (7), 951-993.

Aranguren, M. I.; Mora, E.; Degroot, J. V.; Macosko, C. W., Effect of Reinforcing Fillers on the Rheology of Polymer Melts. *J Rheol* **1992,** *36* (6), 1165-1182.

Bao, R. R.; Zhang, C. Y.; Zhang, X. J.; Ou, X. M.; Lee, C. S.; Jie, J. S.; Zhang, X. H., Self-Assembly and Hierarchical Patterning of Aligned Organic Nanowire Arrays by Solvent Evaporation on Substrates with Patterned Wettability. *Acs Appl Mater Inter* **2013,** *5* (12), 5757-5762.

Baquey, G.; Moine, L.; Degueil-Castaing, M.; Lartigue, J. C.; Maillard, B., Decomposition of di-tert-butyl peroxide in siloxane: An approach of the free radical cross-linking of silicones. *Macromolecules* **2005,** *38* (23), 9571-9583.

Barrie, J. A.; Machin, D., Sorption and Diffusion of Water in Silicone Rubbers .1. Unfilled Rubbers. *J Macromol Sci Phys* **1969,** *B 3* (4), 645-&.

Barton, J. E.; Odom, T. W., Mass-limited growth in zeptoliter beakers: A general approach for the synthesis of nanocrystals. *Nano Lett* **2004,** *4* (8), 1525-1528.

Beach, W. F. L., C.; Bassett, D. R.; Austin, T. M.; Olson, R. In, Encyclopedia of Polymer Science and Engineering. 2nd ed.; Wiley: 1989.

Befahy, S.; Lipnik, P.; Pardoen, T.; Nascimento, C.; Patris, B.; Bertrand, P.; Yunus, S., Thickness and Elastic Modulus of Plasma Treated PDMS Silica-like Surface Layer. *Langmuir* **2010,** *26* (5), 3372-3375.

Bhagat, A. A. S.; Jothimuthu, P.; Papautsky, I., Photodefinable polydimethylsiloxane (PDMS) for rapid lab-on-a-chip prototyping. *Lab Chip* **2007,** *7* (9), 1192-1197.

Bodas, D.; Rauch, J. Y.; Khan-Malek, C., Surface modification and aging studies of addition-curing silicone rubbers by oxygen plasma. *Eur Polym J* **2008,** *44* (7), 2130-2139.

Borde, A.; Larsson, M.; Odelberg, Y.; Hagman, J.; Lowenhielm, P.; Larsson, A., Increased water transport in PDMS silicone films by addition of excipients. *Acta Biomater* **2012,** *8* (2), 579-588.

Bowden, N.; Brittain, S.; Evans, A. G.; Hutchinson, J. W.; Whitesides, G. M., Spontaneous formation of ordered structures in thin films of metals supported on an elastomeric polymer. *Nature* **1998,** *393* (6681), 146-149.

Brasjen, B. J.; van Cuijk, A. W.; Darhuber, A. A., Dip-coating of chemically patterned surfaces. *Chem Eng Process* **2011,** *50* (5-6), 565-568.

Breid, D.; Crosby, A. J., Effect of stress state on wrinkle morphology. *Soft Matter* **2011,** *7* (9), 4490-4496.

Briseno, A. L.; Aizenberg, J.; Han, Y. J.; Penkala, R. A.; Moon, H.; Lovinger, A. J.; Kloc, C.; Bao, Z. A., Patterned growth of large oriented organic semiconductor single crystals on self-assembled monolayer templates. *J Am Chem Soc* **2005,** *127* (35), 12164-12165.

Briseno, A. L.; Mannsfeld, S. C. B.; Ling, M. M.; Liu, S. H.; Tseng, R. J.; Reese, C.; Roberts, M. E.; Yang, Y.; Wudl, F.; Bao, Z. N., Patterning organic single-crystal transistor arrays. *Nature* **2006,** *444* (7121), 913-917.

Briseno, A. L.; Roberts, M.; Ling, M. M.; Moon, H.; Nemanick, E. J.; Bao, Z. N., Patterning organic semiconductors using "dry" poly(dimethylsiloxane) elastomeric stamps for thin film transistors. *J Am Chem Soc* **2006,** *128* (12), 3880-3881.

Buddy D. Ratner, A. S. H., Frederick J. Schoen, Jack E. Lemons, Biomaterial Science: An Introduction to Materials in Medicine. Elservier, Inc.

Burnside, S. D.; Giannelis, E. P., Synthesis and Properties of New Poly(Dimethylsiloxane) Nanocomposites. *Chem Mater* **1995,** *7* (9), 1597-1600.

Cai, G. P.; Weber, W. P., Synthesis of terminal Si-H irregular tetra-branched star polysiloxanes. Pt-catalyzed hydrosilylation with unsaturated epoxides. Polysiloxane films by photo-acid catalyzed crosslinking. *Polymer* **2004,** *45* (9), 2941-2948.

Camenzind, A.; Schweizer, T.; Sztucki, M.; Pratsinis, S. E., Structure & strength of silica-PDMS nanocomposites. *Polymer* **2010,** *51* (8), 1796-1804.

Camino, G.; Lomakin, S. M.; Lazzari, M., Polydimethylsiloxane thermal degradation - Part 1. Kinetic aspects. *Polymer* **2001,** *42* (6), 2395-2402.

Chan, C. K.; Peng, S. L.; Chu, I. M.; Ni, S. C., Effects of heat treatment on the properties of poly(methyl methacrylate)/silica hybrid materials prepared by sol-gel process. *Polymer* **2001,** *42* (9), 4189-4196.

Chen, H.; Brook, M. A.; Sheardown, H., Silicone elastomers for reduced protein adsorption. *Biomaterials* **2004,** *25* (12), 2273-2282.

Chen, H.; Zhang, Z.; Chen, Y.; Brook, M. A.; Sheardown, H., Protein repellant silicone surfaces by covalent immobilization of poly(ethylene oxide). *Biomaterials* **2005,** *26* (15), 2391-2399.

Chen, L.; Yang, G.; Wang, S. T., Air-Grid Surface Patterning Provided by Superhydrophobic Surfaces. *Small* **2012,** *8* (7), 962-965.

Cheng, D. F.; McCarthy, T. J., Using the Fact that Wetting Is Contact Line Dependent. *Langmuir* **2011,** *27* (7), 3693-3697.

Chin Myung Whang, C. S. Y., and Yoo Hang Kim, Preparation and Characterization of Sol-Gel Derived SiO2-TiO2-PDMS Composite Films. *Bull. Korean Chem. Soc.* **2001,** *22*, 1366-1370.

Choi, K. M.; Rogers, J. A., A photocurable poly(dimethylsiloxane) chemistry designed for soft lithographic molding and printing in the nanometer regime. *J Am Chem Soc* **2003,** *125* (14), 4060-4061.

Choi, S.; Stassi, S.; Pisano, A. P.; Zohdi, T. I., Coffee-Ring Effect-Based Three Dimensional Patterning of Micro/Nanoparticle Assembly with a Single Droplet. *Langmuir* **2010,** *26* (14), 11690-11698.

Chung, J. Y.; Nolte, A. J.; Stafford, C. M., Surface Wrinkling: A Versatile Platform for Measuring Thin-Film Properties. *Adv Mater* **2011,** *23* (3), 349-368.

Clarson, S. J., Silicones and Silicone-modified Materials. American Chemical Society: 2000.

Cohenaddad, J. P., Sol or Gel-Like Behavior of Ideal Silica Siloxane Mixtures - Percolation Approach. *Polymer* **1992,** *33* (13), 2762-2767.

Colby, R., Polymer Physics.

Comyn, J., *Polymer Permeability*. Elsevier Applied Science Publishers LTD: 1985.

Darhuber, A. A.; Troian, S. M.; Davis, J. M.; Miller, S. M.; Wagner, S., Selective dip-coating of chemically micropatterned surfaces. *J Appl Phys* **2000,** *88* (9), 5119-5126.

De Souza, E. J.; Gao, L. C.; McCarthy, T. J.; Arzt, E.; Crosby, A. J., Effect of contact angle hysteresis on the measurement of capillary forces. *Langmuir* **2008,** *24* (4), 1391-1396.

deGennes, P. G. B.-W., F, Capillary and Wetting Phenomena. Springer: 2004.

Delamarche, E.; Geissler, M.; Bernard, A.; Wolf, H.; Michel, B.; Hilborn, J.; Donzel, C., Hydrophilic poly (dimethylsloxane) stamps for microcontact printing. *Adv Mater* **2001,** *13* (15), 1164-+.

Dewimille, L.; Bresson, B.; Bokobza, L., Synthesis, structure and morphology of poly (dimethylsiloxane) networks filled with in situ generated silica particles. *Polymer* **2005,** *46* (12), 4135-4143.

Dobrak, A.; Figoli, A.; Chovau, S.; Galiano, F.; Simone, S.; Vankelecom, I. F. J.; Drioli, E.; Van der Bruggen, B., Performance of PDMS membranes in pervaporation: Effect of silicalite fillers and comparison with SBS membranes. *J Colloid Interf Sci* **2010,** *346* (1), 254-264.

Dufour, R.; Brunet, P.; Harnois, M.; Boukherroub, R.; Thomy, V.; Senez, V., Zipping Effect on Omniphobic Surfaces for Controlled Deposition of Minute Amounts of Fluid or Colloids. *Small* **2012,** *8* (8), 1229-1236.

Eral, H. B.; van den Ende, D.; Mugele, F., Say goodbye to coffee stains. *Phys World* **2012,** *25* (4), 33-37.

Estevez, M. C.; O'Donoghue, M. B.; Chen, X. L.; Tan, W. H., Highly Fluorescent Dye-Doped Silica Nanoparticles Increase Flow Cytometry Sensitivity for Cancer Cell Monitoring. *Nano Res* **2009,** *2* (6), 448-461.

Fadeev, A. Y.; McCarthy, T. J., A new route to covalently attached monolayers: Reaction of hydridosilanes with titanium and other metal surfaces. *J Am Chem Soc* **1999,** *121* (51), 12184-12185.

Fadeev, A. Y.; McCarthy, T. J., Trialkylsilane monolayers covalently attached to silicon surfaces: Wettability studies indicating that molecular topography contributes to contact angle hysteresis. *Langmuir* **1999,** *15* (11), 3759-3766.

Fadeev, A. Y.; McCarthy, T. J., Self-assembly is not the only reaction possible between alkyltrichlorosilanes and surfaces: Monomolecular and oligomeric covalently attached layers of dichloro- and trichloroalkylsilanes on silicon. *Langmuir* **2000,** *16* (18), 7268-7274.

Frogley, M. D.; Ravich, D.; Wagner, H. D., Mechanical properties of carbon nanoparticle-reinforced elastomers. *Compos Sci Technol* **2003,** *63* (11), 1647-1654.

Fu, Y. J.; Qui, H. Z.; Liao, K. S.; Lue, S. J.; Hu, C. C.; Lee, K. R.; Lai, J. Y., Effect of UV-Ozone Treatment on Poly(dimethylsiloxane) Membranes: Surface Characterization and Gas Separation Performance. *Langmuir* **2010,** *26* (6), 4392-4399.

Furmidge, C. G., Studies at Phase Interfaces .1. Sliding of Liquid Drops on Solid Surfaces and a Theory for Spray Retention. *J Coll Sci Imp U Tok* **1962,** *17* (4), 309-&.

Fustin, C. A.; Glasser, G.; Spiess, H. W.; Jonas, U., Site-selective growth of colloidal crystals with photonic properties on chemically patterned surfaces. *Adv Mater* **2003,** *15* (12), 1025-+.

Gao, L. C.; McCarthy, T. J., Contact angle hysteresis explained. *Langmuir* **2006,** *22* (14), 6234-6237.

Gao, L. C.; McCarthy, T. J., Ionic liquid marbles. *Langmuir* **2007,** *23* (21), 10445-10447.

Gao, L. C.; McCarthy, T. J., Ionic liquids are useful contact angle probe fluids. *J Am Chem Soc* **2007,** *129* (13), 3804-+.

Gao, L. C.; McCarthy, T. J., Teflon is hydrophilic. Comments on definitions of hydrophobic, shear versus tensile hydrophobicity, and wettability characterization. *Langmuir* **2008,** *24* (17), 9183-9188.

Gao, L. C.; McCarthy, T. J., Wetting 101 degrees. *Langmuir* **2009,** *25* (24), 14105-14115.

Gelest Catalog.

Gentili, D.; Foschi, G.; Valle, F.; Cavallini, M.; Biscarini, F., Applications of dewetting in micro and nanotechnology. *Chem Soc Rev* **2012,** *41* (12), 4430-4443.

Geyer, F. L.; Ueda, E.; Liebel, U.; Grau, N.; Levkin, P. A., Superhydrophobic-Superhydrophilic Micropatterning: Towards Genome-on-a-Chip Cell Microarrays. *Angew Chem Int Edit* **2011,** *50* (36), 8424-8427.

Gilbert, A. R.; Kantor, S. W., Transient Catalysts for the Polymerization of Organosiloxanes. *J Polym Sci* **1959,** *40* (136), 35-58.

Goddard, J. M.; Hotchkiss, J. H., Polymer surface modification for the attachment of bioactive compounds. *Prog Polym Sci* **2007,** *32* (7), 698-725.

Godnjavec, J.; Znoj, B.; Vince, J.; Steinbucher, M.; Znidarsic, A.; Venturini, P., STABILIZATION OF RUTILE TiO2 NANOPARTICLES WITH GLYMO IN POLYACRYLIC CLEAR COATING. *Mater Tehnol* **2012,** *46* (1), 19-24.

Grassie, N.; Macfarlane, I. G., Thermal-Degradation of Polysiloxanes .1. Poly(Dimethylsiloxane). *Eur Polym J* **1978,** *14* (11), 875-884.

Guan, C.; Lu, C. L.; Liu, Y. F.; Yang, B., Preparation and characterization of high refractive index thin films of TiO2/epoxy resin nanocomposites. *J Appl Polym Sci* **2006,** *102* (2), 1631-1636.

Hatton, B. D.; Aizenberg, J., Writing on Superhydrophobic Nanopost Arrays: Topographic Design for Bottom-up Assembly. *Nano Lett* **2012,** *12* (9), 4551-4557.

Helmy, R.; Wenslow, R. W.; Fadeev, A. Y., Reaction of organosilicon hydrides with solid surfaces: An example of surface-catalyzed self-assembly. *J Am Chem Soc* **2004,** *126* (24), 7595-7600.

Herrera-Alonso, M., Surface chemistry of poly(p-xylylene) and nylon. *phD thesis* **2005**.

Heyries, K. A.; Hansen, C. L., Parylene C coating for high-performance replica molding. *Lab Chip* **2011,** *11* (23), 4122-4125.

Hopf, H., [2.2]Paracyclophanes in Polymer Chemistry and Materials Science. *Angew Chem Int Edit* **2008,** *47* (51), 9808-9812.

Hore, M. J. A.; Frischknecht, A. L.; Composto, R. J., Nanorod Assemblies in Polymer Films and Their Dispersion-Dependent Optical Properties. *Acs Macro Lett* **2012,** *1* (1), 115-121.

Huglin, M. B.; Zakaria, M. B., Comments on Expressing the Permeability of Polymers to Gases. *Angew Makromol Chem* **1983,** *117* (Nov), 1-13.

J, C., Mathematics of diffusion. 2nd Edition ed.; Oxford University Press: 1975.

J. Brandrup , E. H. I., E. A. Grulke Polymer Handbook. 4 ed.; John Wiley & Sons, Inc: 1999.

J. Chen, S. S., W. Liu, M. Scott, L. Lacy, S. Allen, S. A. Wickline, X. Yu, Contributions of Collagen Matrix to Restricted Water Diffusion in Post-infarct Rat Heart. *Proc. Intl. Soc. Mag. Reson. Med* **2003,** *11*, 887.

Jie, Y. N.; Niskala, J. R.; Johnston-Peck, A. C.; Krommenhoek, P. J.; Tracy, J. B.; Fan, H. Q.; You, W., Laterally patterned magnetic nanoparticles. *J Mater Chem* **2012,** *22* (5), 1962-1968.

Jo, S.; Park, K., Surface modification using silanated poly(ethylene glycol)s. *Biomaterials* **2000,** *21* (6), 605-616.

Juchniewicz, M.; Stadnik, D.; Biesiada, K.; Olszyna, A.; Chudy, M.; Brzozka, Z.; Dybko, A., Porous crosslinked PDMS-microchannels coatings. *Sensor Actuat B-Chem* **2007,** *126* (1), 68-72.

Kajiyama, T.; Tanaka, K.; Takahara, A., Depth Dependence of the Surface Glass-Transition Temperature of a Poly(Styrene-Block-Methyl Methacrylate) Diblock Copolymer Film on the Basis of Temperature-Dependent X-Ray Photoelectron-Spectroscopy. *Macromolecules* **1995,** *28* (9), 3482-3484.

Kantor, S. W.; Grubb, W. T.; Osthoff, R. C., The Mechanism of the Acid-Catalyzed and Base-Catalyzed Equilibration of Siloxanes. *J Am Chem Soc* **1954,** *76* (20), 5190-5197.

Khorasani, M. T.; Mirzadeh, H.; Kermani, Z., Wettability of porous polydimethylsiloxane surface: morphology study. *Appl Surf Sci* **2005,** *242* (3-4), 339-345.

Koh, S. J., Strategies for controlled placement of nanoscale building blocks. *Nanoscale Res Lett* **2007,** *2* (11), 519-545.

Kohr, J.; Engelhardt, H., Characterization of Quartz Capillaries for Capillary Electrophoresis. *J Chromatogr A* **1993,** *652* (2), 309-316.

Kole, S.; Srivastava, S. K.; Tripathy, D. K.; Bhowmick, A. K., Accelerated Hydrothermal Weathering of Silicone-Rubber, Epdm, and Their Blends. *J Appl Polym Sci* **1994,** *54* (9), 1329-1337.

Kosmulski, M., Chemical Properties of Material Surfaces. CRC Press: 2001.

Krumpfer, J. W.; Bian, P.; Zheng, P. W.; Gao, L. C.; McCarthy, T. J., Contact Angle Hysteresis on Superhydrophobic Surfaces: An Ionic Liquid Probe Fluid Offers Mechanistic Insight. *Langmuir* **2011,** *27* (6), 2166-2169.

Krumpfer, J. W.; McCarthy, T. J., Contact angle hysteresis: a different view and a trivial recipe for low hysteresis hydrophobic surfaces. *Faraday Discuss* **2010,** *146*, 103-111.

Krumpfer, J. W.; McCarthy, T. J., Dip-Coating Crystallization on a Superhydrophobic Surface: A Million Mounted Crystals in a 1 cm(2) Array. *J Am Chem Soc* **2011,** *133* (15), 5764-5766.

Krumpfer, J. W.; McCarthy, T. J., Rediscovering Silicones: "Unreactive" Silicones React with Inorganic Surfaces. *Langmuir* **2011,** *27* (18), 11514-11519.

Kumar, A.; Biebuyck, H. A.; Whitesides, G. M., Patterning Self-Assembled Monolayers - Applications in Materials Science. *Langmuir* **1994,** *10* (5), 1498-1511.

Lai, Y. C., Novel Polyurethane Silicone Hydrogels. *J Appl Polym Sci* **1995,** *56* (3), 301-310.

Lan, Q.; Francis, L. F.; Bates, F. S., Silica nanoparticle dispersions in homopolymer versus block copolymer. *J Polym Sci Pol Phys* **2007,** *45* (16), 2284-2299.

Lane, T. H.; Burns, S. A., Silica, silicon and silicones ... unraveling the mystery. *Curr Top Microbiol* **1996,** *210*, 3-12.

Lee, S.; Shin, H. J.; Yoon, S. M.; Yi, D. K.; Choi, J. Y.; Paik, U., Refractive index engineering of transparent ZrO2-polydimethylsiloxane nanocomposites. *J Mater Chem* **2008,** *18* (15), 1751-1755.

Lee, S.; Voros, J., An aqueous-based surface modification of poly(dimethylsiloxane) with poly(ethylene glycol) to prevent biofouling. *Langmuir* **2005,** *21* (25), 11957-11962.

Lenick, A., The Silicone Conundrum - Silicone Spectator. 2008.

Li, B.; Xu, D.; Zhang, X. F.; Jiang, Z. Y.; Wang, Y.; Ma, J.; Dong, X. A.; Wu, H., Rubbery Polymer-Inorganic Nanocomposite Membranes: Free Volume Characteristics on Separation Property. *Ind Eng Chem Res* **2010,** *49* (24), 12444-12451.

Li, H.; Zhang, J.; Zhou, X. Z.; Lu, G.; Yin, Z. Y.; Li, G. P.; Wu, T.; Boey, F.; Venkatraman, S. S.; Zhang, H., Aminosilane Micropatterns on Hydroxyl-Terminated Substrates: Fabrication and Applications. *Langmuir* **2010,** *26* (8), 5603-5609.

Li, H. Y.; Yu, D. S.; Zhang, J. Y., A novel and facile method for direct synthesis of cross-linked polysiloxanes by anionic ring-opening copolymerization with Ph-12-POSS/D-4/Ph8D4. *Polymer* **2005,** *46* (14), 5317-5323.

Li, J. S. S.; Ueda, E.; Nallapaneni, A.; Li, L. X. X.; Levkin, P. A., Printable Superhydrophilic-Superhydrophobic Micropatterns Based on Supported Lipid Layers. *Langmuir* **2012,** *28* (22), 8286-8291.

Li, Y. F.; Xia, Y. X.; Xu, D. P.; Li, G. L., Surface-Reaction of Particulate Silica with Polydimethylsiloxanes. *J Polym Sci Pol Chem* **1981,** *19* (12), 3069-3079.

Li, Y. Q.; Fu, S. Y.; Yang, Y.; Mai, Y. W., Facile synthesis of highly transparent polymer nanocomposites by introduction of core-shell structured nanoparticles. *Chem Mater* **2008,** *20* (8), 2637-2643.

Lin, Y.; Wang, L. M.; Krumpfer, J. W.; Watkins, J. J.; McCarthy, T. J., Hydrophobization of Inorganic Oxide Surfaces Using Dimethylsilanediol. *Langmuir* **2013,** *29* (5), 1329-1332.

Liu, J. G.; Nakamura, Y.; Ogura, T.; Shibasaki, Y.; Ando, S.; Ueda, M., Optically transparent sulfur-containing polyimide-TiO(2) nanocomposite films with high refractive index and negative pattern formation from poly(amic acid)-TiO(2) nanocomposite film. *Chem Mater* **2008,** *20* (1), 273-281.

Liu, R. X.; Qiao, X. Y.; Chung, T. S., The development of high performance P84 co-polyimide hollow fibers for pervaporation dehydration of isopropanol. *Chem Eng Sci* **2005,** *60* (23), 6674-6686.

Lu, G.; Li, W.; Yao, J. M.; Zhang, G.; Yang, B.; Shen, J. C., Fabricating ordered two-dimensional arrays of polymer rings with submicrometer-sized features on patterned self-assembled monolayers by dewetting. *Adv Mater* **2002,** *14* (15), 1049-+.

Mampallil, D.; Eral, H. B.; van den Ende, D.; Mugele, F., Control of evaporating complex fluids through electrowetting. *Soft Matter* **2012,** *8* (41), 10614-10617.

Mashak, A.; Rahimi, A., Silicone Polymers in Controlled Drug Delivery Systems: A Review. *Iran Polym J* **2009,** *18* (4), 279-295.

Massey, L. K., *Permeability properties of plastics and elastomers- a guide to packaging and barrier materials*. Plastics Design Library/ Willam Andrew Publishing: 2003.

Maury, P.; Escalante, M.; Reinhoudt, D. N.; Huskens, J., Directed assembly of nanoparticles onto polymer-imprinted or chemically patterned templates fabricated by nanoimprint lithography. *Adv Mater* **2005,** *17* (22), 2718-+.

McCarthy, D. W.; Mark, J. E.; Clarson, S. J.; Schaefer, D. W., Synthesis, structure, and properties of hybrid organic-inorganic composites based on polysiloxanes. II. Comparisons between poly(methylphenylsiloxane) and poly(dimethylsiloxane), and between titania and silica. *J Polym Sci Pol Phys* **1998,** *36* (7), 1191-1200.

Mchugh, T. H.; Avenabustillos, R.; Krochta, J. M., Hydrophilic Edible Films - Modified Procedure for Water-Vapor Permeability and Explanation of Thickness Effects. *J Food Sci* **1993,** *58* (4), 899-903.

Merkel, T. C.; Bondar, V.; Nagai, K.; Freeman, B. D.; Yampolskii, Y. P., Gas sorption, diffusion, and permeation in poly(2,2-bis(trifluoromethyl)-4,5-difluoro-1,3-dioxole-co-tetrafluoroethylene). *Macromolecules* **1999,** *32* (25), 8427-8440.

Merkel, T. C.; Freeman, B. D.; Spontak, R. J.; He, Z.; Pinnau, I.; Meakin, P.; Hill, A. J., Sorption, transport, and structural evidence for enhanced free volume in poly(4-methyl-2-pentyne)/fumed silica nanocomposite membranes. *Chem Mater* **2003,** *15* (1), 109-123.

Michael J. Sullivan, S. A., Edmund A. Hebert Golf Ball Surface Patterns Comprising Variable Width/Depth Multiple Channels. 2013.

Mishchenko, L.; Khan, M.; Aizenberg, J.; Hatton, B. D., Spatial Control of Condensation and Freezing on Superhydrophobic Surfaces with Hydrophilic Patches. *Adv Funct Mater* **2013,** *23* (36), 4577-4584.

MSDS sheet of Dow Corning Sylgard 184.

Müller, R., Über Silicone (I). Zur angewandten Chemie der Silicone (Synthese). *Chem. Tech.* **1950,** *2*, 7-13.

Murthy, R.; Cox, C. D.; Hahn, M. S.; Grunlan, M. A., Protein-resistant silicones: Incorporation of poly(ethylene oxide) via siloxane tethers. *Biomacromolecules* **2007,** *8* (10), 3244-3252.

Nakajima, A.; Nakagawa, Y.; Furuta, T.; Sakai, M.; Isobe, T.; Matsushita, S., Sliding of Water Droplets on Smooth Hydrophobic Silane Coatings with Regular Triangle Hydrophilic Regions. *Langmuir* **2013,** *29* (29), 9269-9275.

Nakata, K.; Kimura, H.; Sakai, M.; Ochiai, T.; Sakai, H.; Murakami, T.; Abe, M.; Fujishima, A., UV/Thermally Driven Rewritable Wettability Patterns on TiO2-PDMS Composite Films. *Acs Appl Mater Inter* **2010,** *2* (9), 2485-2488.

Nakayama, N.; Hayashi, T., Preparation and characterization of TiO2 and polymer nanocomposite films with high refractive index. *J Appl Polym Sci* **2007,** *105* (6), 3662-3672.

Nidetz, R.; Kim, J., Directed self-assembly of nanogold using a chemically modified nanopatterned surface. *Nanotechnology* **2012,** *23* (4).

Nisola, G. M.; Beltran, A. B.; Sim, D. M.; Lee, D.; Jung, B.; Chung, W. J., Dimethyl silane-modified silica in polydimethylsiloxane as gas permeation mixed matrix membrane. *J Polym Res* **2011,** *18* (6), 2415-2424.

Niu, X. Z.; Peng, S. L.; Liu, L. Y.; Wen, W. J.; Sheng, P., Characterizing and patterning of PDMS-based conducting composites. *Adv Mater* **2007,** *19* (18), 2682-+.

Odian, G., Principles of Polymerization. fourth ed.; Wiley Interscience.

Olah, A.; Hillborg, H.; Vancso, G. J., Hydrophobic recovery of UV/ozone treated poly(dimethylsiloxane): adhesion studies by contact mechanics and mechanism of surface modification. *Appl Surf Sci* **2005,** *239* (3-4), 410-423.

Oleg Roussak, H. D. G., Applied Chemistry: A Textbook for Engineers and Technologists. second ed.; Springer.

Osthoff, R. C.; Bueche, A. M.; Grubb, W. T., Chemical Stress Relaxation of Polydimethylsiloxane Elastomers. *J Am Chem Soc* **1954,** *76* (18), 4659-4663.

Palkovits, R.; Althues, H.; Rumplecker, A.; Tesche, B.; Dreier, A.; Holle, U.; Fink, G.; Cheng, C. H.; Shantz, D. F.; Kaskel, S., Polymerization of w/o microemulsions for the preparation of transparent SiO2/PMMA nanocomposites. *Langmuir* **2005,** *21* (13), 6048-6053.

Pauling, L., The Nature of Silicon-Oxygen Bonds. *Am Mineral* **1980,** *65* (3-4), 321-323.

Polymer Data Handbook. Mark, J. E., Ed. Oxford University Press, Inc: 1999.

Qin, D.; Xia, Y. N.; Whitesides, G. M., Soft lithography for micro- and nanoscale patterning. *Nat Protoc* **2010,** *5* (3), 491-502.

Qin, D.; Xia, Y. N.; Xu, B.; Yang, H.; Zhu, C.; Whitesides, G. M., Fabrication of ordered two-dimensional arrays of micro- and nanoparticles using patterned self-assembled monolayers as templates. *Adv Mater* **1999,** *11* (17), 1433-1437.

Rajan, G. S.; Sur, G. S.; Mark, J. E.; Schaefer, D. W.; Beaucage, G., Preparation and characterization of some unusually transparent poly(dimethylsiloxane) nanocomposites. *J Polym Sci Pol Phys* **2003,** *41* (16), 1897-1901.

Rajendra, V.; Gonzaga, F.; Brook, M. A., Nearly Monodisperse Silica Microparticles Form in Silicone (Pre)elastomer Mixtures. *Langmuir* **2012,** *28* (2), 1470-1477.

Randall, G. C.; Doyle, P. S., Permeation-driven flow in poly(dimethylsiloxane) microfluidic devices. *P Natl Acad Sci USA* **2005,** *102* (31), 10813-10818.

Rao, H. X.; Liu, F. N.; Zhang, Z. Y., Preparation and oxygen/nitrogen permeability of PDMS crosslinked membrane and PDMS/tetraethoxysilicone hybrid membrane. *J Membrane Sci* **2007,** *303* (1-2), 132-139.

Rimola, A.; Sodupe, M.; Tosoni, S.; Civalleri, B.; Ugliengo, P., Interaction of glycine with isolated hydroxyl groups at the silica surface: First principles B3LYP periodic simulation. *Langmuir* **2006,** *22* (15), 6593-6604.

Riskin, A.; De Dobbelaere, C.; Shan, L.; Boyen, H. G.; D'Haen, J.; Hardy, A.; van Bael, M. K., Dewetting of Patterned Silicon Substrates Leading to a Selective Deposition of Micellar-Based Nanoparticles. *J Phys Chem C* **2012,** *116* (19), 10743-10752.

Rochow, E. G., The Direct Synthesis of Organosilicon Compounds. *J Am Chem Soc* **1945,** *67* (6), 963-965.

Rochow, E. G., An Introduction to the Chemistry of the Silicones. Second ed.; John Wiley & Sons, Inc: 1946.

Rochow, E. G., *Introduction to the Chemistry of Silicones*. Wiley: 1953.

Rochow, E. G.; Rochow, T. G., The Properties and Molecular Weights of Some Silicone Polymers. *J Phys Colloid Chem* **1951,** *55* (1), 9-16.

Rogers, J. A.; Nuzzo, R. G., Recent progress in soft lithography. *Mater Today* **2005,** *8* (2), 50-56.

S.J.Metz. Water Vapor and Gas Transport Through Polymeric Membranes. Universiteit Twente, Enschede, 2003.

Sato, H.; Iba, H.; Naganuma, T.; Kagawa, Y., Effects of the difference between the refractive indices of constituent materials on the light transmittance of glass-particle-dispersed epoxy-matrix optical composites. *Philos Mag B* **2002,** *82* (13), 1369-1386.

Schaefer, D. W.; Kohls, D.; Feinblum, E., Morphology of Highly Dispersing Precipitated Silica: Impact of Drying and Sonication. *J Inorg Organomet P* **2012,** *22* (3), 617-623.

Schaer, E.; Guizani, S.; Choplin, L., Model development for the description of silica particles dispersion in silicone polymer. *Chem Eng Sci* **2006,** *61* (17), 5664-5677.

Schmidt, T.; Mennig, M.; Schmidt, H., New method for the preparation and stabilization of nanoparticulate t-ZrO2 by a combined sol-gel and solvothermal process. *J Am Ceram Soc* **2007,** *90* (5), 1401-1405.

Schweikart, A.; Fery, A., Controlled wrinkling as a novel method for the fabrication of patterned surfaces. *Microchim Acta* **2009,** *165* (3-4), 249-263.

Seethapathy, S.; Gorecki, T., Applications of polydimethylsiloxane in analytical chemistry: A review. *Anal Chim Acta* **2012,** *750*, 48-62.

Sertchook, H.; Elimelech, H.; Avnir, D., Composite particles of silica/poly(dimethylsiloxane). *Chem Mater* **2005,** *17* (18), 4711-4716.

Seyferth, D., Dimethyldichlorosilane and the direct synthesis of methylchlorosilanes. The key to the silicones industry. *Organometallics* **2001,** *20* (24), 4978-4992.

Shao, P.; Huang, R. Y. M., Polymeric membrane pervaporation. *J Membrane Sci* **2007,** *287* (2), 162-179.

Sharpe, R. B. A.; Burdinski, D.; Huskens, J.; Zandvliet, H. J. W.; Reinhoudt, D. N.; Poelsema, B., Chemically patterned flat stamps for microcontact printing. *J Am Chem Soc* **2005,** *127* (29), 10344-10349.

Shim, S. E.; Isayev, A. I., Rheology and structure of precipitated silica and poly(dimethyl siloxane) system. *Rheol Acta* **2004,** *43* (2), 127-136.

Shirazi, Y.; Ghadimi, A.; Mohammadi, T., Recovery of alcohols from water using polydimethylsiloxane-silica nanocomposite membranes: Characterization and pervaporation performance. *J Appl Polym Sci* **2012,** *124* (4), 2871-2882.

Speier, J. L.; Webster, J. A.; Barnes, G. H., The Addition of Silicon Hydrides to Olefinic Double Bonds .2. The Use of Group-Viii Metal Catalysts. *J Am Chem Soc* **1957,** *79* (4), 974-979.

Stannett, V., The transport of gases in synthetic polymeric membranes-an historic perspective. *J Membrane Sci* **1978,** *3* (2), 97-115.

Stein, J.; Lewis, L. N.; Gao, Y.; Scott, R. A., In situ determination of the active catalyst in hydrosilylation reactions using highly reactive Pt(0) catalyst precursors. *J Am Chem Soc* **1999,** *121* (15), 3693-3703.

Stöber, W.; Fink, A.; Bohn, E., Controlled Growth of Monodisperse Silica Spheres in Micron Size Range. *J Colloid Interf Sci* **1968,** *26* (1), 62-&.

Su, B.; Wang, S. T.; Ma, J.; Song, Y. L.; Jiang, L., "Clinging-Microdroplet" Patterning Upon High-Adhesion, Pillar-Structured Silicon Substrates. *Adv Funct Mater* **2011,** *21* (17), 3297-3307.

Suer, M. G.; Bac, N.; Yilmaz, L., Gas Permeation Characteristics of Polymer-Zeolite Mixed Matrix Membranes. *J Membrane Sci* **1994,** *91* (1-2), 77-86.

Suh, K. Y.; Khademhosseini, A.; Eng, G.; Langer, R., Single nanocrystal arrays on patterned poly(ethylene glycol) copolymer microstructures using selective wetting and drying. *Langmuir* **2004,** *20* (15), 6080-6084.

Suloff, E. C. Virginia Tech.

Sun, Y. P.; Gu, A. J.; Liang, G. Z.; Yuan, L., Preparation and Properties of Transparent Zinc Oxide/Silicone Nanocomposites for the Packaging of High-Power Light-Emitting Diodes. *J Appl Polym Sci* **2011,** *121* (4), 2018-2028.

Sylgard 184 Silicone Elastomer Kit Material Safety Data Sheet.

The volume of liquid in the puddles was determined by calculating the height, h, of the circular puddle, assuming that it has a spherical cap: $h = \frac{r}{\sin\theta}(1-\cos\theta)$, θ is the contact angle of N^+S^- on silica, and r is the average radius of the puddles. The average volume of the N^+S^- puddle is $V_{IL} = \frac{1}{6}\pi h(3r^2 + h^2)$ and the average volume of 25% aqueous N^+S^- that was dip-coated is $V = 4V_{IL}$.

Tada, H., Layer-by-Layer Construction of Siox Film on Oxide Semiconductors. *Langmuir* **1995,** *11* (9), 3281-3284.

Tadros, T., Interparticle interactions in concentrated suspensions and their bulk (Rheological) properties. *Adv Colloid Interfac* **2011,** *168* (1-2), 263-277.

Thalladi, V. R.; Whitesides, G. M., Crystals of crystals: Fabrication of encapsulated and ordered two-dimensional arrays of microcrystals. *J Am Chem Soc* **2002,** *124* (14), 3520-3521.

Thanawala, S. K.; Chaudhury, M. K., Surface modification of silicone elastomer using perfluorinated ether. *Langmuir* **2000,** *16* (3), 1256-1260.

Tian, D. L.; Song, Y. L.; Jiang, L., Patterning of controllable surface wettability for printing techniques. *Chem Soc Rev* **2013,** *42* (12), 5184-5209.

Topcuoglu, O.; Altinkaya, S. A.; Balkose, D., Characterization of waterborne acrylic based paint films and measurement of their water vapor permeabilities. *Prog Org Coat* **2006,** *56* (4), 269-278.

Ueda, E.; Levkin, P. A., Emerging Applications of Superhydrophilic-Superhydrophobic Micropatterns. *Adv Mater* **2013,** *25* (9), 1234-1247.

Unger, M. A.; Chou, H. P.; Thorsen, T.; Scherer, A.; Quake, S. R., Monolithic microfabricated valves and pumps by multilayer soft lithography. *Science* **2000,** *288* (5463), 113-116.

Vaeth, K. M.; Jensen, K. F., Transition metals for selective chemical vapor deposition of parylene-based polymers. *Chem Mater* **2000,** *12* (5), 1305-1313.

Vanderweij, F. W., The Action of Tin-Compounds in Condensation-Type Rtv Silicone Rubbers. *Makromol Chem* **1980,** *181* (12), 2541-2548.

Vesaratchanon, J. S.; Nikolov, A.; Wasan, D. T., Sedimentation of concentrated monodisperse colloidal suspensions: Role of collective particle interaction forces. *J Colloid Interf Sci* **2008,** *322* (1), 180-189.

Vladkova, T., Surface modification of silicone rubber with poly(ethylene glycol) hydrogel coatings. *J Appl Polym Sci* **2004,** *92* (3), 1486-1492.

Vondracek, P.; Schatz, M., Nh3-Modified Swelling of Silica-Filled Silicone-Rubber. *J Appl Polym Sci* **1979,** *23* (9), 2681-2694.

W.R.R.Park, *Plastics film technology*. Reinhold Book Corporation: 1969.

Wan, V. C. H.; Kim, M. S.; Lee, S. Y., Water vapor permeability and mechanical properties of soy protein isolate edible films composed of different plasticizer combinations. *J Food Sci* **2005,** *70* (6), E387-E391.

Wang, L. M.; McCarthy, T. J., Shear Distortion and Failure of Capillary Bridges. Wetting Information Beyond Contact Angle Analysis. *Langmuir* **2013,** *29* (25), 7776-7781.

Warrick, E. L.; Lauterbur, P. C., Filler Phenomena in Silicone Rubber. *Ind Eng Chem* **1955,** *47* (3), 486-491.

Watson, J. M.; Baron, M. G., The behaviour of water in poly(dimethylsiloxane). *J Membrane Sci* **1996,** *110* (1), 47-57.

We measured viscosity values of N^+S^- between 1100 and 1229 cP (4 measurements) using a parallel plate rheometer. 25% aq. N^+S^- exhibited a viscosity of ~2 cP. For comparison, water and glycerol exhibited 1.1 and 1002 cP with this instrument.

Wen, B.; Wang, F.; Zhang, S. M.; Ding, Y. F.; Yang, M. S., ZnO and ZnO-SiO2 core-shell structured fillers on properties of polycarbonate nanocomposites. *Plast Rubber Compos* **2010,** *39* (9), 419-424.

Wier, K. A., COMPOSITE POLYMER COATINGS PREPARED IN SUPERCRITICALCARBON DIOXIDE *phD thesis* **2006**.

Winzenberg, K. N.; Kemppinen, P.; Fanchini, G.; Bown, M.; Collis, G. E.; Forsyth, C. M.; Hegedus, K.; Singh, T. B.; Watkins, S. E., Dibenzo[b,def]chrysene Derivatives: Solution-Processable Small Molecules that Deliver High Power-Conversion Efficiencies in Bulk Heterojunction Solar Cells. *Chem Mater* **2009,** *21* (24), 5701-5703.

Wright, P. S., Soft lining materials: their status and prospects. *J Dent* **1976,** *4*, 246-256.

Xia, Y. N.; Whitesides, G. M., Soft lithography. *Annu Rev Mater Sci* **1998,** *28*, 153-184.

Xiang, H. P.; Ge, J. F.; Cheng, S. H.; Han, H. M.; Cui, S. W., Synthesis and characterization of titania/MQ silicone resin hybrid nanocomposite via sol-gel process. *J Sol-Gel Sci Techn* **2011,** *59* (3), 635-639.

Xu, J. J.; Gleason, K. K., Conformal, Amine-Functionalized Thin Films by Initiated Chemical Vapor Deposition (iCVD) for Hydrolytically Stable Microfluidic Devices. *Chem Mater* **2010,** *22* (5), 1732-1738.

Xue, L. J.; Han, Y. C., Pattern formation by dewetting of polymer thin film. *Prog Polym Sci* **2011,** *36* (2), 269-293.

Yan Liu, Z. L., Xueying Zhao, Kyoung-sik Moon, Sehoon Yoo, J Choi, C. P. Wong, High Refractive Index and Transparency Nanocomposites as Encapsulant for High Brightness LED packaging. *Electronic Components and Technology Conference* **2013**, 553-556.

Yang, X. F.; Shao, Q.; Yang, L. L.; Zhu, X. B.; Hua, X. L.; Zheng, Q. L.; Song, G. X.; Lai, G. Q., Preparation and performance of high refractive index silicone resin-type materials for the packaging of light-emitting diodes. *J Appl Polym Sci* **2013,** *127* (3), 1717-1724.

Young, T., An Essay on the Cohesion of Fluids *Philosophical Transactions of the Royal Society* **1805,** *95*, 65-87.

Zhang, Y. H.; Ishida, M.; Kazoe, Y.; Sato, Y.; Miki, N., Water-Vapor Permeability Control of PDMS by the Dispersion of Collagen Powder. *Ieej T Electr Electr* **2009,** *4* (3), 442-449.

Zheng, P. W.; McCarthy, T. J., Rediscovering Silicones: Molecularly Smooth, Low Surface Energy, Unfilled, UV/Vis-Transparent, Extremely Cross-Linked, Thermally Stable, Hard, Elastic PDMS. *Langmuir* **2010,** *26* (24), 18585-18590.

Zheng, P. W.; McCarthy, T. J., Rediscovering silicones, part 1, extremely crosslinked PDMS: A low surface energy, unfilled, UV/vis-transparent, thermally stable, molecularly smooth, hard, and elastic material. *Abstr Pap Am Chem S* **2011,** *241*.

Zheng, P. W.; McCarthy, T. J., A Surprise from 1954: Siloxane Equilibration Is a Simple, Robust, and Obvious Polymer Self-Healing Mechanism. *J Am Chem Soc* **2012,** *134* (4), 2024-2027.

Zhou, J. W.; Ellis, A. V.; Voelcker, N. H., Recent developments in PDMS surface modification for microfluidic devices. *Electrophoresis* **2010,** *31* (1), 2-16.